forests

Disturbance Effects on Soil Carbon and Greenhouse Gas Emissions in Forest Ecosystems

Edited by

Scott X. Chang and Yanjiang Cai

Printed Edition of the Special Issue Published in *Forests*

www.mdpi.com/journal/forests

MDPI

Disturbance Effects on Soil Carbon and Greenhouse Gas Emissions in Forest Ecosystems

Disturbance Effects on Soil Carbon and Greenhouse Gas Emissions in Forest Ecosystems

Special Issue Editors

Scott X. Chang
Yanjiang Cai

MDPI • Basel • Beijing • Wuhan • Barcelona • Belgrade • Manchester • Tokyo • Cluj • Tianjin

Special Issue Editors
Scott X. Chang
University of Alberta
Canada

Yanjiang Cai
Zhejiang A&F University
China

Editorial Office
MDPI
St. Alban-Anlage 66
4052 Basel, Switzerland

This is a reprint of articles from the Special Issue published online in the open access journal *Forests* (ISSN 1999-4907) (available at: https://www.mdpi.com/journal/forests/special_issues/Disturbance_Effects_on_Soil_Carbon_and_Greenhouse_Gas_Emissions).

For citation purposes, cite each article independently as indicated on the article page online and as indicated below:

LastName, A.A.; LastName, B.B.; LastName, C.C. Article Title. *Journal Name* **Year**, *Article Number*, Page Range.

ISBN 978-3-03928-666-9 (Pbk)
ISBN 978-3-03928-667-6 (PDF)

Cover image courtesy of Scott X. Chang

Contents

About the Special Issue Editors

Scott X. Chang (Professor of Forest Soils and Nutrient Dynamics) received his B.Sc. from Zhejiang Agricultural University, his M.Sc. from the Chinese Academy of Sciences, and his Ph.D. from the University of British Columbia. He has held academic positions in New Zealand and the United States prior to taking up his current position at the University of Alberta. His main research interests are in forest soils, soil nutrient cycling, and plant nutrition. He served as Chair of the Soil Fertility and Plant Nutrition Commission of the International Union of Soil Science; President of the Association of Chinese Soil & Plant Scientists in North America; Chair for the Forest, Range, and Wildland Soils Division of the Soil Science Society of America; and Chair of the Alberta Soil Science Workshop. He has served as an Associate/Guest Editor or Editorial Board member for Biology and Fertility of Soils, Pedosphere, Soil Science Society of America Journal, Canadian Journal of Soil Science, Journal of Environmental Quality, Environmental Science and Pollution Research, Forests, and Forest Ecology and Management. He is a fellow of the Soil Science Society of America, the American Society of Agronomy, and the Canadian Society of Soil Science.

Yanjiang Cai (Professor of Soil Science) received his B.Sc. from the Hebei University, his M.Sc. from the Dalian Jiaotong University, and his Ph.D. from the Chinese Academy of Sciences. He was a visiting Professor at the University of Alberta in Canada and a JSPS postdoctoral researcher at the National Agriculture and Food Research Organization in Japan. He held an academic position in Chinese Academy of Sciences prior to taking up his current position at the Zhejiang A&F University. His main research interests are soil carbon and nitrogen transformations and fluxes in forest and grassland ecosystems, as well as management options towards greenhouse gas mitigation and climate change adaptation. He has served as an Editorial Board member for Biology and Fertility of Soils and a Guest Editor for Forests. He received the JSPS Fellowship for Overseas Researchers and the Excellent Young Scientist Award from the Association of Chinese Soil and Plant Scientists in North America.

forests

MDPI

Editorial

Disturbance Effects on Soil Carbon and Greenhouse Gas Emissions in Forest Ecosystems

Yanjiang Cai [1] and Scott X. Chang [1,2,*]

[1] State Key Laboratory of Subtropical Silviculture, Zhejiang A&F University, Hangzhou 311300, China; yjcai@zafu.edu.cn

[2] Department of Renewable Resources, University of Alberta, 442 Earth Sciences Building, Edmonton, AB T6G 2E3, Canada

* Correspondence: scott.chang@ualberta.ca; Tel.: +1-780-492-6375

Received: 28 February 2020; Accepted: 5 March 2020; Published: 7 March 2020

Abstract: Forests cover around 30% of the global land area and forest ecosystems can store over 70% of total soil organic carbon (SOC) of all terrestrial ecosystems, but SOC stocks and greenhouse gas (GHG) emissions may be affected by both natural and anthropogenic disturbances. Even though the changes in forest soil C pool can have a significant effect on climate change, there are some contradictory results regarding the role of forest disturbance on SOC sequestration, GHG emissions, and the mitigation of global changes. Therefore, there is a need to better understand the impact of different disturbance regimes on forest soil C storage and GHG emissions. A Special Issue was therefore organized for discussing the responses of soil C storage and GHG emissions to various types of disturbances in forest ecosystems and a total of 15 studies were accepted for this special issue to assess these responses. This Special Issue includes the effects of storms and beetle outbreaks, Karstification, rock desertification, warming, nitrogen addition, land-use change, field tillage, and biochar application on soil C dynamics and/or GHG emissions.

Keywords: CH_4 emissions; CO_2 emissions; climate change mitigation; global change; land-use change; N_2O emissions; soil carbon sequestration

Disturbances from natural (e.g., insect outbreaks, geologic processes and wildfires) and anthropogenic (e.g., logging, applying soil amendments and land use change) are important drivers of changes of ecological processes in forest ecosystems, and the impact of disturbances on ecosystem processes may vary with the type and level of disturbances [1–3]. These disturbances are expected to markedly affect the amount, form and stability of soil organic carbon (SOC) and the emission of three major trace greenhouse gases (GHGs) (CO_2, CH_4 and N_2O) from forest ecosystems [4,5]. More than 70% of total SOC of all terrestrial ecosystems can be found in forest ecosystems [6] and thus, a minor change in the size of the forest SOC pool can exert a large impact on climate change on a global scale. The assessment of the variability in forest SOC storage and GHG emissions is thus a critical consideration for evaluating regional and global climate change [7]. It is vitally important to improve the understanding of the impact of different disturbance regimes on forest SOC storage and GHG emissions for guiding future research, forest management practices, and policy development. We therefore organized a Special Issue to bring together researchers working on different aspects of forest ecology to share their findings on disturbance effects on SOC storage and GHG emissions in forest ecosystems. We are pleased that we received a strong response from the scientific community to this call for the Special Issue and a total of 15 papers have ultimately been accepted for inclusion in this Special Issue.

Three papers in this Special Issue address the effect of natural disturbances on SOC content and GHG emissions. Storms and beetle outbreaks are two major forms of disturbance in European forests,

but Kosunen et al. did not find any consistent effect of either storm or European spruce bark beetle (*Ips typographus* L.) outbreak on soil total and heterotrophic respiration, and soil total respiration rates were found to be related to the basal area of living trees, and also to soil temperature and soil moisture content [8]. Karstification, the dissolution of calcite and the formation of the karst landform in an area where the bedrock is dominated by limestone, can also affect soil C dynamics; in this respect, Huang et al. found that the C sink in karstified calcareous soils was 11.97 times that of non-karstified red soils, while the role of calcareous soils as a C source was only 1.12 times that in red soils [9]. The overall mean $\delta^{13}C$-CO_2 value in calcareous soils was 0.87‰ higher than that in red soils, and these results indicate that karst soils play a key role in the reduction of atmospheric CO_2 [9]. Rock desertification is a process of land degradation that may reduce soil productivity and some natural environmental factors can induce this process [10], but the effect of desertification on forest soil stoichiometry remains poorly understood. Yang et al. reported that soil C:N (nitrogen) ratio was not significantly affected by the degree of desertification, but soil C:P (C: phosphorus) and N:P ratios increased with increasing degree of desertification [11]. Yang et al. also pointed out that P might be the limiting factor for plant growth during restoration and calcium could play an important role in soil C, N and P stoichiometry in the ecosystem they studied [11].

Eleven papers in this Special Issue address the effect of anthropogenic disturbances on soil C and GHG emissions. Soil C and N cycling can be significantly affected by climate warming and N deposition that are caused by human activities [12,13]. An eight-year experiment with warming and N addition treatments in a subalpine spruce (*Picea asperata* Mast.) plantation forest showed that soil CO_2 emissions were solely influenced by warming while both N addition and its interaction with warming significantly elevated soil N_2O emissions, there were different response patterns and different factors governed soil CO_2 and N_2O emissions in the forest ecosystem [14]. Interestingly, Zhou et al. found that in a subtropical forest dominated by *Castanopsis carlesii* Hayata and *Schima superba* Gardn. et Champ, a high-level N addition treatment significantly reduced but a low-level N addition treatment markedly enhanced soil respiration, with the high-level N addition treatment reduced soil pH and increased C and P co-limitation of microorganisms, which resulted in decreases in total phospholipid fatty acid (PLFA) content and alterations in microbial community structures [15]. Zhou et al. also concluded that the altered microbial community structure and suppressed microbial biomass under increasing N deposition could ultimately lead to the accumulation of recalcitrant C and reduction in soil C emissions in the studied subtropical forest [15].

Changes in land use patterns can also alter soil C and N cycling and the structure of soil microbial communities [5,6]. The research in Qiu et al. indicated that *Proteobacteria*, *Verrucomicrobia* and *Acidobacteria* were the dominant bacteria and their relative abundances were different in the woodland, shrubland and grassland soils in a karst graben basin in subtropical China, and soil bacterial communities were markedly influenced by SOC, total N, and available potassium contents [16]. Studying SOC mineralization under different land uses is essential for improving our understanding of SOC responses to land-use change. The study of Yang et al. in the karst region showed that the establishment of plum (*Prunus salicina* Lindl.) plantations markedly reduced the SOC content as compared with abandoned lands, but the SOC content did not vary with plum plantation age; however, the cumulative and potential SOC mineralization rates were different among plum plantation ages, and both increased with increasing soil calcium concentration; thus, more attention should be paid in the future to the critical role of calcium in SOC mineralization in the studied subtropical area [17]. In contrast, the study conducted by Zhao et al. in a larch (*Larix principis-rupprechtii* Mayr) forest showed that the contents of SOC, total N and total K were all increased with increasing stand age, and clear-cutting reduced SOC, total N, and total K contents [18]. The effect of the conversion of natural evergreen broadleaved forests to an assisted natural regeneration and Chinese fir (*Cunninghamia lanceolata* (Lamb.) Hook) and mason pine (*Pinus massoniana* Lamb.) plantations was conducted by Yang et al. in subtropical China [19]. The conversion led to 42%, 60%, and 64% reductions in SOC contents for assisted natural regeneration, Chinese fir, and mason pine plantations, respectively, with

microbial residue C accumulation varying with SOC content and rate of litter input [19]. In addition, Zhu et al. investigated the responses of SOC and soil organic N to soil erosion and forest conversion in the development of sloping economic forests in mountain areas in Jiangsu province in China; they reported that the conversion of coniferous broadleaved mixed forests into economic forests aggravated soil erosion, and the intensive management of the economic forest also reduced soil C storage and increased the loss of soil nutrients; the loss of soil C and N caused by soil erosion can therefore be detrimental to the development of local agriculture and forestry [20].

Although tillage in forest ecosystems does not take place as often as in agricultural ecosystems, tree planting and tillage are practices commonly used for vegetation restoration [21]. In a forest soil profile inversion and mixing study, Wang et al. showed that CO_2 concentration in forest soil profiles was governed by both soil properties related to CO_2 production such as SOC and soil microbial biomass content and those related to gas diffusion, such as soil bulk density and gas molecular weight; however, soil surface CO_2 emissions were not affected by soil profile inversion but were increased by soil profile mixing; soil surface CO_2 emissions were mainly controlled by soil surface temperature [21].

Mangrove wetlands are a potential source for atmospheric CH_4, but there remain considerable uncertainties regarding the importance of mangrove wetlands for contributing climate warming [22]. Through a field study at three tidal zones of two mangrove ecosystems in southeastern China, Zheng et al. found highly variable CH_4 emission patterns among the three zones and attributed this phenomenon to the heterogeneity in the mangrove soil environment [23]. After analyzing the data from these three zones and those from 24 mangrove wetlands worldwide, the authors summarized that undisturbed mangrove sites had very low rates of CH_4 emissions, which were much lower than the global warming potentials generated by soil CO_2 emissions from the same sites. Although CH_4 emissions from mangrove soils were not significantly affected by plant species, study site, tidal position, sampling time, and soil characteristics, the nutrient inputs driven by anthropogenic activities could markedly elevate mangrove soil CH_4 emissions, and the estimates of regional or biglobal inventory of CH_4 emission should affirmatively consider the part from mangrove wetlands intensively affected by human activities [23].

Even though biochar has a great potential to mitigate climate change, much less research on biochar effects has been carried out in forest ecosystems in comparison to agricultural ecosystems [24]. Two papers in this Special Issue address the effect of biochar on altering forest soil C storage and mitigating GHG emissions. The study of Criscuoli et al. in northern Italy showed that conifer woodchip-derived biochar application did not significantly influence the temperature sensitivity of soil CO_2 and N_2O emissions, but significantly reduced the sensitivity of soil CH_4 uptake [25]. In the second biochar study included in this Special Issue, Deng et al. conducted an in situ experiment to examine the effects of shell-derived biochar and dicyandiamide (DCD) on soil N_2O emissions from a tea oil camellia (*Camellia oleifera* Abel) plantation with intensive N application in Jiangxi province, China [26]. The authors found that N application enhanced cumulative soil N_2O emissions by 307%, adding biochar and DCD to the N-fertilized field reduced cumulative soil N_2O emissions by 36 and 44%, respectively, suggesting that the mitigation potential of biochar on soil N_2O emissions may reach that of DCD under the conditions studied [26].

It should be noted that estimating forest C stock and improving the accuracy of GHG inventory for each country are very important for evaluating the impact of land management and land use change on regional and global climate change [5–7]. The work done by Lee et al. in South Korea showed that forests could continue to store C and absorb CO_2 even under the declining total forest area and their study provides methodologies to facilitate the estimation of C stock changes and CO_2 removal by different forest types or plant species [27].

We are pleased to make this Special Issue available to readers. As guest editors, we would like to thank the authors for their valuable contribution to this Special Issue and express our deep appreciation to the many reviewers for their insightful comments that improved the quality of an earlier version

of each of the published papers. We would also like to express our sincere gratitude to the Editorial Office for their valuable assistance throughout the publication process.

Author Contributions: Y.C. wrote the first draft. S.X.C. went through several rounds of review/editing and added content. All authors have read and agreed to the published version of the manuscript.

Funding: This work was supported by the National Natural Science Foundation of China (41877085, 41877088), the Research and Development Fund of Zhejiang A&F University (2018FR005, 2018FR006), the Open Research Fund Program of the State Key Laboratory of Subtropical Silviculture, Zhejiang A&F University (ZY20180301, ZY20180205).

Conflicts of Interest: The authors declare no conflict of interest.

References

1. Danneyrolles, V.; Dupuis, S.; Fortin, G.; Leroyer, M.; de Römer, A.; Terrail, R.; Vellend, M.; Boucher, Y.; Laflamme, J.; Bergeron, Y.; et al. Stronger influence of anthropogenic disturbance than climate change on century-scale compositional changes in northern forests. *Nat. Commun.* **2019**, *10*, 1265. [CrossRef]
2. Moreno-Mateos, D.; Barbier, E.B.; Jones, P.C.; Jones, H.P.; Aronson, J.; López-López, J.A.; McCrackin, M.L.; Meli, P.; Montoya, D.; Rey Benayas, J.M. Anthropogenic ecosystem disturbance and the recovery debt. *Nat. Commun.* **2017**, *8*, 14163. [CrossRef]
3. Thom, D.; Seidl, R. Natural disturbance impacts on ecosystem services and biodiversity in temperate and boreal forests. *Biol. Rev.* **2016**, *91*, 760–781. [CrossRef]
4. Bradford, J.B.; Birdsey, R.A.; Joyce, L.A.; Ryan, M.G. Tree age, disturbance history, and carbon stocks and fluxes in subalpine Rocky Mountain forests. *Glob. Change Biol.* **2008**, *14*, 2882–2897. [CrossRef]
5. Oertel, C.; Matschullat, J.; Zurba, K.; Zimmermann, F.; Erasmi, S. Greenhouse gas emissions from soils—A review. *Geochemistry* **2016**, *76*, 327–352. [CrossRef]
6. Jandl, R.; Lindner, M.; Vesterdal, L.; Bauwens, B.; Baritz, R.; Hagedorn, F.; Johnson, D.W.; Minkkinen, K.; Byrne, K.A. How strongly can forest management influence soil carbon sequestration? *Geoderma* **2007**, *137*, 253–268. [CrossRef]
7. IPCC. Climate Change 2014: Synthesis Report. In *Contribution of Working Groups I, II and III to the Fifth Assessment Report of the Intergovernmental Panel on Climate Change*; Core Writing Team, Pachauri, R.K., Meyer, L.A., Eds.; IPCC: Geneva, Switzerland, 2014; p. 151.
8. Kosunen, M.; Lyytikäinen-Saarenmaa, P.; Ojanen, P.; Blomqvist, M.; Starr, M. Response of soil surface respiration to storm and *Ips typographus* (L.) disturbance in boreal Norway spruce stands. *Forests* **2019**, *10*, 307. [CrossRef]
9. Huang, F.; Cao, J.; Zhu, T.; Fan, M.; Ren, M. CO_2 transfer characteristics of calcareous humid subtropical forest soils and associated contributions to carbon source and sink in Guilin, southwest China. *Forests* **2020**, *11*, 219. [CrossRef]
10. Yang, Q.Q.; Wang, K.L.; Zhang, C.; Yue, Y.M.; Tian, R.C.; Fan, F.D. Spatio-temporal evolution of rocky desertification and its driving forces in karst areas of Northwestern Guangxi, China. *Environ. Earth Sci.* **2011**, *64*, 383–393. [CrossRef]
11. Yang, H.; Zhang, P.; Zhu, T.; Li, Q.; Cao, J. The characteristics of soil C, N, and P stoichiometric ratios as affected by geological background in a karst graben area, southwest China. *Forests* **2019**, *10*, 601. [CrossRef]
12. Battye, W.; Aneja, V.P.; Schlesinger, W.H. Is nitrogen the next carbon? *Earth's Future* **2017**, *5*, 894–904. [CrossRef]
13. Reay, D.S.; Dentener, F.; Smith, P.; Grace, J.; Feely, R.A. Global nitrogen deposition and carbon sinks. *Nat. Geosci.* **2008**, *1*, 430–437. [CrossRef]
14. Li, D.; Liu, Q.; Yin, H.; Luo, Y.; Hui, D. Differential responses and controls of soil CO_2 and N_2O fluxes to experimental warming and nitrogen fertilization in a subalpine coniferous spruce (*Picea asperata* Mast.) plantation forest. *Forests* **2019**, *10*, 808. [CrossRef]
15. Zhou, J.; Liu, X.; Xie, J.; Lyu, M.; Zheng, Y.; You, Z.; Fan, Y.; Lin, C.; Chen, G.; Chen, Y.; et al. Nitrogen addition affects soil respiration primarily through changes in microbial community structure and biomass in a subtropical natural forest. *Forests* **2019**, *10*, 435. [CrossRef]
16. Qiu, J.; Cao, J.; Lan, G.; Liang, Y.; Wang, H.; Li, Q. The influence of land use patterns on soil bacterial community structure in the karst graben basin of Yunnan province, China. *Forests* **2019**, *11*, 51. [CrossRef]

17. Yang, H.; Mo, B.; Zhou, M.; Zhu, T.; Cao, J. Effects of plum plantation ages on soil organic carbon mineralization in the karst rocky desertification ecosystem of southwest China. *Forests* **2019**, *10*, 1107. [CrossRef]
18. Zhao, K.; Fahey, T.J.; Liang, D.; Jia, Z.; Ma, L. Effects of long-term successive rotations, clear-cutting and stand age of prince rupprecht's larch (*Larix principis-rupprechtii* Mayr) on soil quality. *Forests* **2019**, *10*, 932. [CrossRef]
19. Yang, L.; Chen, S.; Li, Y.; Wang, Q.; Zhong, X.; Yang, Z.; Lin, C.; Yang, Y. Conversion of natural evergreen broadleaved forests decreases soil organic carbon but increases the relative contribution of microbial residue in subtropical China. *Forests* **2019**, *10*, 468. [CrossRef]
20. Zhu, X.; Lin, J.; Dai, Q.; Xu, Y.; Li, H. Evaluation of forest conversion effects on soil erosion, soil organic carbon and total nitrogen based on ^{137}Cs tracer technique. *Forests* **2019**, *10*, 433. [CrossRef]
21. Wang, X.; Fu, S.; Li, J.; Zou, X.; Zhang, W.; Xia, H.; Lin, Y.; Tian, Q.; Zhou, L. Forest soil profile inversion and mixing change the vertical stratification of soil CO_2 concentration without altering soil surface CO_2 Flux. *Forests* **2019**, *10*, 192. [CrossRef]
22. Chen, G.; Chen, B.; Yu, D.; Tam, N.F.Y.; Ye, Y.; Chen, S. Soil greenhouse gas emissions reduce the contribution of mangrove plants to the atmospheric cooling effect. *Environ. Res. Lett.* **2016**, *11*, 124019. [CrossRef]
23. Zheng, X.; Guo, J.; Song, W.; Feng, J.; Lin, G. Methane emission from mangrove wetland soils is marginal but can be stimulated significantly by anthropogenic activities. *Forests* **2018**, *9*, 738. [CrossRef]
24. Li, Y.; Hu, S.; Chen, J.; Mueller, K.; Li, Y.; Fu, W.; Lin, Z.; Wang, H. Effects of biochar application in forest ecosystems on soil properties and greenhouse gas emissions: A review. *J. Soils Sediments* **2018**, *18*, 546–563. [CrossRef]
25. Criscuoli, I.; Ventura, M.; Sperotto, A.; Panzacchi, P.; Tonon, G. Effect of woodchips biochar on sensitivity to temperature of soil greenhouse gases emissions. *Forests* **2019**, *10*, 594. [CrossRef]
26. Deng, B.; Fang, H.; Jiang, N.; Feng, W.; Luo, L.; Wang, J.; Wang, H.; Hu, D.; Guo, X.; Zhang, L. Biochar is comparable to dicyandiamide in the mitigation of nitrous oxide emissions from *Camellia oleifera* Abel. fields. *Forests* **2019**, *10*, 1076. [CrossRef]
27. Lee, S.J.; Yim, J.S.; Son, Y.M.; Son, Y.; Kim, R. Estimation of forest carbon stocks for national greenhouse gas inventory reporting in South Korea. *Forests* **2018**, *9*, 625. [CrossRef]

forests

MDPI

Article

Response of Soil Surface Respiration to Storm and *Ips typographus* (L.) Disturbance in Boreal Norway Spruce Stands

Maiju Kosunen *, Päivi Lyytikäinen-Saarenmaa, Paavo Ojanen, Minna Blomqvist and Mike Starr

Department of Forest Sciences, University of Helsinki, P.O. Box 27, FI-00014, 00100 Helsinki, Finland; paivi.lyytikainen-saarenmaa@helsinki.fi (P.L.-S.); paavo.ojanen@helsinki.fi (P.O.); minna.blomqvist@helsinki.fi (M.B.); mike.starr@helsinki.fi (M.S.)

* Correspondence: maiju.kosunen@helsinki.fi

Received: 28 February 2019; Accepted: 24 March 2019; Published: 3 April 2019

Abstract: Disturbances such as storm events and bark beetle outbreaks can have a major influence on forest soil carbon (C) cycling. Both autotrophic and heterotrophic soil respiration may be affected by the increase in tree mortality. We studied the effect of a storm in 2010 followed by an outbreak of the European spruce bark beetle (*Ips typographus* L.) on the soil surface respiration (respiration by soil and ground vegetation) at two Norway spruce (*Picea abies* L.) dominated sites in southeastern Finland. Soil surface respiration, soil temperature, and soil moisture were measured in three types of plots—living trees (undisturbed), storm-felled trees, and standing dead trees killed by *I. typographus*—during the summer–autumn period for three years (2015–2017). Measurements at storm-felled tree plots were separated into dead tree detritus-covered (under storm-felled trees) and open-vegetated (on open areas) microsites. The soil surface total respiration for 2017 was separated into its autotrophic and heterotrophic components using trenching. The soil surface total respiration rates at the disturbed plots were 64%–82% of those at the living tree plots at one site and were due to a decrease in autotrophic respiration, but there was no clear difference in soil surface total respiration between the plots at the other site, due to shifts in either autotrophic or heterotrophic respiration. The soil surface respiration rates were related to plot basal area (living and all trees), as well as to soil temperature and soil moisture. As storm and bark beetle disturbances are predicted to become more common in the future, their effects on forest ecosystem C cycling and CO_2 fluxes will therefore become increasingly important.

Keywords: forest soils; autotrophic respiration; heterotrophic respiration; CO_2 effluxes; decomposition; forest disturbance; tree mortality; storm damage; insect outbreak

1. Introduction

Abiotic disturbances, such as storms, and biotic disturbances, such as bark beetle outbreaks, are important drivers of forest ecosystem functioning [1,2]. Such disturbances increase tree mortality, resulting in—at least temporarily—diminished forest C fixation (CO_2 influx) and autotrophic respiration (CO_2 efflux from plant and rhizosphere metabolism) and, in some cases, increased heterotrophic respiration (CO_2 efflux from organic matter decomposition) due to increased decomposition [2–6]. Over extended periods of time, the effect of natural disturbances on the carbon (C) balance can thus result in a forest turning from being a C sink into a C source and so add to global warming [4,7]. However, the effects on C balance may be less drastic and transient if the productivity of the remaining trees and secondary structure is increased or if decreased forest stand productivity is accompanied with a reduction in ecosystem respiration [8,9]. Besides disturbance severity, changes in forest ecosystem C fluxes are dependent on several other factors, e.g., pre-disturbance forest composition

and structure, growth of the remaining trees and ground vegetation, and tree regeneration [5,8,10–12]. Hence, the responses and recovery of a forest after disturbance may differ among forest management strategies as well as between non-managed and commercially managed forests [3,8,13–15].

Soil respiration is one of the largest terrestrial C fluxes globally [16]. It has been estimated that 55% of the C fixed annually by forests in gross primary production is returned back to the atmosphere as a result of soil respiration [17]. Disturbance may alter soil respiration in several ways. Tree death reduces soil autotrophic respiration due to the cessation of C allocation to roots and soil [18,19]. Disturbance-induced tree mortality also results in changes in litter quality and quantity [20,21], light and water availability and soil temperature and moisture [2,6,12,22,23], soil microbial community dynamics [24–26], and the composition of the ground vegetation [13,27], all of which can be expected to lead to changes in the decomposition process and, hence, soil heterotrophic respiration.

Besides spatial variation in the alterations, the direction and magnitude of these alterations may change with time after the disturbance [5]. As a result, both increases [23,28] and decreases [9,29] as well as no change [6,22,23,30,31] in soil total respiration over periods varying from months to several years after disturbance have been reported. However, few studies have studied the effects of natural disturbance separately on the autotrophic and heterotrophic components of soil respiration. Mayer et al. [6,23] found that storm disturbance increased heterotrophic respiration for some years after the storm and attributed this to increases in soil temperature and associated accelerated decomposition of soil organic matter, whereas in another study [29], storm and bark beetle disturbance was shown to have decreased autotrophic soil respiration but to have had no clear effect on heterotrophic respiration.

Storms and European spruce bark beetle (*Ips typographus* L.) outbreaks are two major forms of disturbance in European forests [32,33], and both are predicted to result in greater tree damage in the future [34,35]. Whilst storms immediately alter the structure and functioning of the forest by breaking and uprooting (killing) trees and mixing soil [1], the changes brought about by bark beetle outbreaks are gradual [2]. Wind disturbance especially creates various microsites [1,36] where tree stand and soil properties differ. For example, undisturbed soil with decomposing residue piles [37] or gaps [38,39] created after disturbance can have different soil properties and dynamics compared to the less affected areas or pre-disturbance conditions. Storm events can predispose forests to insect outbreaks, as wind-fallen trees provide optimal breeding material for bark beetles [40,41]. Where there is more than one disturbance event, changes in the C balance and soil respiration can be expected to be more complicated.

In this study, the effects of a storm event followed by an outbreak of *I. typographus* on soil surface total (SR_{tot}, soil CO_2 efflux from soil and ground vegetation), autotrophic (SR_a), and heterotrophic (SR_h) respiration were investigated at two forest sites in southeastern Finland. The aims of the study were to determine the effect of storm damage and *I. typographus* outbreak on (1) SR_{tot} and its autotrophic and heterotrophic components and (2) the degree to which disturbance-related differences in respiration were due to differences in tree stand characteristics and tree mortality or in environmental conditions. We hypothesized that (1) SR_a from storm-damaged and from *I. typographus*-infested plots would be lower and SR_h higher compared to control (undisturbed) plots; (2) storm-damaged SR_a and SR_h would differ between open microsites having ground vegetation and microsites under storm-felled trees covered with dead tree detritus; and (3) respiration would be related to stand basal area (dead tree basal area resulting from the storm and *I. typographus* disturbances), disturbance-related differences in soil microclimate (temperature and moisture), or both.

2. Materials and Methods

2.1. Research Area

The study was carried out in two Norway spruce (*Picea abies* L.) dominated forest sites, Paajasensalo (56 ha) and Viitalampi (73 ha), located in the municipality of Ruokolahti (61°17′30″ N, 28°49′10″ E) in southeastern Finland. The distance between the two sites is about 6 km. A large-scale storm occurred

in the region in July 2010 and was followed by an outbreak of *I. typographus* from 2011 onwards. The forests at the Paajasensalo site were in commercial use until 2010 and those in the Viitalampi site until 2011, but afterwards they were conserved as METSO (Forest Biodiversity Program for Southern Finland) sites and no forest management actions have been carried out since. Thus, contrary to normal forestry practice, all the trees killed by the storm and bark beetle were left in the forest after the disturbance events, making the sites ideal for the purposes of this research.

The soils at the study sites were Podzols, mostly cambic, and developed in till deposits. The soil texture (fine-earth fraction) was either sandy loam or loamy sand, and the thickness of the surface humus layer varied between 2.3 and 8.0 cm. According to the Cajanderian site type classification [42], which describes site stand productivity, the sites were mainly medium-rich Myrtillus (MT) and rich Oxalis-Myrtillus (OMT) types. The ground vegetation under closed canopy was dominated by blueberry (*Vaccinium myrtillus* L.), with lingonberry (*Vaccinium vitis-idaea* L.) and several herbaceous species (e.g., small cow-wheat (*Melampyrum sylvaticum* L.), twinflower (*Linnea borealis* L.), wood sorrel (*Oxalis acetosella* L.), and oak fern (*Gymnocarpium dryopteris* L. Newman)) being present. The forest floor moss layer was dominated by red-stemmed feather-moss (*Pleurozium schreberi* (Brid.) Mitt.), stairstep moss (*Hylocomium splendens* (Hedw.) BSG), and fork-moss (*Dicranum* sp.). The storm and, to a lesser degree, the bark beetle outbreaks modified the ground vegetation composition towards more light-demanding pioneer species such as fireweed (*Chamerion angustifolium* L.), wavy hair-grass (*Deschampsia flexuosa* L. Trin), and raspberry (*Rubus ideaus* L.). Although dominated by spruce, isolated Scots pine (*Pinus sylvesteris* L.), silver birch (*Betula pendula* Roth), downy birch (*Betula pubescens* L.), European aspen (*Populus tremula* L.), grey alder (*Alnus incana* L.), common alder (*Alnus glutinosa* L. Gaertn), rowen (*Sorbus aucuparia* L.), and willow (*Salix* spp.) trees also grew within the stands. The long-term (1981–2010) mean annual air temperature for the study sites was 4.2 °C and the mean annual precipitation was 653 mm [43]. The mean air temperature and precipitation for the study months (May–Oct) were 12.3 °C and 38 mm in 2015, 13.0 °C and 52 mm in 2016, and 11.3 °C and 61 mm in 2017 [44].

2.2. Study Layout

After exploring both study sites, three types of disturbance areas were identified: those having living trees with no clear signs of storm or bark beetle damage (LT), areas with fallen trees resulting from the storm (SF), and areas of living and dead standing trees showing bark beetle attack (ID). A circular plot (radius 11.28 m, area 400 m^2) was then established in each of three areas in both study sites in June 2015 (Figure 1), resulting in a total of 12 plots (6 in Paajasensalo and 6 in Viitalampi). In order to have a more encompassing data set, another set (block) of plots were established in both study sites in June 2016 (Figure 1). Photographs of each plot type (LT, SF, and ID) are presented in Figure S1. As the three plots (disturbance treatments) were spatially interspersed within the two blocks and the blocks were replicated at two study sites, bias and problems of pseudoreplication were reduced [45].

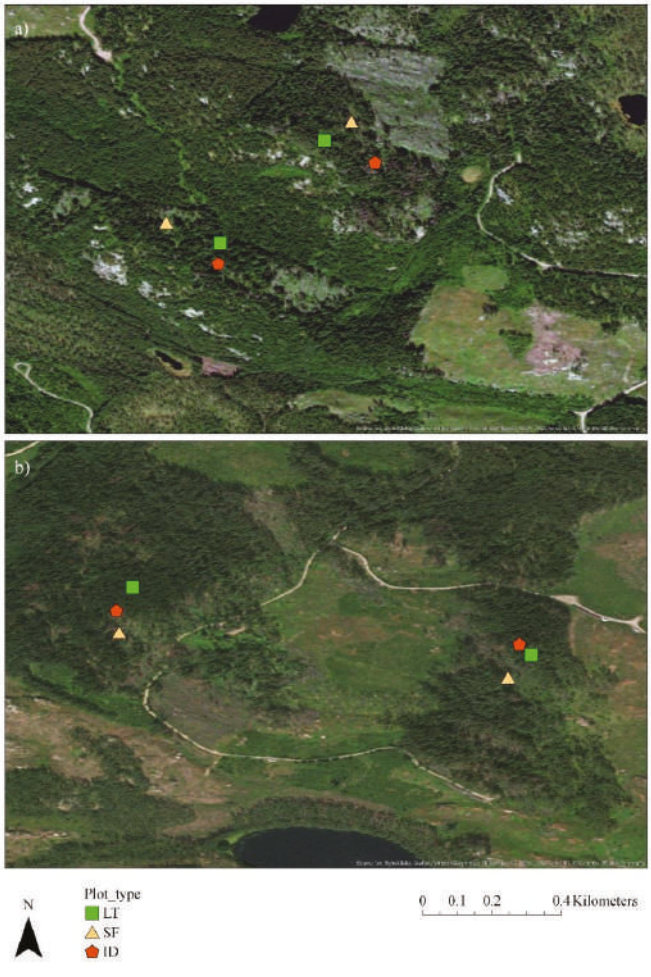

Figure 1. Locations of study plots in Paajasensalo (**a**) where plots established in 2015 are on the left and plots established in 2016 are on the right, and Viitalampi (**b**) where plots established in 2015 are on the right and plots established in 2016 are on the left. LT = living tree plot (green squares), SF = storm-felled tree plot (light brown triangles), and ID = tree killed by *I. typographus* plot (red pentagons). Created using ArcGIS (ESRI, Redlands, CA, USA).

2.3. Tree Measurements

All trees growing on the plots were numbered and the diameter at breast height (dbh) of each living and dead tree, both standing and fallen, with a dbh of >6 cm was measured. All spruce trees were inspected for symptoms of *I. typographus* colonization (discoloration, defoliation, entrance and exit holes, resin flow spots, and bark loss) [46] to confirm the initial cause of each spruce tree's death as *I. typographus* and to monitor the population level of the living trees during the study. Although some spruce trees on the LT plots showed incipient symptoms caused by *I. typographus*, they remained living and vigorous during the study period. We are not able to identify the specific time of death of the *I. typographus*-killed trees in our plots, but it took place during 2013–2014 [47]. In addition to the storm in July 2010, the warm summers of 2010, 2011, and 2013 [48] likely contributed to the development of the *I. typographus* outbreak. The two disturbance types also interacted on some of the

plots. For example, 50% of the standing dead trees on the Viitalampi ID plot established in 2015 broke and fell due to another storm in October 2015. On the other plots, however, only single standing dead trees and none of the living trees fell during the study period. In addition, many of the wind-thrown trees on the SF plots had maternal galleries of *I. typographus*. However, the initial cause of tree death on SF plots was the storm in 2010 and the beetle outbreak on the ID plots that occurred from 2011 onwards. Some dead trees were also found at the LT plots, but they had already died before the 2010 storm and start of the beetle outbreak.

2.4. Soil Surface Respiration, Temperature, and Moisture Measurements

Soil surface respiration, soil temperature, and soil moisture were measured at a number of locations in each plot. For the LT and ID plots, the location of the sampling point was based on a random selection of the numbered trees. A stone-free sampling area ≥2 m from the randomly selected tree stem (or other measurement point) was selected. In the case of the SF plots, all fallen tree(s)–detritus-covered microsites (SF_d) and ground vegetated–open (i.e., no fallen trees above) microsites (SF_o) were identified and numbered, and then a set of each microsite type was chosen using a random number sequence generator. These two types of microsite reflected a clear dichotomy in conditions created by the storm. If a respiration measurement point was considered unsuitable (stony or <1.5 m to another measurement point or tree), it was rejected and the next measurement point in the random sequence was chosen. Accordingly, 30 soil respiration measurement points were established in each study site in summer 2015: eight in the LT plots, seven each in the SF_d and SF_o microsites, and eight in ID plots at each forest (Figure S2). A PVC collar (diameter = 20.1 cm, height ~ 15 cm) for respiration measurements was installed at each selected measurement point by pressing the collar into the ground to a depth of ca. 1 cm and sealed from the outside with sand (Figure 2, Figure S2). At this stage, vegetation was not removed from inside the collars so that SR_{tot} measurements included respiration by soil and ground vegetation. In 2016, collars were installed in the new plots using the same procedure as in 2015: three collars in the LT plots, three in each of the two microsites in the SF plots, and three in ID plots at both study sites.

Figure 2. Soil surface respiration chamber darkened with aluminum foil and containing the CARBOCAP® GMP343 CO_2 probe and a data logger on the ground in front. The measurement point is one of the trenched measurement points. Photo: Maiju Kosunen.

In order to quantify the proportions of SR_a and SR_h, 15 of the measurement points in the plots established in 2015 (4 in LT, 3 or 4 in SF_d and 3 or 4 in SF_o, and 4 in ID selected at random in both study sites) were trenched in July–August 2016. A knife and a spade were used to cut the roots in an area of ca 0.25 m^2 surrounding the selected collars to a depth of ca. 30 cm, the maximum depth of most *P. abies* roots in Finnish conditions [49]. A 30 cm wide strip of strong fabric was then inserted into the cut to inhibit further root ingrowth. After trenching, the ground vegetation was carefully removed from inside the collars. Mosses were, however, left growing in the collars to avoid direct radiation from topsoil, but were not considered to have significantly affected the respiration measurements. Any regrowth of vegetation was removed inside the trenched collars before each measurement.

Trenching may bias soil autotrophic and heterotrophic respiration estimates, for example, because of changes in the soil microclimate brought about by root decease [50]. In our study, trenching, however, had no clear effect on soil moisture and increased the soil temperature only slightly at some plots. Nevertheless, for example, re-sprouting of the clipped vegetation at trenched points in between measurements as well as inclusion of ground vegetation respiration to measurements at intact collars may have also caused inaccuracy to estimations. Thus, the SR_a and SR_h values should only be considered as estimates of the proportions.

The respiration measurements were carried out approximately weekly during 18 Jun–6 Oct 2015 and 24 May–27 Sept 2016 and approximately biweekly during 16 May–19 Oct 2017 (intervals varying from 4 to 18 days) using a closed and darkened chamber (D = 19.0 cm, height = 24.7 cm) made of Perspex fitted with a CARBOCAP®GMP343 CO_2 probe (Vaisala Ltd., Vantaa, Finland) and an air mixing fan (Figure 2). After carefully placing the chamber on top of the collar, the increase in the CO_2 concentration inside the chamber was recorded every 5 seconds over a 5 minute period. The lower edge of the chamber was fitted with a rubber O-ring washer so as to prevent any airflow between the collar and chamber. The air in the chamber was mixed during each measurement by means of a small fan fitted inside the chamber. Between each measurement, the chamber was ventilated by exposing the chamber to the air. Immediately following the respiration measurements, soil temperature and moisture were measured at three spots around each collar (ca. 0.2 m distance from the collar). Soil temperature (°C) was measured at a depth of 10.5 cm using a S3 11B thermometer (Fluke corp., Everett, WA, USA) probe and the soil moisture (% vol) was measured at a depth of 6.0 cm with a ML3 ThetaKit soil moisture meter (Delta-T devices Ltd., Cambridge, UK).

2.5. Calculation of Soil Surface Total, Heterotrophic, and Autotrophic Respiration

Respiration (mg CO_2 m^{-2} s^{-1}) was calculated as the slope of the linear regression between CO_2 concentration in the chamber and time. Respiration measurements from the intact (non-trenched) collars (n = 30 in both Paajasensalo and Viitalampi until Aug 2016, after which n = 27) in both study sites over the whole study period in 2015–2017 were taken to be SR_{tot}. Respiration measured from the trenched collars (n = 15 in both Paajasensalo and 15 in Viitalampi) was considered to be SR_h, and the difference between SR_{tot} and SR_h was therefore assumed to be SR_a.

However, as we observed a difference in the mean SR_{tot} values between the intact collars and the collars to be trenched already before the trenching for some plots, we used linear regression to estimate the SR_{tot} values for the trenched collars in order to correct for this baseline difference. Thus, for each plot established in 2015, a linear regression model was computed using pre-trench data (up to June 2016) to predict the SR_{tot} of the collars to be trenched from that of the collars that would remain intact. These regression models were then used to derive post-trenching SR_{tot} values for the trenched collars as if they had not been trenched. All regression models had high R^2 values (0.73–0.96). The difference between the predicted mean SR_{tot} values and the measured mean values from the trenched collars (SR_h) was then taken to be SR_a. Values of SR_a were thus weekly treatment means, including one value that was negative. The SR_h values were individual collar measurements; however, weekly treatment means of SR_h for each plot were used to compare with SR_a values.

The disturbance caused by root cutting and fast decay could be expected to keep the levels of respiration high for some time after trenching. In our treatments, respiration of the trenched collars in comparison to the intact collars decreased mostly 1–3 weeks (but ca. 2 months at the latest) after the root cutting; therefore, only the respiration measurements starting from 2017 were used to estimate the proportions of SR_a and SR_h.

2.6. Statistical Analyses

For comparing SR_{tot} and SR_h (measured and temperature-adjusted), temperature, and moisture between treatments, analyses of variance (ANOVA) with a linear mixed-effects model structure followed by Scheffe's post hoc tests were used. Treatment (LT, SF_o, SF_d, and ID) was set as a fixed variable, and measurement date (running number of days cumulated over the study period) and collar number were set as random crossed variables. If the produced linear mixed model did not fulfil the assumptions of normality and homogeneity of residuals, appropriate transformations were applied. Because there was only one value for SR_a at each treatment for each measurement day in 2017, it was not appropriate to test for differences in SR_a between treatments.

To control for the effect of treatment differences in soil temperature on respiration, each measured SR_{tot} and SR_h value was adjusted to a soil temperature value of 10 °C. This was done by fitting a nonlinear regression [51] between soil temperature and respiration for each collar separately. The adjusted flux at a soil temperature at 10 °C was then calculated by adding the estimated value of respiration at 10 °C of each collar to the residual of each measurement.

Spearman's rank correlation coefficients were computed to describe the relationship between the plot (n = 16) mean SR_{tot} (measured and temperature-adjusted), soil temperature and soil moisture, and plot basal area (living, dead, and total), i.e., across treatments. Basal area values of the entire SF plots were used for both SF_d and SF_o microsites. Spearman's rank correlation coefficients were also computed to describe the relationship between plot (n = 8) mean SR_a and SR_h and plot basal area, i.e., across treatments.

All the analyses were done using the R statistical computing environment [52] with utilization of *lme4* [53] for the mixed modeling, *car* [54] for ANOVA, and *emmeans* [55] for the post hoc tests.

3. Results

3.1. Tree Mortality

The characteristics of the stands on each plot are shown in Table 1. Spruce was the dominant species, although several plots also had a considerable proportion of pine (*Pinus sylvestris* L.) and broadleaved trees (mostly silver birch, *Betula Pendula* Roth) present. An exception was the Viitalampi LT plot established in 2016, where only 45% of the trees were spruce; however, 59% of the living trees on that plot were spruce. The Viitalampi ID plot established in 2016 had the highest stem density, and the Viitalampi SF plot established in 2015 had the lowest, with all being dead. Of the disturbed plots (SF and ID), the greatest proportion of dead trees was in the Viitalampi SF plot established in 2015 (100%) and the lowest was in the Viitalampi ID plot established in 2015 (69%). The proportion of dead trees on the LT plots varied between 8% and 27%.

Table 1. Study plot disturbance and stand characteristics (mean ± standard deviation). Abbreviations: Year = year of plot establishment, dbh = tree diameter at breast height, Stems/ha = number of trees per hectare, Basal area = basal area of trees, Species (%) = percentage of basal area of certain tree species from all measured trees on plot, Sp = spruce, Pi = pine, De = deciduous, PS = Paajasensalo, VL = Viitalampi, LT = living trees, ID = trees killed by *I. typographus*, SF = storm-felled trees, MT = medium-rich Myrtillus type, OMT = Oxalis-Myrtillus type.

						Basal Area (m^2/ha)			Species (%)		
Site	**Year**	**Plot Type**	**Site Type**	**dbh (cm)**	**Stems/ha**	**Living**	**Dead**	**Total**	**Sp**	**Pi**	**De**
PS	2015	LT	MT	21 ± 8	1350	42.2 ± 0.6	9.3 ± 1.4	51.5 ± 0.8	65	22	13
PS	2015	SF	MT	22 ± 7	925	13.6 ± 0.7	24.6 ± 0.6	38.2 ± 0.7	81	14	5
PS	2015	ID	OMT	25 ± 8	625	5.5 ± 1.2	27.4 ± 0.7	33.0 ± 0.8	96	0	4
PS	2016	LT	MT	20 ± 10	925	34.3 ± 0.8	0.9 ± 0.2	35.2 ± 0.8	89	0	11
PS	2016	SF	MT	17 ± 7	1725	10.6 ± 0.3	36.8 ± 0.7	47.4 ± 0.6	88	0	12
PS	2016	ID	MT	15 ± 7	1525	2.3 ± 0.3	29.3 ± 0.5	31.7 ± 0.5	100	0	0
VL	2015	LT	MT	21 ± 7	975	35.9 ± 0.4	0.4 ± 0.0	36.3 ± 0.5	97	0	3
VL	2015	SF	MT	25 ± 3	600	0 ± 0.0	28.6 ± 0.3	28.6 ± 0.3	100	0	0
VL	2015	ID	MT	24 ± 4	650	9.8 ± 0.4	20.1 ± 0.3	30.0 ± 0.3	100	0	0
VL	2016	LT	MT	20 ± 10	1275	39.8 ± 0.8	9.5 ± 1.0	49.2 ± 0.9	45	4	51
VL	2016	SF	MT	19 ± 9	800	0.7 ± 0.1	26 ± 0.8	26.7 ± 0.8	63	0	38
VL	2016	ID	OMT	19 ± 9	1800	22.8 ± 0.7	39.7 ± 0.7	62.5 ± 0.7	96	0	4

3.2. Soil Surface Total Respiration, Soil Temperature, and Soil Moisture

At Paajasensalo, the mean SR_{tot} of the three disturbed treatments was lower than that of the LT treatment, although only significantly so in the case of the SF_o treatment (Table 2). At Viitalampi, the disturbed treatment mean SR_{tot} was also lower than that of the LT treatment, but none of the differences were significant. After adjusting SR_{tot} for soil temperature, the differences in mean values between treatments were reduced, but LT and SF_o still significantly differed from each other at Paajasensalo (Table 2). Adjusting the respiration values for soil temperature did not change the pattern in SR_{tot} among the treatments at Viitalampi.

Table 2. Treatment mean total soil surface respiration (SR_{tot}) and soil-temperature-adjusted soil surface total respiration values ($SR_{tot\_ST\ adj.}$), soil temperature (ST) and soil moisture (SM; non-trenched collars 2015–2017 data only), and heterotrophic soil respiration (SR_h) and soil-temperature-adjusted heterotrophic soil respiration (SR_{tot_STadj}; 2017 data from trenched collars only) for the Paajasensalo and Viitalampi study sites. Values are linear mixed-effects model adjusted means. Treatment means followed by the same subscript letter are not significantly different (p = 0.05; Scheffe's post hoc tests). LT = living trees, SF_d = storm damaged, tree detritus, SF_o = storm damaged, open-vegetated, ID = trees killed by *I. typographus*.

	LT		**SF_d**		**SF_o**		**ID**	
Paajasensalo								
SR_{tot} (mg CO_2 m^{-2} s^{-1})	0.28	a	0.23	ab	0.18	b	0.22	ab
$SR_{tot\_STadj.}$ (mg CO_2 m^{-2} s^{-1})	0.24	a	0.22	ab	0.17	b	0.20	ab
ST (°C)	10.7	a	10.2	b	10.2	b	10.5	ab
SM (% vol/vol)	13.3	a	18.3	b	22.8	bc	26.0	c
SR_h (mg CO_2 m^{-2} s^{-1})	0.14	a	0.13	ab	0.10	b	0.12	ab
$SRh_{\_STadj.}$ (mg CO_2 m^{-2} s^{-1})	0.15	a	0.15	a	0.12	a	0.13	a
Viitalampi								
SR_{tot} (mg CO_2 m^{-2} s^{-1})	0.22	a	0.18	a	0.21	a	0.20	a
$SR_{tot\_STadj.}$ (mg CO_2 m^{-2} s^{-1})	0.20	a	0.17	a	0.19	a	0.17	a
ST (°C)	10.5	a	10.3	a	10.6	a	11.0	b
SM (% vol/vol)	20.1	a	26.1	a	26.3	a	26.3	a
SR_h (mg CO_2 m^{-2} s^{-1})	0.11	a	0.14	a	0.12	a	0.11	a
$SRh_{\_STadj.}$ (mg CO_2 m^{-2} s^{-1})	0.12	a	0.15	a	0.12	a	0.11	a

Mean soil temperatures were slightly lower, but significantly so only at SF_d and SF_o for the disturbed treatments compared to the LT treatment at Paajasensalo (Table 2). At Viitalampi, mean soil temperatures were significantly highest in the case of the ID treatment. The mean soil moisture content at Paajasensalo was significantly higher for the three disturbed treatments compared to the LT treatment. At Viitalampi, the disturbed treatment mean soil moisture was also higher than the LT treatment mean value, but not significantly so (Table 2). The mean SR_{tot}, temperature, and moisture of plots established in 2015 and 2016 as well as those of the to-be-trenched and intact collars are presented in Table S1.

The seasonal patterns in SR_{tot}, soil temperature, and soil moisture contents for the three study years are shown in Figure 3. At Paajansensalo, the LT treatment had higher SR_{tot} values compared to the disturbed treatments during the mid-summer to autumn months, whereas the differences between treatments were not that visible in the early summer periods (Figure 3a). At Viitalampi, no clear differences in the seasonal pattern of SR_{tot} among the treatments were observed (Figure 3b). However, at both Paajasensalo and Viitalampi, SR_{tot} followed the seasonal pattern in soil temperature (Figure 3c,d). The seasonal pattern in soil moisture in each year was similar at both Paajasensalo and Viitalampi. At Paajasensalo, soil moisture was consistently the highest in the ID treatment and lowest in the LT treatment throughout each year (Figure 3e). While the treatment differences in soil moisture at Viitalampi during 2015 were similar to those at Paajasensalo, the differences evened out during 2016 and 2017 (Figure 3f).

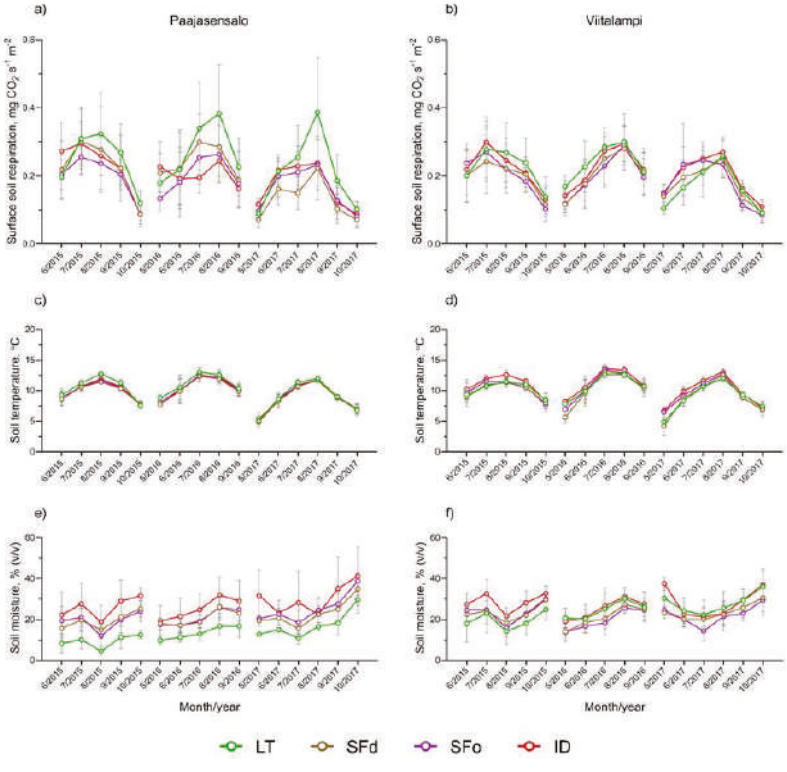

Figure 3. Monthly means and standard deviations for soil surface total respiration (**a,b**), soil temperature (**c,d**), and soil moisture (**e,f**) of each treatment in Paajasensalo (left) and Viitalampi (right). Values are based on measurements from the intact collars on plots established in 2015, i.e., the data set is consistent throughout 2015–2017. LT = living trees, SF_d = storm dead tree detritus, SF_o = storm open-vegetated, and ID = trees killed by *I. typographus*.

3.3. Heterotrophic and Autotrophic Soil Respiration

At Paajasensalo, the mean SR_a values from the disturbed plots were 23% (SF_d), 39% (SF_o), and 57% (ID) of the mean value from LT. At Viitalampi, the mean SR_a value from the SF_d treatment was 45% of the mean value in LT, whereas the mean values from the SF_o microsite and ID plot were 195% and 124%, respectively, of the mean value of LT. The mean SR_h at Paajansensalo was lowest in SF_o (70% of the mean in LT) (Figure 4) and differed significantly from LT. The respective soil-temperature-adjusted mean respiration values, however, did not differ significantly from each other (Table 2). At Viitalampi, the highest mean SR_h was found in SF_d (124% of mean in LT), but the mean did not differ significantly from those of other treatments (Table 2).

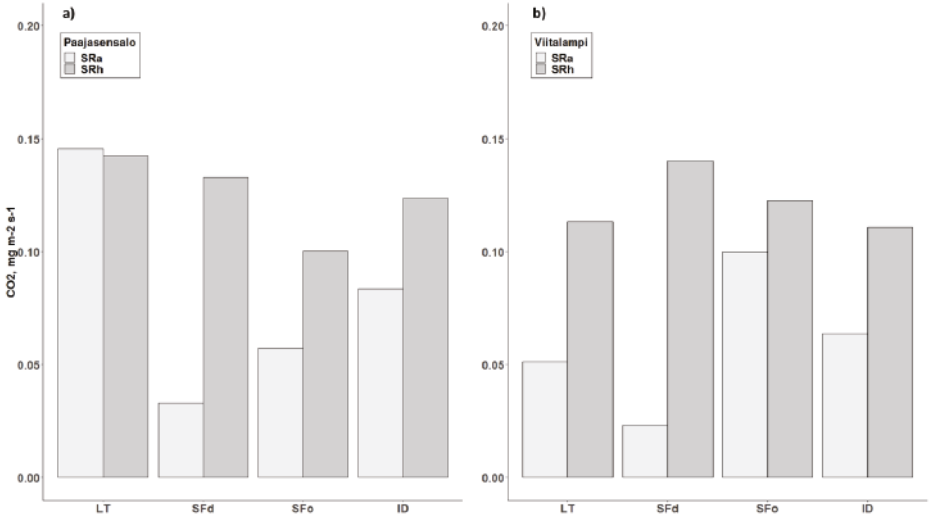

Figure 4. Means of autotrophic (SR_a) and heterotrophic (SR_h) soil surface respiration, based on the measurements in May–Sept 2017, of each treatment (one weekly mean value per treatment) in plots established in 2015 for (**a**) Paajasensalo and (**b**) Viitalampi. LT = living trees, SF_d = storm dead tree detritus, SF_o = storm open-vegetated, ID = trees killed by *I. typographus*.

The proportion of SR_a relative to SR_{tot} at Paajasensalo was 51% for LT, 20% for SF_d, 36% for SF_o, and 40% for ID treatment. The corresponding proportions at Viitalampi were 31% for LT, 14% for SF_d, 45% for SF_o, and 36% for ID. This resulted in a shift in SR_{tot} towards SR_h at disturbed plots with exception of the SF_o microsite and ID plot in Viitalampi, where the proportions of SR_a were higher than at the LT plot.

3.4. Relationships between Variables

Combining data from both sites, the plot mean (treatment mean in SF) SR_{tot} was significantly and positively correlated with the basal area of living trees (Table 3). SR_a or SR_h, however, were not significantly correlated with the basal area of living trees or that of all trees. Neither did soil temperature correlate with the tree stand variables, but soil moisture showed a significant negative correlation with both basal areas of living and all trees (Table 3). Using soil-temperature-adjusted SR_{tot} values for correlations did lower the correlations. Across both sites, treatment and plot mean soil temperature also showed a significant positive correlation with soil total respiration (Table 3), as it did inside each treatment (Table S2). Mean soil moisture, on the contrary, showed significant negative correlations with SR_{tot} and SR_h across both sites and treatments (Table 3) but showed weaker correlations inside each treatment (Table S2).

Table 3. Spearman's correlation coefficients between various plot mean soil surface respiration and soil temperature, soil moisture, and stand basal area. BA_L = living, BA_D = dead, and BA_{tot} = all trees, ST = soil temperature, SM = soil moisture, SR_{tot} = soil surface total respiration, $SR_{tot\_STadj.}$ = temperature-adjusted soil surface total respiration (Aug–Oct 2016 and May–Oct 2017 data, n = 16). SR_a = autotrophic respiration, SR_h = measured, and $SR_{h\_STadj.}$ = soil-temperature-adjusted heterotrophic respiration (May–Oct 2017 data, n = 8).

	BA_L	BA_D	BA_{tot}	ST	SM
SR_{tot}	0.55 *	−0.41	0.40	0.54 *	−0.67 **
$SR_{tot\_STadj.}$	0.43	−0.36	0.31	-	−0.69 **
SR_a	0.14	−0.12	0.17	-	-
SR_h	0.02	0.17	0.12	−0.29	−0.83 *
$SR_{h\_STadj.}$	0.16	0.13	0.33	-	−0.88 **
ST	0.17	−0.18	−0.01	-	−0.13
SM	−0.56 *	0.25	−0.59 **	−0.13	-

* = $p < 0.05$ and ** = $p < 0.01$.

4. Discussion

4.1. Soil Surface Total, Autotrophic, and Heterotrophic Respiration

We hypothesized that the loss of living trees (roots) resulting from storm damage (5–7 years ago) and *I. typographus* infestation (tree mortality circa 2–4 years ago) would result in reduced SR_a, while the death of trees and roots would increase the amount of surface organic debris and soil organic matter available for microbial decomposition and hence increase SR_h. Our results went some way to supporting this hypothesis. Thus, SR_a at both the *I. typographus*-infested and storm-damaged plots was lower than at the living tree plot in Paajasensalo, and the same was true for the storm-damaged SF_d microsite, but not for the storm-damaged SF_o microsite and *I. typographus*-infested plot, at Viitalampi. Furthermore, the lower SR_a/SR_{tot} ratios of the disturbed plots compared to the living tree plots supported the hypothesis that disturbance results in a shift in total respiration away from SR_a towards SR_h at Paajasensalo, but not at Viitalampi. Although significant differences in SR_h were only found between the SF_o and LT treatments in Paajasensalo, the values at disturbed treatments were mainly lower in Paajasensalo and higher in Viitalampi in comparison to LT. As a result of these patterns in SR_a and SR_h, significant differences (lower) in SR_{tot} compared to living tree plots were only associated with the storm-damaged open microsites at Paajasensalo.

The higher-than-expected level of SR_a at the Viitalampi SF_o microsite and ID plot might have been due to a response of ground vegetation cover and/or the remaining living trees to changes brought about by the tree mortality. As the ground vegetation at the Viitalampi SF_o microsite was observed to be more developed than at the other plots, the higher-than-expected SR_a value was however probably due to the inclusion of the associated autotrophic respiration. The ID plot was also damaged by a storm which broke and felled 50% of the beetle-killed standing dead trees, resulting in increased light to the forest floor and subsequent development of the ground vegetation, which is typical especially after wind disturbance [27]. The effect of developing ground vegetation after disturbance (bark beetle, storm and clearance) has been implicated in increased autotrophic soil respiration observed in a study carried out in Norway spruce stands in Austria [50]. In addition, the productivity of the remaining living trees at the ID plot may have been stimulated by an increase in light, water, and nutrient availability after the death of surrounding trees by *I. typographus*, as was shown in a study on mountain pine beetle (*Dendroctonus ponderosae* Hopkins) attack on lodgepole pine stands in British Columbia [8], and resulted in increased SR_a. Also, seedlings which were growing at all plot types may have contributed to some extent to the SR_a at the disturbed treatment plots. However, rather than stimulating growth, mechanical damage to the remaining living trees caused by the storm-felled trees may have hampered their growth [56], resulting in the lower SR_a in SF_d plot compared to the ID plot at Paajasensalo. That

there was still relatively high SR_a in the SF_d microsite in Viitalampi in spite of there being no living mature trees, may be because some of the respiration measurement points also had living ground vegetation, which would have contributed to the SR_a component.

That the difference in SR_h rates between treatments was weaker than expected may be related to the length of time since tree mortality. Following tree mortality, the C/N and lignin/N ratios of the needle litter decrease [20,22], while litterfall [21] and the mortality of fine roots and ectomycorrhizal fungi [19,57] increase, all of which could potentially stimulate decomposition and SR_h. With time after disturbance, the more easily decomposable compounds would be utilized, leaving more recalcitrant debris and lowering the rate of decomposition [24]. The SR_h rates at our disturbed plots may thus have been considerably higher in the first weeks, or even years, following the death of the trees, i.e., before our measurements started. Nevertheless, small branches and twigs on the SF_d microsites were probably a sufficiently good substrate for decomposition, keeping SR_h rates relatively high even seven years after the storm. However, such an effect could be expected to be less visible in the case of managed forests where trees are cleared away after disturbance. Increasing ground vegetation growth accompanied with lowering heterotrophic respiration can considerably mitigate C emissions already three to six years after storm and beetle disturbance and clearing of damaged trees [50]. In our study, the higher SR_a at the SF_o microsite in comparison to LT at Viitalampi and lower (although not significantly) SR_h at SF_o microsite in comparison to SF_d at both sites could indicate such a pattern. However, we have no data to support this possibl effect.

On a larger spatial scale with greater variability in tree mortality, forest structure and composition, and disturbance-created microhabitats, different or more notable effects in soil surface respiration after the two disturbance types could possibly be found. Although our disturbed study plots on average had a similar dead tree basal area, storm- and *I. typographus*-induced tree mortality patterns across the study forests were rather heterogeneous, varying from individual to stand-level tree decease. Noteworthy also is that at our sites, trees were not cleared away after the events, which would be expected to lead to differing response and recovery patterns of C balance compared to managed forests, due to differences in, e.g., litter quantity, incoming radiation, and ground vegetation changes [13,27].

4.2. Relationships between Basal Area, Soil Microclimate, and Respiration

Although we hypothesized that respiration would be related to the amount of dead tree biomass resulting from the disturbances, SR_{tot} was more strongly correlated to the basal area of living trees than to that of the dead trees. The weaker correlations with dead tree basal area are probably because much of the dead fine root biomass, needles, and small branch detritus that decompose much faster than the bigger tree parts [58,59] had already decomposed by the time of our respiration measurements. Also, since detritus for decomposition is also supplied by the living trees, SR_h cannot be attributed to dead trees only; therefore, correlations with basal area likely were relatively weak.

As we had hypothesized, soil temperature and moisture conditions differed among the treatments. The higher soil moisture contents in the disturbed plots compared to the living tree plots in Paajasensalo are likely related to a reduction in transpiration resulting from tree mortality. The effect of tree mortality on transpiration and soil moisture contents was also clearly indicated by a significant negative correlation between soil moisture content and living tree basal area. However, in Viitalampi, the diminishing soil moisture differences between treatments during the study period may be related to the dense herbaceous ground vegetation further developing during the study and potentially enhanced tree growth taking up moisture from the soil. Soil temperature did not differ so clearly between treatments as moisture, but the higher soil temperatures recorded in Viitalampi ID treatment compared to other treatments may be explained by an increase in light (radiation) conditions brought about by the storm felling of dead trees, as discussed earlier.

To assess the extent to which soil surface respiration were determined more by soil temperature than by plant metabolism and the supply of detritus (living and dead basal area), we examined temperature-adjusted respiration values. However, adjusting respiration for temperature had little

effect on the treatment mean respiration rates, indicating that treatment differences in soil surface respiration were determined more by differences in plant metabolism and the supply of detritus than by differences in soil temperature per se.

Collar-wise correlations between soil moisture and SR_{tot} were generally poor, which is why we were not able to examine the effect of soil moisture on respiration differences between treatments. There were, however, clear differences in mean soil moisture contents between treatments, and plot-wise mean SR_{tot} and SR_h rates were strongly and significantly correlated to plot mean soil moisture contents, indicating that disturbance-driven effects on soil surface respiration are related to changes in soil moisture conditions. However, as basal area and soil moisture were also strongly correlated, it is not possible to determine whether differences in respiration were due to differences in basal area or soil moisture.

5. Conclusions

We found no consistent effect of either storm or *I. typographus* disturbances (tree mortality) on SR_{tot} and SR_h. However, SR_a was lower and SR_{tot} rates showed a shift towards a greater proportion of SR_h in the disturbed forest areas, except at the SF_o microsite and ID plot at Viitalampi, where SR_a was higher than expected. These higher-than-expected SR_a values may have been related to the development of ground vegetation and growth stimulation of remaining living trees. Soil surface respiration was found to be related to basal area (living trees) and soil moisture and temperature conditions, factors which would further relate to plant metabolism, the supply and availability of organic matter for decomposition, forest floor light (radiation) conditions, and stand transpiration.

Despite the mainly similar effects of the two disturbances on soil C dynamics found in this study, the influence of the disturbances on tree mortality patterns, stand structure and composition, and created microsites differs over larger areas. Since storm and bark beetle disturbances are predicted to become more common in the future, their effects on forest C dynamics may become even more complex and considerable. Therefore, for future research, studies concentrating on several disturbances and their effects on forest C fluxes and C balance at greater spatial and temporal scales would be important in order to clarify and estimate the potential effects of disturbances on forest C dynamics.

Supplementary Materials: The following are available online at http://www.mdpi.com/1999-4907/10/4/307/s1, Figure S1: Example photos of plot types, Figure S2: Example photos of soil surface respiration measurement points, Table S1: Mean soil surface respiration, temperature and moisture of each treatment at each plot separately, Table S2: Correlation coefficients between soil surface total and heterotrophic respiration, temperature and moisture.

Author Contributions: Conceptualization, M.K., P.L.-S., M.B. and M.S.; Data curation, M.K. and M.B.; Formal analysis, M.K.; Funding acquisition, M.K., P.L.-S. and M.S.; Investigation, M.K., P.O. and M.S.; Methodology, M.K., P.L.-S., P.O. and M.S.; Project administration, M.K. and M.S.; Resources, M.K.; Software, M.K.; Supervision, P.L.-S., P.O. and M.S.; Visualization, M.K. and M.S.; Writing—original draft, M.K.; Writing—review and editing, P.L.-S., P.O., M.B. and M.S.

Funding: This research was funded by AGFOREE Doctoral Programme, Finnish Cultural Foundation—South-Karelia Regional Fund, Nessling Foundation, Niemi Foundation and Societas pro Fauna et Flora Fennica.

Acknowledgments: We wish to thank Pentti Henttonen, Eetu Hirvonen, Risto Tanninen and Jaana Turunen for irreplaceable help with field work. Tuula Kantola, Kajar Köster and Jukka Pumpanen we acknowledge for their valuable advice in relation to the study design and field measurements. Stora Enso and Tornator Ltd, especially Jarmo Hakalisto and Maarit Sallinen, we thank for enabling this study to be carried out in the Viitalampi and Paajasensalo forests.

Conflicts of Interest: The authors declare no conflict of interest.

References

1. Mitchell, S.J. Wind as a natural disturbance agent in forests: A synthesis. *Forestry* **2013**, *86*, 147–157. [CrossRef]
2. Edburg, S.L.; Hicke, J.A.; Brooks, P.D.; Pendall, E.G.; Brent, E.; Norton, U.; Gochis, D.; Gutmann, E.D.; Meddens, A.J.H.; Edburg, S.L.; et al. Cascading impacts of bark beetle-c mortality on coupled biogeophysic biogeochemical processes. *Front. Ecol. Environ.* **2012**, *10*, 416–424. [CrossRef]

3. Knohl, A. Carbon exchange of a Russian boreal forest after windthrow Carbon dioxide exchange of a Russian boreal forest after disturbance by wind throw. *Glob. Chang. Biol.* **2002**, *8*, 231–246. [CrossRef]
4. Kurz, W.A.; Dymond, C.C.; Stinson, G.; Rampley, G.J.; Neilson, E.T.; Carroll, A.L.; Ebata, T.; Safranyik, L. Mountain pine beetle and forest carbon feedback to climate change. *Nature* **2008**, *452*, 987–990. [CrossRef]
5. Hicke, J.A.; Allen, C.D.; Desai, A.R.; Dietze, M.C.; Hall, R.J.; Hogg, E.H.T.; Kashian, D.M.; Moore, D.; Raffa, K.F.; Sturrock, R.N.; et al. Effects of biotic disturbances on forest carbon cycling in\r\nthe United States and Canada. *Glob. Chang. Biol.* **2012**, *18*, 7–34. [CrossRef]
6. Mayer, M.; Sandén, H.; Rewald, B.; Godbold, D.L.; Katzensteiner, K. Increase in heterotrophic soil respiration by temperature drives decline in soil organic carbon stocks after forest windthrow in a mountainous ecosystem. *Funct. Ecol.* **2017**, *31*, 1163–1172. [CrossRef]
7. Lindroth, A.; Lagergren, F.; Grelle, A.; Klemedtsson, L.; Langvall, O.; Weslien, P.; Tuulik, J. Storms can cause Europe-wide reduction in forest carbon sink. *Glob. Chang. Biol.* **2009**, *15*, 346–355. [CrossRef]
8. Brown, M.; Black, T.A.; Nesic, Z.; Foord, V.N.; Spittlehouse, D.L.; Fredeen, A.L.; Grant, N.J.; Burton, P.J.; Trofymow, J.A. Impact of mountain pine beetle on the net ecosystem production of lodgepole pine stands in British Columbia. *Agric. For. Meteorol.* **2010**, *150*, 254–264. [CrossRef]
9. Moore, D.J.P.; Trahan, N.A.; Wilkes, P.; Quaife, T.; Stephens, B.B.; Elder, K.; Desai, A.R.; Negron, J.; Monson, R.K. Persistent reduced ecosystem respiration after insect disturbance in high elevation forests. *Ecol. Lett.* **2013**, *16*, 731–737. [CrossRef]
10. Hicke, J.A.; Meddens, A.J.H.; Allen, C.D.; Kolden, C.A. Carbon stocks of trees killed by bark beetles and wildfire in the western United States. *Environ. Res. Lett.* **2013**, *8*, 035032. [CrossRef]
11. Hansen, E.M.; Amacher, M.C.; Van Miegroet, H.; Long, J.N.; Ryan, M.G. Carbon dynamics in central US Rockies lodgepole pine type after mountain pine beetle outbreaks. *For. Sci.* **2015**, *61*, 665–679. [CrossRef]
12. Reed, D.E.; Ewers, B.E.; Pendall, E. Impact of mountain pine beetle induced mortality on forest carbon and water fluxes. *Environ. Res. Lett.* **2014**, *9*, 105004. [CrossRef]
13. Jonášová, M.; Prach, K. The influence of bark beetles outbreak vs. salvage logging on ground layer vegetation in Central European mountain spruce forests. *Biol. Conserv.* **2008**, *141*, 1525–1535. [CrossRef]
14. Seidl, R.; Rammer, W.; Jäger, D.; Lexer, M.J. Impact of bark beetle (*Ips typographus* L.) disturbance on timber production and carbon sequestration in different management strategies under climate change. *For. Ecol. Manag.* **2008**, *256*, 209–220. [CrossRef]
15. Jonášová, M.; Vávrová, E.; Cudlín, P. Western Carpathian mountain spruce forest after a windthrow: Natural regeneration in cleared and uncleared areas. *For. Ecol. Manag.* **2010**, *259*, 1127–1134. [CrossRef]
16. Schlesinger, W.; Andrews, J. Soil Respiration and Global Carbon Cycle. *Biogeochemistry* **2000**, *48*, 7–20. [CrossRef]
17. Janssens, I.A.; Lankreijer, H.; Matteucci, G.; Kowalski, A.S.; Buchmann, N.; Epron, D.; Pilegaard, K.; Kutsch, W.; Longdoz, B.; Grünwald, T.; et al. Productivity overshadows temperature in determining soil and ecosystem respiration across European forests. *Glob. Chang. Biol.* **2002**, *7*, 269–278. [CrossRef]
18. Bhupinderpal-Singh; Nordgren, A.; Löfvenius Ottosson, M.; Högberg, M.N.; Mellander, P.E.; Högberg, P. Tree root and soil heterotrophic respiration as revealed by girdling of boreal Scots pine forest: Extending observations beyond the first year. *Plant Cell Environ.* **2003**, *26*, 1287–1296. [CrossRef]
19. Högberg, P.; Bhupinderpal-Singh; Löfvenius, M.O.; Nordgren, A. Partitioning of soil respiration into its autotrophic and heterotrophic components by means of tree-girdling in old boreal spruce forest. *For. Ecol. Manag.* **2009**, *257*, 1764–1767.
20. Sariyildiz, T.; Akkuzu, E.; Küçük, M.; Duman, A.; Aksu, Y. Effects of *Ips typographus* (L.) damage on litter quality and decomposition rates of oriental spruce [*Picea orientalis* (L.) Link.] in Hatila Valley National Park, Turkey. *Eur. J. For. Res.* **2008**, *127*, 429–440. [CrossRef]
21. Kopáček, J.; Cudlín, P.; Fluksová, H.; Kaňa, J.; Picek, T.; Šantrůčková, H.; Svoboda, M.; Vaněk, D. Dynamics and composition of litterfall in an unmanaged *Norway spruce* (*Picea abies*) forest after bark-beetle outbreak. *Boreal Environ. Res.* **2015**, *20*, 305–323.
22. Morehouse, K.; Johns, T.; Kaye, J.; Kaye, M. Carbon and nitrogen cycling immediately following bark beetle outbreaks in southwestern ponderosa pine forests. *For. Ecol. Manag.* **2008**, *255*, 2698–2708. [CrossRef]
23. Mayer, M.; Matthews, B.; Schindlbacher, A.; Katzensteiner, K. Soil CO_2 efflux from mountainous windthrow areas: Dynamics over 12 years post-disturbance. *Biogeosciences* **2014**, *11*, 6081–6093. [CrossRef]

24. Šťursová, M.; Šnajdr, J.; Cajthaml, T.; Bárta, J.; Šantrůčková, H.; Baldrian, P. When the forest dies: The response of forest soil fungi to a bark beetle-induced tree dieback. *ISME J.* **2014**, *8*, 1920–1931. [CrossRef]
25. Mikkelson, K.M.; Brouillard, B.M.; Bokman, C.M.; Sharpa, J.O. Ecosystem resilience and limitations revealed by soil bacterial community dynamics in a bark beetle-impacted forest. *MBio* **2017**, *8*, 1–13. [CrossRef]
26. Pec, G.J.; Karst, J.; Taylor, D.L.; Cigan, P.W.; Erbilgin, N.; Cooke, J.E.K.; Simard, S.W.; Cahill, J.F. Change in soil fungal community structure driven by a decline in ectomycorrhizal fungi following a mountain pine beetle (*Dendroctonus ponderosae*) outbreak. *New Phytol.* **2017**, *213*, 864–873. [CrossRef] [PubMed]
27. Fischer, A.; Lindner, M.; Abs, C.; Lasch, P. Vegetation dynamics in central european forest ecosystems (near-natural as well as managed) after storm events. *Folia Geobot.* **2002**, *37*, 17–32. [CrossRef]
28. Zhang, B.; Zhou, X.; Zhou, L.; Ju, R. A global synthesis of below-ground carbon responses to biotic disturbance: A meta-analysis. *Glob. Ecol. Biogeogr.* **2015**, *24*, 126–138. [CrossRef]
29. Kobler, J.; Jandl, R.; Dirnböck, T.; Mirtl, M.; Schindlbacher, A. Effects of stand patchiness due to windthrow and bark beetle abatement measures on soil CO_2 efflux and net ecosystem productivity of a managed temperate mountain forest. *Eur. J. For. Res.* **2015**, *134*, 683–692. [CrossRef]
30. Köster, K.; Püttsepp, Ü.; Pumpanen, J. Comparison of soil CO_2 flux between uncleared and cleared windthrow areas in Estonia and Latvia. *For. Ecol. Manag.* **2011**, *262*, 65–70. [CrossRef]
31. Borkhuu, B.; Peckham, S.D.; Ewers, B.E.; Norton, U.; Pendall, E. Does soil respiration decline following bark beetle induced forest mortality? Evidence from a lodgepole pine forest. *Agric. For. Meteorol.* **2015**, *214–215*, 201–207. [CrossRef]
32. Schelhaas, M.-J.; Nabuurs, G.-J.; Schuck, A. Natural disturbances in the European forests in the 19th and 20th centuries. *Glob. Chang. Biol.* **2003**, *9*, 1620–1633. [CrossRef]
33. Jeger, M.; Bragard, C.; Caffier, D.; Candresse, T.; Chatzivassiliou, E.; Dehnen-Schmutz, K.; Gilioli, G.; Jaques Miret, J.A.; MacLeod, A.; Navajas Navarro, M.; et al. Pest categorisation of *Ips amitinus*. *EFSA J.* **2017**, *15*, 5038.
34. Seidl, R.; Thom, D.; Kautz, M.; Martin-Benito, D.; Peltoniemi, M.; Vacchiano, G.; Wild, J.; Ascoli, D.; Petr, M.; Honkaniemi, J.; et al. Forest disturbances under climate change. *Nat. Clim. Chang.* **2017**, *7*, 395–402. [CrossRef] [PubMed]
35. Seidl, R.; Schelhaas, M.J.; Lexer, M.J. Unraveling the drivers of intensifying forest disturbance regimes in Europe. *Glob. Chang. Biol.* **2011**, *17*, 2842–2852. [CrossRef]
36. Ulanova, N.G. The effects of windthrow on forest at different spatial scales: A review. *For. Ecol. Manag.* **2000**, *135*, 155–167. [CrossRef]
37. Pumpanen, J.; Westman, C.J.; Ilvesniemi, H. Soil CO_2 efflux from a podzolic forest soil before and after forest clear-cutting and site preparation. *Boreal Environ. Res.* **2004**, *9*, 199–212.
38. Müller, K.H.; Wagner, S. Fine root dynamics in gaps of Norway spruce stands in the German Ore Mountains. *Forestry* **2003**, *76*, 149–158. [CrossRef]
39. Gray, A.N.; Spies, T.A.; Easter, M.J. Microclimatic and soil moisture responses to gap formation in coastal Douglas-fir forests. *Can. J. For. Res.* **2002**, *32*, 332–343. [CrossRef]
40. Wermelinger, B. Ecology and management of the spruce bark beetle Ips typographus—A review of recent research. *For. Ecol. Manag.* **2004**, *202*, 67–82. [CrossRef]
41. Eriksson, M.; Pouttu, A.; Roininen, H. The influence of windthrow area and timber characteristics on colonization of wind-felled spruces by *Ips typographus* (L.). *For. Ecol. Manag.* **2005**, *216*, 105–116. [CrossRef]
42. Mikola, P. Application of vegetation science to forestry in Finland. In *Handbook of Vegetation Science, Part 12*; Jahn, G., Ed.; Dr W. Junk Publishers: The Hague, The Netherlands; Boston, MA, USA; London, UK, 1982; pp. 199–224.
43. Pirinen, P.; Simola, H.; Aalto, J.; Kaukoranta, J.-P.; Karlsson, P.; Ruuhela, R. *CLIMATOLOGICAL statistics of Finland 1981–2010*; Reports 2012-1; Finnish Meteorological Institute: Helsinki, Finland, 2012.
44. Finnish Meteorological Institute. Open Source Weather Observations. Available online: https://en.ilmatieteenlaitos.fi/download-observations#!/ (accessed on 19 October 2018).
45. Hurlbert, S.H. Pseudoreplication and the Design of Ecological Field Experiments. *Ecol. Monogr.* **1984**, *54*, 187–211. [CrossRef]
46. Blomqvist, M.; Kosunen, M.; Starr, M.; Kantola, T.; Holopainen, M.; Lyytikäinen-Saarenmaa, P. Modelling the predisposition of Norway spruce to *Ips typographus* L. infestation by means of environmental factors in southern Finland. *Eur. J. For. Res.* **2018**, *137*, 675–691. [CrossRef]

47. Lyytikäinen-Saarenmaa, P.; (Department of Forest Sciences, University of Helsinki). Personal communication, 2014.
48. Finnish Meteorological Institute. Annual Weather Statistics. Available online: https://ilmatieteenlaitos.fi/vuositilastot (accessed on 3 January 2019).
49. Helmisaari, H.-S.; Derome, J.; Nojd, P.; Kukkola, M. Fine root biomass in relation to site and stand characteristics in Norway spruce and Scots pine stands. *Tree Physiol.* **2007**, *27*, 1493–1504. [CrossRef]
50. Zehetgruber, B.; Kobler, J.; Dirnböck, T.; Jandl, R.; Seidl, R.; Schindlbacher, A. Intensive ground vegetation growth mitigates the carbon loss after forest disturbance. *Plant Soil* **2017**, *420*, 239–252. [CrossRef] [PubMed]
51. Lloyd, J.; Taylor, J. On the Temperature Dependence of Soil Respiration. *Funct. Ecol.* **1994**, *8*, 315–323. [CrossRef]
52. R Core Team. *R: A Language and Environment for Statistical Computing*; R Foundation for Statistical Computing: Vienna, Austria, 2018.
53. Bates, D.; Maechler, M.; Bolker, B.; Walker, S. Fitting Linear Mixed-Effects Models Using lme4. *J. Stat. Softw.* **2015**, *67*, 1–48. [CrossRef]
54. Fox, J.; Weisberg, S. *An {R} Companion to Applied Regression*, 2nd ed.; Sage: Thousand Oaks, CA, USA, 2011.
55. Lenth, R. *Emmeans: Estimated Marginal Means, aka Least-Squares Means*; R Core Team: Vienna, Austria, 2018.
56. Seidl, R.; Blennow, K. Pervasive Growth Reduction in Norway Spruce Forests following Wind Disturbance. *PLoS ONE* **2012**, *3*, e33301. [CrossRef]
57. Högberg, M.N.; Högberg, P.; Högberg, M.N. Extramatrical ectomycorrhizal mycelium contributes one-third of microbial biomass and produces, together with associated roots, half the dissolved organic carbon in a forest soil. *New Phytol.* **2002**, 791–795. [CrossRef]
58. Lõhmus, K.; Ivask, M. Decomposition and nitrogen dynamics of fine roots of Norway spruce (*Picea abies* (L.) Karst.) at different sites. *Plant Soil* **1995**, *168*, 89–94. [CrossRef]
59. Hyvonen, R.; Olsson, B.A.; Lundkvist, H.; Staaf, H. Decomposition and nutrient release from *Picea abies* (L.) Karst. and *Pinus sylvestris* L. logging residues. *For. Ecol. Manag.* **2000**, *126*, 97–112. [CrossRef]

forests

MDPI

Article

CO_2 Transfer Characteristics of Calcareous Humid Subtropical Forest Soils and Associated Contributions to Carbon Source and Sink in Guilin, Southwest China

Fen Huang [1,2], Jianhua Cao [1,2,*], Tongbin Zhu [1,2], Mingzhu Fan [1,2] and Mengmeng Ren [1,3]

1 Key Laboratory of Karst Dynamics, Institute of Karst Geology (CAGS), Ministry of Natural Resourses (MNR) and Guangxi, Guilin 541004, China; hfen@karst.ac.cn (F.H.); zhutongbin@gmail.com (T.Z.); fanmingzhu3071@163.com (M.F.); luckdevin@163.com (M.R.)

2 International Research Center on Karst, Under the Auspices of United Nations Educational, Scientific and Cultural Organization (UNESCO), Guilin 541004, China

3 School of Water Resources and Environment, China University of Geosciences (Beijing), Beijing 100083, China

* Correspondence: jhcaogl@163.com; Tel.: +86-773-779-6626

Received: 4 January 2020; Accepted: 11 February 2020; Published: 14 February 2020

Abstract: In karst landscapes, soil CO_2 is a key factor in weathering processes and carbon cycling, where its distribution and migration characteristics directly affect fluxes in carbon source–sink dynamics. We measured the CO_2 emission and dissolution rates of carbonate tablets in calcareous soil developed from limestone and red soil developed from clastic rock, in karst and non-karst subtropical forests, in Guilin, southwest China between 2015 and 2018, to analyze their CO_2 transfer characteristics and source–sink effects. The results showed similar average soil respiration rates between calcareous soil and red soil, with an average CO_2 emission flux of 1305 and 1167 t C km^{-2} a^{-1}, respectively. Carbonate tablet dissolution rates were bidirectional with increasing depth and were greater in red soil than calcareous soil, averaging 13.88 ± 5.42 and 7.20 ± 2.11 mg cm^{-2} a^{-1}, respectively. CO_2 concentration was bidirectional with increasing soil depth, reaching a maximum at the base of the soil–atmosphere interface (50–60 cm), and the bidirectional gradient was more distinctive in red soil. Change in the carbon isotope value of soil CO_2 was also bidirectional in calcareous soils, for which the overall average was 0.87‰ heavier in calcareous than red soil. The carbon sink in calcareous soil in karst regions was estimated to be 11.97 times that of red soil in non-karst regions, whereas its role as a carbon source is just 1.12 times that of red soil, thus indicating the key role of karst soil in the reduction of atmospheric CO_2.

Keywords: subtropical forest; calcareous soils; red soils; soil CO_2; carbon source–sink

1. Introduction

As the largest carbon pool of the terrestrial ecosystem, the amount of total carbon stored in soil (2300 Pg) is about two times and three times higher than the amount stored in the atmosphere (750 Pg) and in living biomass (650 Pg), respectively [1]. Global soil CO_2 emission rates are now up to approximately 98 ± 12 Pg a^{-1}, which is an order of magnitude greater than total annual CO_2 emissions from human activities (6.8 Pg a^{-1}); thus, small fluctuations in soil CO_2 emissions can greatly affect concentrations of atmospheric CO_2 [2,3].

Notably, soil CO_2 is soluble in water and readily forms carbonic acid, which can react with some types of bedrock (e.g., carbonate rock) to consume soil CO_2 and act as an important carbon sink of atmospheric CO_2 [4]. China has a karst area of 3.44 million km^2 [5], and the net recovery of atmospheric

CO_2 from the weathering of carbonate rocks (karstifiction) can reach 36 million t C a^{-1} [6], accounting for 48% of China's forest carbon sink (75 million t C a^{-1}) [7] between 1981 and 2000. The karst area of eight provinces in southwest China totals 1.12 million km^2, of which the bare karst area, depicted as carbonate rock exposed to the atmosphere directly, is 460,000 km^2 [5].

According to previous studies, the karstification that occurred in the soil–rock interface has affected the carbon isotope value ($\delta^{13}C$) of CO_2 from soil respiration and its distribution in the soil profile [8–12]. The CO_2 concentration in the limestone soil profile has a bidirectional gradient, with CO_2 concentration peaks typical in the middle layer [8–11]. In contrast, the CO_2 concentration in the red soil profile has a unidirectional gradient; that is to say, the deeper the red soil layer, the higher the CO_2 concentration [9]. However, unidirectional gradients with depth have also been recorded from 60 cm depths in limestone and dolomite soil profiles [12]. In the non-karst soil profile, the bidirectional gradient of CO_2 distribution was also reported [13,14]. The CO_2 concentration and amount of CO_2 emitted from soil respiration in limestone soil are both lower in karst areas than those of red soil in non-karst areas [9]. The $\delta^{13}C$ value of CO_2 from soil respiration in the karst area is 4‰ heavier than that of the non-karst area [9]. This difference may be related to consummation and absorption of soil CO_2 in the carbonate rock dissolution at the soil–rock interface of karst regions [9]. In the soil–atmosphere interface layer, the $\delta^{13}C$ value of soil CO_2 ($\delta^{13}C$-CO_2) decreased with an increase in soil depth; whereas, below the soil–atmosphere interface layer, the $\delta^{13}C$-CO_2 is basically unchanged in a karst soil [15].

Analysis of the $\delta^{13}C$ may be used to explore the source of CO_2 in soil. If the karstification effect is sufficiently large enough to influence soil CO_2 concentration distribution, it should first arouse the CO_2 isotope's response to the soil profiles, because the CO_2 dissociated from bicarbonate formed by karstification is one of the sources of the soil CO_2 in karst areas [12]. Therefore, to understand how it may affect $\delta^{13}C$-CO_2 and the release of CO_2, and evaluate the CO_2 source and sink effect of karst soils, we determined the CO_2 concentration and isotope value in three calcareous soil profiles, developed from limestone found in a subtropical forest, for three years, for which red soils developed from clastic rock of the same zone were chosen for comparison. The source of CO_2 emission in calcareous soil was collected by the chamber method, and the sink produced by karstification was calculated by the standard carbonate tablet method.

2. Materials and Methods

2.1. Study Site

The study area was located near Maocun village, about 30 km southeastof Guilin (110°30′00″–110°33′45″ E, 25°10′11″–25°12′30″ N), in a typical karst peak cluster depression and valley landscape, with a catchment of about 10 km^2 (Figure 1). The climate in the area is mid-subtropical humid monsoon, hot and humid summer, characterized by spatio–temporal variations in rainfall; the annual average temperature is 19.64–20.39 °C, and the annual average rainfall is 1160–1378 mm (Figure S1). The geology of karst areas consists of Upper Devonian Rongxian Formation (D_3r) pure limestone. Vegetation in the studied sites was comprised of an evergreen broad-leaved forest dominated by *Cyclobalanopsis glauca*, *Loropetalum chinense*, *Alchornea trewioides*, and *Nephrolepis auriculata*, whose soil type was brown calcareous soil of the primosol order in the genetic soil classification of China (GSCC) [16], with a depth of 0.2–1 m. The geology of non-karst areas comprises iron clastic rock (D_2^1). Vegetation in this studied site was comprised of an evergreen broad-leaved forest, dominated by *Castanopsis fargesii*, *Schima superba*, *Itea chinensis*, and a small amount of *Miscanthus* spp.; the soil type was red soil of the ferralosol order in GSCC [16], with a depth of >1 m [9].

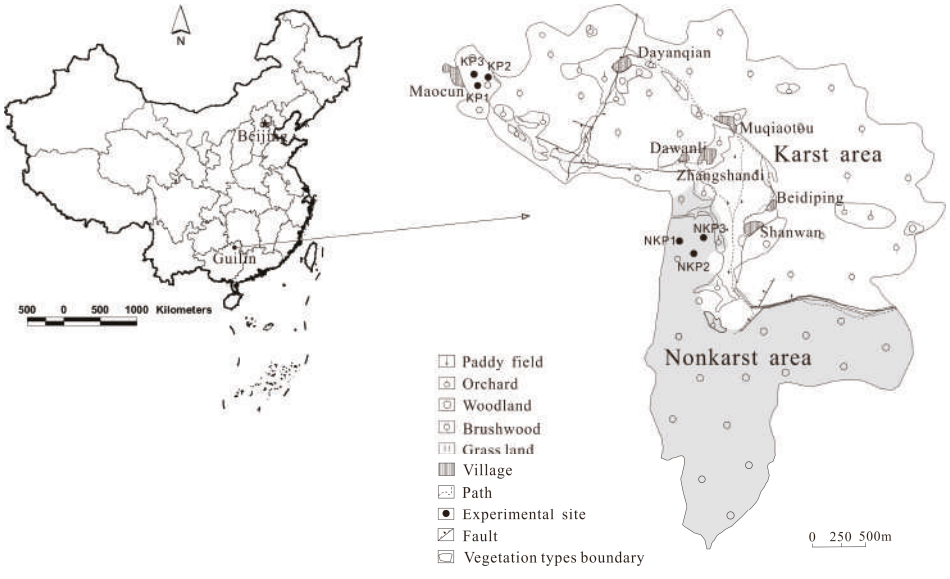

Figure 1. Land use of study area and location of study sites.

2.2. Soil Physicochemical Properties

For each layer (10, 20, 30, 40, 50, 60, 80, and 100 cm) in the 1-m deep soil profiles, we recorded water volume concentration, conductivity, and temperature using a WET sensor and HH2 moisture meter (Delta, Wakefield, UK); the corresponding range and resolutions are 0–100%, 0.1%, 0–300 mS m^{-1}, 1.0 mS m^{-1} and–5–+50 °C, 0.1 °C. Soil pH was measured by a US IQ150 (0.00–14.00, 0.01) soil in situ acidity meter on 24 March 2015. The water volume concentration, conductivity, and temperature of the surface calcareous soil and red soil were measured monthly for one year (Table 1; Figure 2). Soil organic matter was determined by the potassium dichromate volumetric method.

Table 1. Properties at different depths in calcareous and red soils.

	Depth (cm)	pH	Organic Matter (%)	Water Content (%)	Conductivity (mS m^{-1})	Soil Temperature (°C)
Calcareous soil (KP1)	10	7.32	4.57 ± 0.05	26.7	92	16.3
	20	7.29	2.57 ± 0.03	22.6	106	16.4
	30	7.35	1.92 ± 0.04	23.4	112	16.1
	40	7.27	1.78 ± 0.03	22.3	115	16.1
	50	7.25	1.89 ± 0.08	22.2	118	16.0
	60	7.13	2.02 ± 0.05	20.8	123	16.0
	80	7.21	1.34 ± 0.01	26.2	117	15.8
	100	7.24	0.86 ± 0.00	32.2	116	15.7
Red soil (NKP1)	10	5.48	4.02 ± 0.03	21.9	12	17.1
	20	5.96	3.67 ± 0.05	23.3	16	16.6
	30	5.33	3.15 ± 0.05	20.3	12	16.6
	40	5.40	2.72 ± 0.03	22.0	13	16.8
	50	5.48	2.01 ± 0.08	19.5	11	17.0
	60	5.36	1.65 ± 0.00	18.1	10	17.4
	80	5.69	1.14 ± 0.01	16.2	7	17.6
	100	6.39	1.04 ± 0.06	10.7	7	17.5

Data are the mean ± standard deviation (SD). N = 3.

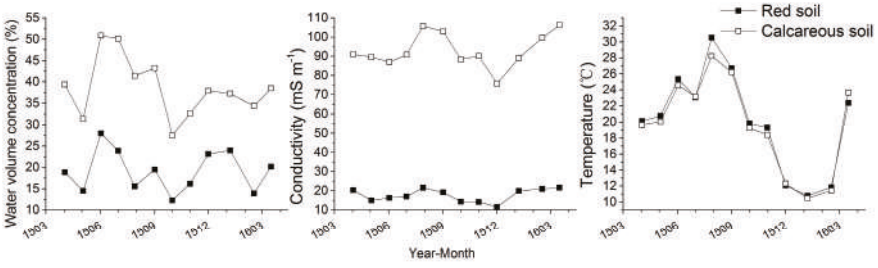

Figure 2. Temperature, water volume concentration and conductivity in the calcareous and red soils.

2.3. Soil CO_2 Concentrations and Emissions

We installed a CO_2 collection pipe in the calcareous (KP1) and red (NKP1) soil profiles in March 2015; two additional profiles in each soil type were included in January 2016 (KP2, KP3, and NKP2, NKP3), and monitoring points were separated by 5–50 m. Monthly monitoring continued from April 2015 to March 2018.

CO_2 concentrations in the eight soil layers were measured and recorded monthly (April 2015–March 2018) using a self-made soil collection pipe, comprising a 100 mL test tube in which gas was collected using a vacuum pump (GAS-TECQ Kitagawa, Japan). If CO_2 concentration >2.6%, we collected 50 mL of gas, and CO_2 concentration was doubled to give a concentration per 100 mL of gas.

Soil respiration CO_2 was collected from relatively flat ground, from which litter and weeds were removed to control for photosynthesis and the respiration of plants; the bare ground was immediately covered with a metal cylinder (25 cm diameter, 32 cm high), and the lower, open end of the cylinder was embedded 2 cm below the soil surface. A rubber tube was embedded in the soil within the cylinder and exposed to the atmosphere; a water stop clip was used to seal the end of the tube exposed to the atmosphere. Monthly atmospheric samples (April 2015–March 2018) were taken from the profiles at about 2 m above ground level to calculate background CO_2 levels; 1 h later, 200 mL of gas in the cylinder was continuously collected using a 100 mL medical syringe and injected into a vacuumed aluminum foil gas sampling bag. CO_2 concentration (ppm) was determined using an Agilent SP1 7890-0468 meteorological chromatograph (Agilent, Santa Clara, CA, USA) at the Ministry of Natural Resources/Guangxi Key Laboratory of Karst Dynamics, Guilin, Guangxi. Air pressure and temperature were simultaneously recorded. Sampling was done between 09:00 and 11:00, when soil respiration rates tend to reflect daily averages [17], to minimize diurnal variations in emissions. Soil CO_2 concentration and respiration in KP1 and NKP1 were sampled 33 times, and 23 times from the remaining profiles.

The $\delta^{13}C$-CO_2 was measured from the eight layers in the soil profiles in June and December 2015, and July 2017, where we used a vacuum to extract soil CO_2 into sealed aluminum bags. The $\delta^{13}C$-CO_2 analysis was completed at the isotope laboratory of the Chinese Academy of Agricultural Sciences, Beijing, China using a MAT253 mass spectrometer. Samples were collected from KP1 and NKP1 three times, and once from the remaining profiles.

2.4. Dissolution Rate of Carbonate Rock

The rate was acquired through the standard carbonate tablet method [18]. Carbonate tablets were determined from high purity, 4 cm diameter × 0.3 cm thick calcareous tablets that were washed and subsequently dried at 70 °C to constant weight after cooling, through a repeated dry-weigh process. In March 2015, in KP1 and NKP1, three tablets were placed 150 cm above the ground, at the soil surface, and inserted at the 20, 50, and 100 cm soil layers. In June, September, and December 2015, and March 2016, the tablets were recovered, analyzed, and re-buried following the washing and drying process described above.

2.5. Data Analysis

The units of CO_2 measurement (ppm) were converted to mg m^{-3} using:

$$CO_2 = \frac{M}{22.4} \times ppm \times \frac{273}{273 + T} \times \frac{Ba}{101325} \quad (1)$$

where M is the molecular weight of the gas; ppm is the measured volume concentration; T is the atmospheric temperature (°C); and, Ba is atmospheric pressure (Pa).

Soil respiration rate (V_R; mg C m^{-2} h^{-1}) was calculated as:

$$V_R = \frac{(C_1 - C_0) \times V}{S \times h} \times \frac{12}{44} \quad (2)$$

where C_1 is CO_2 concentration in the cylinder (mg m^{-3}); C_0 is the corresponding background CO_2 concentration (mg m^{-3}); V is the sampling box volume (m^3); S is the area of sampled soil (m^2); and, h is the monitoring time (h).

Annual soil CO_2 emission flux (F; t C km^{-2} a^{-1}) was calculated as:

$$F = \frac{\sum_{i=1}^{n} V_n \times (T_n - T_{n-1}) \times 24 \times 10^{-3}}{\frac{(T_n - T_1)}{365}} \quad (3)$$

where V_n is the nth measured soil respiration rate (mg C m^{-2} h^{-1}); $T_n - T_{n-1}$ and $T_n - T_1$ are the nth and (n−1)th, the nth and 1st sampling intervals (d), respectively.

The annual dissolution rate of the carbonate tablet (ER; mg cm^{-2} a^{-1}) was calculated as:

$$ER = (W_1 - W_2) \times 1000 \times \frac{T}{365 \times S} \quad (4)$$

where W_1 is the initial weight of the tablet (g); W_2 is the weight after embedding (g); T is the embedding duration (d); and S is the tablet surface area (about 28.9 cm^2).

CO_2 recovery in calcareous soil (CR_C; t C km^{-2} a^{-1}) was calculated according to the stoichiometric coefficient ratio of the carbonate dissolution reaction:

$$CaCO_3 + CO_2 + H_2O \leftrightarrow Ca^{2+} + HCO_3^- \quad (5)$$

$$CR_C = ER \times 97\% \times \frac{12}{100} \times 10 \quad (6)$$

where ER is the annual dissolution rate of the carbonate tablet (mg cm^{-2} a^{-1}); 97% is the purity of the standard carbonate tablet.

The dissolution rate of carbonate rocks in calcareous soil is 23.8 times that of clastic rocks in red soil at the study site [19]. According to the clastic rock dissolution reaction:

$$2CO_2 + 3H_2O + CaSiO_3 = Ca^{2+} + 2HCO_3^- + H_4SiO_4 \quad (7)$$

the CO_2 recovery in red soil (CR_R; t C km^{-2} a^{-1}) was calculated this way:

$$CR_R = \frac{CR_C}{23.8} \times 2 \quad (8)$$

We used one-way analysis of variance (ANOVA) to analyze the differences in soil respiration rate, CO_2 concentration, and $\delta^{13}C$-CO_2 among the soil layers between the two soil types at $p = 0.05$. A Pearson correlation analysis was used to test for association between CO_2 concentration and $\delta^{13}C$-CO_2 in different layers. Analyses were performed in Statistical Package Social Science (SPSS ver. 20.0; IBM Crop., Armonk, NY, USA).

3. Results

3.1. Soil Respiration Rate and Flux

There was a single peak in the soil respiration rate in one year of the karst and non-karst soil profiles, and soil respiration rates varied among the three calcareous soil profiles (range: 9.02–437.33 mg C m^{-2} h^{-1}, average: 134.84 mg C m^{-2} h^{-1}), where they were greater in KP2 than KP1; there were no differences among the red soil profiles (range: 23.21–361.42 mg C m^{-2} h^{-1}, average: 137.93 mg C m^{-2} h^{-1}) (Figure 3). No difference in the mean soil respiration rate was found between the two soil types, but the variation was greater in calcareous soil. The average CO_2 emission flux in calcareous soil and red soil was 1305 and 1167 t C km^{-2} a^{-2} (Table S1), being 12% higher in calcareous soil.

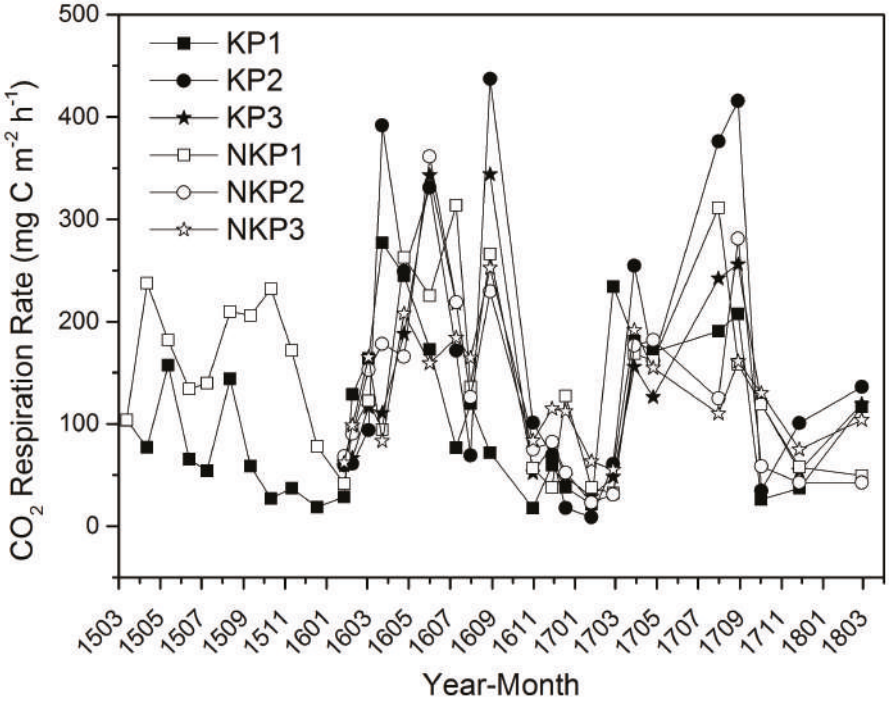

Figure 3. Respiration rates in the calcareous and red soils.

3.2. Variation in CO_2 Concentration among Soil Layers

Consistent with changes in soil respiration rate, the seasonal variation in soil CO_2 concentration in the layers tended to be unimodal, and concentrations were universally greater in summer and autumn than in winter and spring; an anomaly was the low value recorded in July 2015 and August 2016 (Figure 4). Overall, CO_2 concentrations were greatest and most variable in KP2, and lowest in KP1. There were no differences in CO_2 concentrations among the three red profiles.

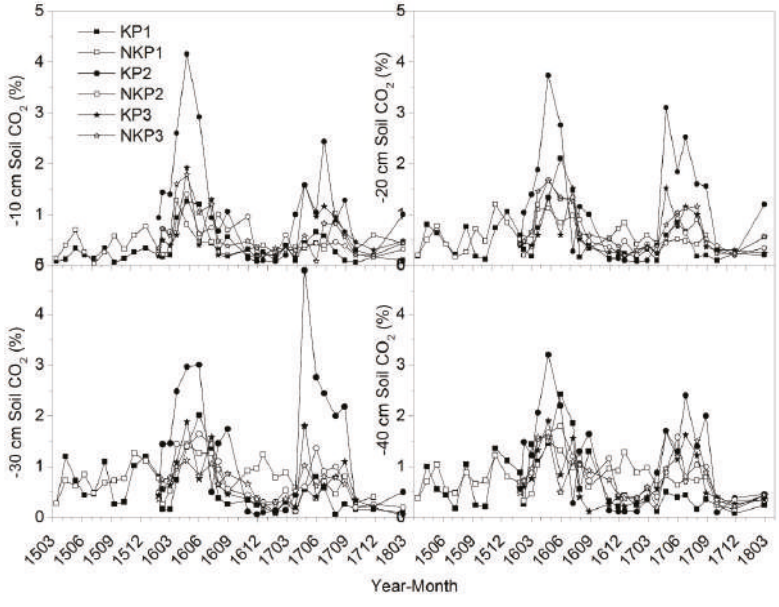

(**a**)

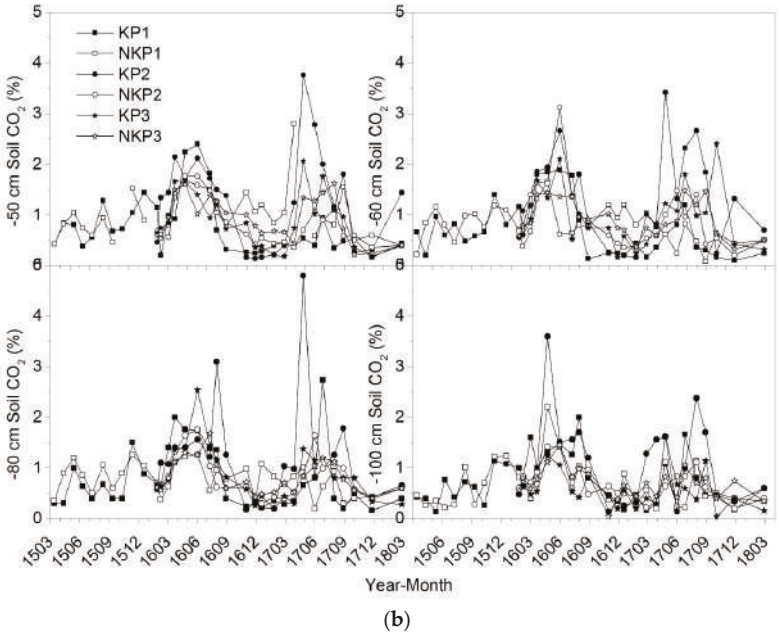

(**b**)

Figure 4. Soil CO_2 concentrations at 10–40 cm (**a**) and 50–100 cm (**b**) depths in calcareous and red soils.

Soil CO_2 concentration in the calcareous soil and red soil profiles varied with depth, where it tended to be higher at 50–60 cm and lower in the upper and deeper layers; this pattern was clearer in the red soils (Figure 5). The mean CO_2 concentrations in the three calcareous soils were 11% greater than in the red soils (Table S2).

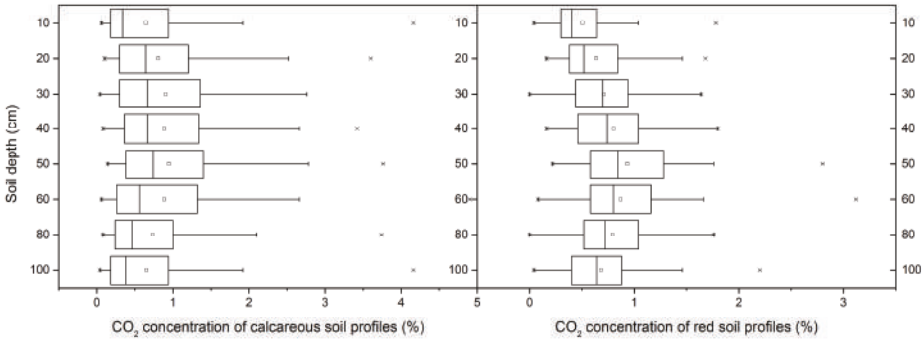

Figure 5. Summary statistics of overall mean soil CO_2 concentrations in calcareous and red soils. Open square: average; vertical line: median; box: upper and lower quartiles; horizontal lines: 1st and 99th percentiles; ×: minimum and maximum values. N = 168.

3.3. Changes in δ^{13}C-CO_2 among Soil Layers

In the calcareous soils, there was a bidirectional gradient of δ^{13}C-CO_2 with a depth in KP1 and KP3, and values at 60 cm were lighter than those of either the upper or deeper layers; the δ^{13}C-CO_2 values were lightest in KP2 and heaviest in KP1, with respective averages of −26.28‰ and −24.24‰ (Figure 6). In the red soils, δ^{13}C-CO_2 decreased with a depth of up to 50 cm, but it remained stable from 50 cm to 100 cm. The mean value of three plots for all layers was 0.87‰ heavier in calcareous soil than red soil (Table S3).

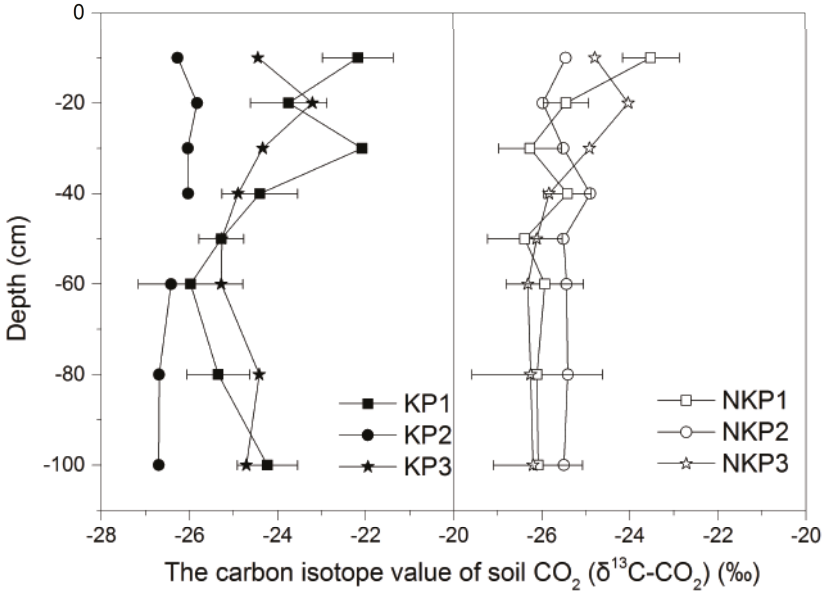

Figure 6. δ^{13}C-CO_2 values in different depth layers of the calcareous and red soils.

3.4. Dissolution Rates of the Carbonate Tablets in Different Layers

The dissolution rates of carbonate tablets were greater in the two soil types than in the air above the profiles, and their rates were greatest in the summer (Figure 7). The rates were bidirectional with

increasing depth and were greater in red soil than calcareous soil, except in calcareous soil during summer. There was no difference in the mean rates in the air above the calcareous and red soils, with averages of 2.50 ± 0.91 and 2.03 ± 1.07 mg cm^{-2} a^{-1}, respectively. The corresponding rates in the soil were 7.20 ± 2.11 and 13.88 ± 5.42 mg cm^{-2} a^{-1}, being 48% lower in calcareous soil (Table S4).

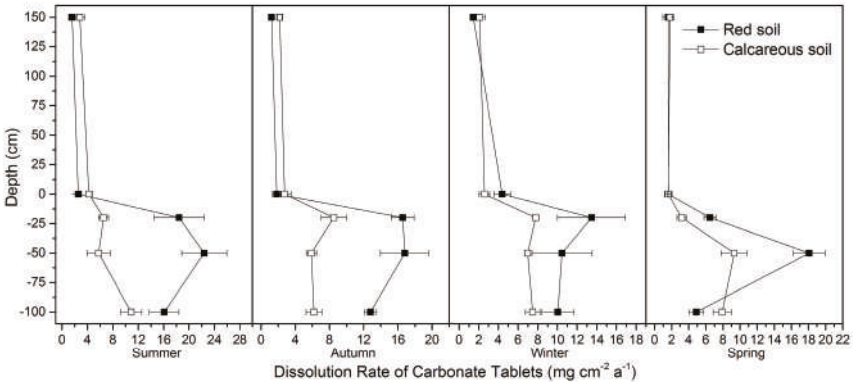

Figure 7. Dissolution rates in calcareous and red soils.

4. Discussion

4.1. Bidirectional Gradient of Soil CO_2 Concentrations and CO_2 Emissions in Red and Calcareous Soil Profile

Wang [13] and Dai [14] found that soil concentrations of CO_2 increased with a greater depth (up to 50 cm) but then diminished below 60 cm, due to the low associated organic carbon content. In our study, soil CO_2 concentrations in the two soil types had a bidirectional gradient trend, though this was more pronounced in the red soil, where the maximum values were recorded in the 50–60 cm layer. Soil organic matter (SOM) on the surface of calcareous soil was clearly higher than that of red soil (Table 1), but it exhibited the opposite trend deeper in the profile. Additionally, there is only a single trend of a gradually decreasing SOM content in red soil, while calcareous soil has a tendency to increase slightly at 50–60 cm. Therefore, the distribution of SOM should be a major reason why the concentration of CO_2 in deep layers of red soil decreases faster than in calcareous soil.

Our experiment showed that the diffusion input of atmospheric CO_2 was greater until the 50–60 cm layer, indicating that the thickness of the soil–atmosphere interface layer was 50–60 cm, while soil CO_2 in deeper layers was probably controlled by oxidative decomposition of organic matter. It is likely that the physical structure of soil particles and porosity, clay content, and soil flooding may also affect the thickness of the soil–atmosphere interface layer [20–22].

The annual soil respiration flux varies greatly in southwest China, ranging from 4.5 t C ha^{-1} a^{-1} (450 t C km^{-2} a^{-1}) in Yaji, Guilin, Guangxi, to 150 mg C m^{-2} h^{-1} (1314 t C km^{-2} a^{-1}) in Qingmuguan, Chongqing [9,23–25]. The results of our study are close to the largest value in those studies. The results were four to six times greater than those of typical meadow and dryland systems in a temperate continental monsoon climate zone (2.8–4.8 t C ha^{-1} a^{-1} = 280–480 t C km^{-2} a^{-1}) [22], perhaps due to lower temperatures in the temperate zone. Soil temperature, which is a key driver of soil respiration, is exponentially related to soil CO_2 [26].

Soil moisture also drives the soil respiration rate, and directly and indirectly regulates soil CO_2 emissions. It is believed that soil respiration increases with increasing soil moisture, until it reaches a threshold, after which it declines [20]. For example, when soil moisture is >60% in shallow soil, CO_2 flux rapidly decreases, due to the restriction of gas transport by the moisture [21], and a soil water content of 25–45% is optimal for microbe activity [27]. Soil moisture in the profile of calcareous soil was horizontally and vertically higher than that of the profile of red soil (Table 1, Figure 2), which may

have been responsible for the higher CO_2 concentration and respiration characterizing the calcareous soil profile.

4.2. Soil CO_2 Concentration and δ^{13}C-CO_2 Affected by Karstification

Consistent with our results, the CO_2 produced in soil had a lighter mean δ^{13}C value of −21 ± 1.5‰ than CO_2 with heavier isotopes in the surface atmosphere did (−9.82‰) [15], indicating a greater exchange of soil and air CO_2 at the soil–atmosphere interface. Therefore, δ^{13}C-CO_2 from the soil–atmosphere interface layer and upward gradually becomes heavier.

We found heavier δ^{13}C-CO_2 in the calcareous karst soils below 50–60 cm, due to two possible reasons. Firstly, karstification consumes soil CO_2, and lighter C is moved downward; the nearer the bedrock, the greater the likelihood of consumption of lighter C, resulting in heavier δ^{13}C-CO_2 in the soil. Secondly, the δ^{13}C of the rock is 0‰, and the theoretical CO_2 isotope value for bicarbonate formed by karstification at the soil–rock interface dissociation into soil CO_2 is −14‰ [28]; therefore, lighter δ^{13}C-CO_2 derived from root respiration, soil organic matter oxidative decomposition, and soil microbe activity could be mixed with this part of CO_2, resulting in a decreased overall CO_2 isotope value.

The δ^{13}C-CO_2 in the red soil below 50–60 cm tended to be stable; this finding is consistent with other studies in non-karst areas [29]. This stability with increasing soil depth may be attributed to the composition of stable carbon isotopes of CO_2 produced from the soil or the limited impacts of the climate on the physical properties of deep soils. The lightest value of soil CO_2 occurred at 50–60 cm, both in calcareous and red soils, which further corroborated that the 50–60 cm layer was the bottom of the soil–atmosphere interface layer.

Below the soil–atmosphere interface layer, karstification at the soil–rock interface consumes CO_2 and drives the downward migration of CO_2 [9]. This process may also have caused slow declines in CO_2 concentration at the bottom profile of the calcareous soil, resulting in a less pronounced bidirectional gradient than in the red soil profile. The δ^{13}C-CO_2 in calcareous soil became heavier: both the CO_2 concentration and its isotopes of calcareous soil show a bidirectional gradient due to the contribution from karstification, so a significant positive correlation arose between the CO_2 concentration and its isotopes (Figure 8). However, this was not the case in the red soil profile.

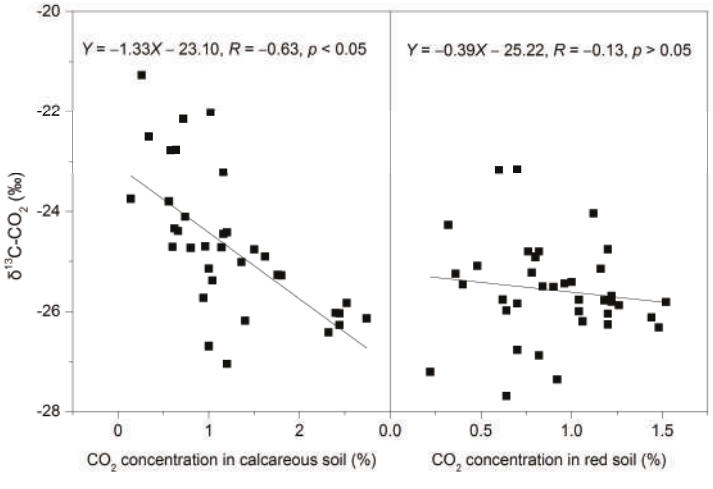

Figure 8. Association between δ^{13}C-CO_2 and the CO_2 concentration in calcareous and red soils.

4.3. Source–Sink Effect of Karst Soil Carbon Pools

In this study, the dissolution rate of the carbonate tablet in the red soil was found to be 1.93 times that of the calcareous soil (Table 2); however, soil CO_2 concentration and soil respiration rates were not as high (1.16 and 1.42 times, respectively, for NKP1 versus KP1), possibly due to a lower soil pH in the red soil affecting the rate of soil organic matter decomposition and erosion by soil microorganisms [30].

Table 2. The ratio of CO_2 recovery to CO_2 emission in calcareous soil and red soil.

	Calcareous Soil	Red Soil
Carbonate dissolution rate in air (mg cm^{-2} a^{-1})	2.50	2.03
Carbonate dissolution rate in soil (mg cm^{-2} a^{-1})	7.20	13.88
CO_2 recovery (t C km^{-2} a^{-1})	8.38	0.70
Soil CO_2 emission flux (t C km^{-2} a^{-1})	1305	1167
CO_2 recovery/CO_2 emission (%)	0.64	0.06

Influenced by soil temperature, water, soil CO_2, soil organic matter and pH, in addition to soil pores and other conditions [31], the dissolution rate of carbonate tablets in the soil in forests in karst areas in southwest China vary widely, ranging from 1.99 mg cm^{-2} a^{-1} in Yaji, Guilin, Guangxi [24], to 357.93 mg m^{-2} d^{-1} (13.06 mg cm^{-2} a^{-1}) in Dalongdong, Hunan [32]. The corresponding value obtained in our study is in the middle of these (Table 2), which can be considered as a better representative. The dissolution rate of carbonate tablets in the air is mainly controlled by the concentration of atmospheric CO_2 and rainfall intensity [18], and the difference between the data in this study (Table 2) and that from Jinfo Mountain, Chongqing, (21.4 t km^{-2} a^{-1} = 2.14 mg cm^{-2} a^{-1}) [18] is not large.

According to Table 2, CO_2 recovery accounts for 0.64% of the soil carbon source for calcareous soil. It is clear, then, that although karstification is an active weathering process, decomposition of soil organic matter and associated CO_2 respiratory emissions dominate the transport and cycling of carbon in the soil system. Thus, karstification and its impact on the carbon cycle represent an Earth-surface carbon transfer process.

Although the carbon source of calcareous soil was 1.12 times that of red soil, its carbon sink effect is 11.97 times that of red soil, suggesting that karst soil contributes greatly to the reduction of atmospheric CO_2. Nonetheless, the dissolution rate of carbonate tablets in the air could be indicative of the carbonate rock dissolution rate in bare karst areas, which is only 0.35 times that of calcareous soil. However, due to the wide distribution of bare karst in southwest China, its carbon sink potentiality cannot be ignored. The high carbonate dissolution rate in red soil also indicated the huge carbon sink potential of zonal red soil-intercalated carbonate rocks.

5. Conclusions

The CO_2 concentrations in calcareous and red soil layers exhibited bidirectional responses to soil depth. The influence of the soil–atmosphere interface on CO_2 exchange extended to a depth of 50–60 cm, where CO_2 concentration increased with depth; below this, CO_2 concentration decreases with depth and is mainly controlled by organic matter decomposition.

Soil $\delta^{13}C$-CO_2 in the two soils was controlled by CO_2 exchange at the soil–atmosphere interface and downward—where isotopes become lighter with depths of 50–60 cm; beyond this, $\delta^{13}C$-CO_2 gradually became heavier in calcareous soil layers, being mainly controlled by karstification. The CO_2 in the red clastic soils was derived from organic matter with stable isotopes, and so $\delta^{13}C$-CO_2 values were stable at depths >50–60 cm. The overall average of $\delta^{13}C$-CO_2 was 0.87‰ heavier in calcareous soils than red soils.

There were also bidirectional differences evident in the dissolution rates of carbonate rock in the two contrasting soils. The rates in the calcareous soil and red soil were 7.20 ± 2.11 and 13.88 ± 5.42 mg cm^{-2} a^{-1}, and, thus, almost half as low (48% lower) in calcareous soil.

Although karstification is an active weathering process, the decomposition of soil organic matter and associated CO_2 respiratory emissions dominate the transport and cycling of carbon in the system. The soil carbon sink only accounts for 0.64% of carbon sources in the karst areas. However, the CO_2 recovery in karst soil is estimated to be 11.97 times that of the clastic rock area and 1.12 times the latter as a carbon source, indicating the key role of karst soil in reducing atmospheric CO_2.

Supplementary Materials: The following are available online at http://www.mdpi.com/1999-4907/11/2/219/s1, Figure S1: Temperature and rainfall in Maocun village, Table S1: Respiration rates in calcareous and red soils, Table S2: CO_2 Concentrations in different layers in calcareous and red soils, Table S3: $\delta^{13}C$-CO_2 values at different depths of calcareous and red soils, Table S4: Seasonal carbonate dissolution rates in calcareous and red soils.

Author Contributions: Conceptualization, J.C.; writing—original draft preparation, F.H.; investigation, M.R. and M.F., writing—review and editing, J.C. and T.Z. All authors have read and agreed to the published version of the manuscript.

Funding: This study was supported by the National and Guangxi Natural Science Foundation of China (Grant Nos. 41772385, 2016GXNSFAA380034, 41530316), the National Key Research Projects (Grant No. 2016YFC05025), and the China Geological Survey (Grant No. DD20160305).

Acknowledgments: Special thanks go to the anonymous referees for their valuable comments and suggestions.

Conflicts of Interest: The authors declare no conflict of interest.

References

1. Jobbagy, E.G.; Jackson, R. The Vertical Distribution of Soil Organic Carbon and Its Relation to Climate and Vegetation. *Ecol. Appl.* **2000**, *10*, 423–436. [CrossRef]
2. Sheng, H.; Yang, Y.S.; Yang, Z.J.; Chen, G.S.; Xie, J.S.; Guo, J.F.; Zou, S.Q. The dynamic response of soil respiration to land-use changes in subtropical China. *Glob. Chang. Biol.* **2010**, *16*, 1107–1121. [CrossRef]
3. Ben, B.L.; Allison, T. Temperature-associated increases in the global soil respiration record. *Nature* **2010**, *464*, 579–582.
4. Cao, J.; Yang, H.; Kang, Z. Preliminary regional estimation of carbon sink flux by carbonate rock corrosion: A case study of the Pearl River Basin. *Chin. Sci. Bull.* **2011**, *56*, 3766–3773. [CrossRef]
5. Li, D.; Luo, Y. Measurement of carbonate rocks distribution area in China. *Carsologica Sin.* **1983**, *2*, 147–150. (In Chinese)
6. Liu, Z.; Wolfgang, D. Comparison of carbon sequestration capacity between carbonate weathering and forests: The necessity to change traditional ideas and methods of study of carbon sinks. *Carsologica Sin.* **2012**, *31*, 345–348. (In Chinese)
7. Fang, J.; Guo, Z.; Piao, S.; Chen, A. Estimation of terrestrial vegetation carbon sink in China from 1981 to 2000. *Sci. China Ser. D* **2007**, *37*, 804–812. (In Chinese)
8. Huang, Q.; Qin, X.; Liu, P.; Zhang, L.; SU, C. Proportion of pedogenic carbonates and the impact on carbon sink calculation in karst area with semiarid environment. *Carsologica Sin.* **2016**, *35*, 164–172. (In Chinese)
9. Cao, J.; Zhou, L.; Yang, H.; Lu, Q.; Kang, Z. Comparison of carbon transfer between forest soils in karst and clasolite areas and the karst carbon sink effect in Maocun village of Guilin. *Quat. Sci.* **2011**, *31*, 431–437. (In Chinese)
10. He, S.; Zhang, M.; Xu, S. Observation on soil CO_2 concentration, hydrochemistry, and thier relationship with karst processes. *Carsologica Sin.* **1997**, *16*, 319–324.
11. Xu, S.; He, S. The CO_2 regime of soil profile and its drive to dissolution of carbonbate rock. *Carsologica Sin.* **1996**, *15*, 50–57. (In Chinese)
12. Li, T.; Wang, S.; Zheng, L. Comparative study on sources of CO_2 from overlying carbonate rocks and non-carbonate rocks, in the middle parts of Guizhou province. *Sci. China Ser. D* **2001**, *31*, 777–782. (In Chinese)
13. Wang, C.; Huang, Q.; Yang, Z.; Huang, R.; Chen, G. Analysis of vertical profiles of soil CO_2 efflux in Chinese fir plantation. *Acta Ecol. Sin.* **2011**, *31*, 5711–5719. (In Chinese)
14. Dai, W.; Wang, Y.; Huang, Y.; Liu, J.; Zhao, L. Seasonal dynamic of CO_2 concentration in lou soil and impact by environmental factors. *Acta Pedol. Sin.* **2004**, *41*, 827–831. (In Chinese)
15. Zheng, L. The stable carbon isotope composition of soil CO_2 in the karst areas, the middle parts of Guizhou province. *Sci. Chin. Ser. D* **1999**, *29*, 514–519. (In Chinese)

16. Huang, C. *Soil Science*; China Agriculture Press: Beijing, China, 2000; pp. 224–227. (In Chinese)
17. Bubier, J.; Crill, P.; Mosedale, A.; Frolking, S.; Linder, E. Peatland responses to varying interannual moisture conditions as measured by automatic CO_2 chambers. *Glob. Biogeochem. Cycles* **2003**, *17*. [CrossRef]
18. Zhang, C. Carbonate rock dissolution rates in different landuses and their carbon sink effect. *Chin. Sci. Bull.* **2011**, *56*, 2174–2180. [CrossRef]
19. Huang, F.; Zhang, C.L.; Xie, Y.C.; Li, L.; Cao, J.H. Inorganic carbon flux and its source in the karst catchment of Maocun, Guilin, China. *Environ. Earth Sci.* **2015**, *74*, 1079–1089. [CrossRef]
20. Gong, X.; Li, Y.; Wang, X.; Niu, Y.; Lian, J.; Luo, Y. Characteristics of soil CO_2 emission in relation to hydrothermal factors during the growing season in horqin sandy land. *Ecol. Environ.* **2018**, *27*, 634–642. (In Chinese)
21. Gabriel, C.E.; Kellman, L. Investigating the role of moisture as an environmental constraint in the decomposition of shallow and deep mineral soil organic matter of a temperate coniferous soil. *Soil Biol. Biochem.* **2014**, *68*, 373–384. [CrossRef]
22. Jiang, C.; Hao, Q.; Song, C.; Hu, B. Effects of marsh reclamation on soil respiration in the Sanjiang Plain. *Acta Ecol. Sin.* **2010**, *30*, 4539–4548. (In Chinese)
23. Wu, X.; Pan, M.; Zhu, X.; Zhang, M.; Bai, X.; Zhang, B. Precipitation effect on soil respiration in epikarst during summer. *J. South. Agric.* **2015**, *46*, 575–580. (In Chinese)
24. Pan, G.; He, S.; Cao, J.; Tao, Y.; Sun, Y. Variation of $\delta^{13}C$ value in karst soil system in the surface zone of Yaji Village, Guilin. *Chin. Sci. Bull.* **2001**, *46*, 1919–1922. (In Chinese)
25. Li, L.; Xian, H.; Kuang, M.; Xie, S.; Zhang, Y.; Jiang, Y.; Liu, Y. The regularity of CO_2 release from soils of the epikarst ecosystem in the Jinfu mountain, Chongqing. *Acta Geosci. Sin.* **2006**, *27*, 329–334. (In Chinese)
26. Wang, X.; Wang, X.; Han, G.; Wang, J.; Song, W.; You, Z. Dynamics of soil CO_2 concentration and CO_2 efflux in non-growing season of the Yellow River Delta wetland. *Chin. J. Ecol.* **2018**, *37*, 2698–2706.
27. Schindlbacher, A.; Zechmeister-Boltenstern, S.; Kitzler, B.; Jandl, R. Experimental forest soil warming: Response of autotrophic and heterotrophic soil respiration to a short-term 10 °C temperature rise. *Plant Soil* **2008**, *303*, 323–330. [CrossRef]
28. Jiang, Y.J. The contribution of human activities to dissolved inorganic carbon fluxes in a karst underground river system: Evidence from major elements and delta $\delta^{13}C_{DIC}$ Nandong, Southwest China. *J. Contam. Hydrol.* **2013**, *152*, 1–11. [CrossRef]
29. Ding, P.; Shen, C.; Wang, N.; Yi, W.; Ding, X.; Fu, D.; Liu, K.; Zhao, P. Carbon isotopic composition turnover and origins of soil of soil CO_2 in a monsoon evergreen hroad leaf forest in Dinghushan Biosphere Reservior, South China. *Chin. Sci. Bull.* **2010**, *55*, 779–787. (In Chinese) [CrossRef]
30. Zhao, R.; Lv, X.; Jiang, J.; Duan, Y. Factors affecting soil CO_2 and karst carbon cycle. *Acta Ecol. Sin.* **2015**, *35*, 4257–4264. (In Chinese)
31. Liu, W.; Zhang, Q.; Jia, Y. The influence of meteorological factors and soil physicochemical properties on karst processes in six land-use patterns in summer and winter in a typical karst valley. *Acta Ecol. Sin.* **2014**, *34*, 1418–1428. (In Chinese)
32. Wang, W.; Lan, F.; Jiang, Z.; Qin, X.; Lao, W. Corrosion rate of carbonate tablet under diverse land use and lithology in the Dalongdong basin, Hunan. *Carsologica Sin.* **2013**, *32*, 29–33. (In Chinese)

forests

MDPI

Article

The Characteristics of Soil C, N, and P Stoichiometric Ratios as Affected by Geological Background in a Karst Graben Area, Southwest China

Hui Yang [1,2], Peng Zhang [1,2,3], Tongbin Zhu [1,2,*], Qiang Li [1,2] and Jianhua Cao [1,2]

1 Institute of Karst Geology, CAGS, Karst Dynamics Laboratory, MNR and Guangxi, Guilin 541004, China
2 International Research Centre on Karst, Under the Auspices of UNESCO, Guilin 541004, China
3 School of Water Resources and Environment, China University of Geosciences (Beijing), Beijing 100083, China
* Correspondence: zhutongbin@gmail.com; Tel.: +86-773-5837840

Received: 31 May 2019; Accepted: 17 July 2019; Published: 19 July 2019

Abstract: Understanding ecological stoichiometric characteristics of soil nutrient elements is crucial to guide ecological restoration and agricultural cultivation in karst rocky desertification region, but the information about the effect of the geological background on ecological stoichiometric ratios remains unknown. Soils from different landforms, including a basin, slope, and plateau, were sampled to investigate the spatial variance of the ecological stoichiometric characteristics of soil carbon (C), nitrogen (N), and phosphorus (P) under different rocky desertification grades (LRD: light rocky desertification; MRD: moderate rocky desertification; and SRD: severe rocky desertification) in a karst graben basin of Southwest China. Soil C:N ratio was not significantly influenced by rocky desertification grade, which was at a relatively stable level in the same landform, but soil C:P and N:P ratios increased with increasing rocky desertification grade. This change was consistent with increased soil organic carbon (SOC) and total nitrogen (TN) concentrations in the same geomorphic location along with the intensification of rocky desertification, but soil P concentration remained at a relatively stable level, indicating that P may be the limiting macronutrient for plant growth during vegetation restoration in a karst graben area. The soil C:N ratio of slope land was larger than that of the basin and plateau, while the soil C:P ratio and N:P ratio of the slope and plateau were significantly larger than that of the basin. The correlations between pH and C, N, and P stoichiometry decreased significantly when Ca was used as a control variable. In sharp contrast, the correlations between Ca and C, N, and P stoichiometry were highly significant no matter whether pH was used as a control variable, suggesting the important role of Ca in soil C, N, and P stoichiometry in karst graben basins.

Keywords: stoichiometric ratios; landform; rocky desertification; karst graben basin

1. Introduction

Karst, which accounts for 12% of the world's total land area, is a calcium (Ca)-rich environment and a unique ecological system [1]. China has approximately 3.44 million km^2 of karst areas, including buried, covered, and exposed carbonate rock areas, accounting for 15.6% of all karst areas in the world [2]. The karst ecosystem is extremely fragile, and it is ranked as the four fragile eco-environmental zones in China along with loess, desert, and cold desert [3]. Due to the fragile ecological environment, complex human-land system, and unreasonable social and economic activities, the rocky desertification widely occurs in the southwest karst region of China (Figure S1) [4]. Noticeably, the karst graben basin is a unique geomorphological form, more fragile than other karst regions in the Southwest China, due to the obvious differences in the topography and climate between basins and mountainous areas in graben basins. Furthermore, geographical environment factors (e.g., hydrology, climate,

and soil) are complex and vegetation site conditions are poor, all of which induce serious rocky desertification [5,6]. Thus, rocky desertification control has become an important part of China's social and economic construction. In addition, vegetation after rocky desertification control is characterized by simple structure, poor stability, and weak resistance. However, the theoretical research of karst rocky desertification restoration lags far behind the practice of rocky desertification control, which seriously limits the restoration and reconstruction of rocky desertification.

It has been widely accepted that the eco-stoichiometry in terrestrial ecosystems plays an important role in biogeochemical cycle research, because it can be used to evaluate the equilibrium and coupling relationships of the main components of an ecosystem [7,8]. Among various elements, soil carbon (C), nitrogen (N), and phosphorus (P) are considered to be the most important components, because the soil C:N:P stoichiometric ratio can reflect soil fertility, plant nutritional status, and the coupling changes between these elements can also affect the growth and distribution of vegetation [9]. In the past several decades, the ratios and relationships among soil C, N, and P have been extensively studied to indicate whether plant growth is limited by these nutrients [10]. The stoichiometric ratio of soil C, N, and P is strongly influenced by soil type, vegetation community characteristics, climatic condition, and vegetation development stage [11,12]. Noticeably, soil is highly heterogeneous in time and space, especially for karst landform. With the development of rock desertification grades, except for plant loss (i.e., the reverse succession of plant communities), the changes in soil quality (e.g., physical, chemical, and biological properties) and quantity have also been significantly taken place [13,14]. In general, the positive succession of plant communities facilitates soil nutrient accumulation, while the reverse succession of plant communities exacerbates soil degradation [15], which can be further enhanced with an increasing rocky desertification grade [16–18]. However, the response of soil physical and chemical properties during the evolution of rocky desertification can show the different patterns as follows: With the increasing rocky desertification grade, the aggregation effect of bare rocks becomes more and more obvious, and the input of soil total N (TN) and soil organic carbon (SOC) is increased through atmospheric sedimentation nutrients and the karst process, while soil erosion becomes weak due to the less soil that can be lost, and subsequently soil nutrient loss is weak, which may improve soil nutrients and physical properties in a rocky desertification environment [16]. Thus, it is possible that soil quality varies with the grade of rocky desertification. Noticeably, soils that widely exist in different landforms in the karst graben basin also have different physical and chemical properties. Therefore, soil stoichiometry may be simultaneously affected by rocky desertification and topography. However, the existing reports mainly focus on the spatial distribution characteristics of soil nutrients and changing patterns during rocky desertification evolution [19]. There is no systematic study on the relationships, ratios between soil C, N, and P elements, and the affecting factors under different rocky desertification in different landforms in the karst graben basin. In addition, calcareous soil developed on carbonate rock is characterized by high pH, magnesium (Mg), and Ca materials in a karst region [2,20], which may lead to the obvious differences in the eco-stoichiometry of soil C, N, and P compared to other soil types. We hypothesized that the karst geological background, especially soil pH, Mg, and Ca concentrations, may play an important role in controlling soil C, N, and P stoichiometry.

In this study, soils from different landforms, including a basin, slope, and plateau, were sampled to investigate the spatial variance of the ecological stoichiometric characteristics of soil C, N, and P under different rocky desertification grades in the karst graben basin. In addition, other soil properties, especially pH, Mg, and Ca concentrations, were also determined to reveal the influencing geochemical factors for soil C, N, and P stoichiometric ratios.

2. Material and Methods

2.1. Study Area

The study site was located in Mengzi county, Hani-Yi Autonomous Prefecture of Honghe, Yunnan Province, China (Figure 1). It is characterized by a typical karst landscape and the topography is

dominated by mountains and basins. Rocky desertification is usually distributed in mountainous areas with a large elevation difference and steep slopes, which results in gradient effects of water, energy, and other factors, and then forms the vertical changes in climate, biology, soil, and so on [21]. The development degree of rocky desertification in the graben basin area is restricted by geological-climatic conditions, resulting in the formation of the eco-environmental characteristics of the basin with thicker soil cover, shallow hills in the basin, slopes around the basin, and plateau areas where rocks are exposed and rocky desertification is serious [5]. According to the characteristics of the Mengzi karst graben basin, soil samples were collected along the basin, slope, and plateau (Figure 1). The annual average temperature of the basin, slope, and plateau is 19.0, 15.6, and 13.7 °C, respectively, and the annual rainfall of the basin, slope, and plateau is 663, 575, and 1027 mm, respectively [22].

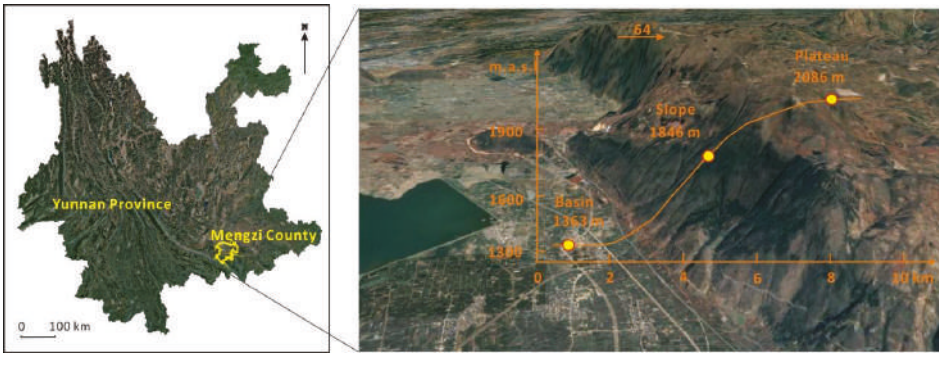

Figure 1. The location of the study area.

2.2. Soil Sampling

The classification of the severity of rocky desertification referred to the method of Jiang et al. (2014) [2], which has been classified into four categories according to the rock exposure rate in China: (1) No rocky desertification with a rock exposure rate <30% of the land; (2) LRD (light rocky desertification with a rock exposure rate ranging from 30% to 50%); (3) MRD (moderate rocky desertification with a rock exposure rate ranging from 50% to 70%); and (4) SRD (severe rocky desertification with a rock exposure rate >70%).

Soil samples were collected from different geomorphic sites, including the basin, slope, and plateau. Different rocky desertification grades, including LRD, MRD, and SRD, were selected in the same landform. The details of the sampling sites, including the vegetation and rocky desertification, are shown in Table 1 and Figure S2.

Table 1. Basic information of the study area and sampling sites.

Location	Latitude and Longitude	Altitude (m)	Rocky Desertification and Vegetation
Basin	103°23′47″ E, 23°28′22″ N	1363	LRD: *Eucalyptus* forest with short planting years and single community structure. The rock bareness rate was ~35%. MRD: Herbs, dominated by Miscanthus. The rock bareness rate was ~55%. SRD: Herbs, herb of Spanishneedles (*Bidens bipinnata* Linn.) and Canadian fleabane (*Conyza canadensis* (Linn.) Cronq.) was dominant specie. The rock bareness rate was >70%.
Slope	103°26′13″ E, 23°27′43″ N	1846	LRD: Artificially planted cypress forests, with high canopy density. The rock bareness rate was ~30%. MRD: Shrub, domained by Purpus Priver (*Ligustrum quihoui* Carr.) and Euphorbiae Pekinensis Radix (*Euphorbia pekinensis* Rupr). The rock bareness rate was ~50% SRD: Ferns are the main species. The rock bareness rate was >70%.
Plateau	103°27′09″ E, 23°27′08″ N	2086	LRD: Forest, the main vegetation types are *Ligustrum quihoui* Carr. and Chinese mugwort (*Artemisia argyi* H. Lév.) and Vaniot. The rock bareness rate was ~30%. MRD: the main vegetation types are Miscanthus. The rock bareness rate was ~50%. SRD: Herbs, domained by Miscanthus with a small amount of *Conyza canadensis* (Linn.) Cronq. The rock bareness rate was >70%.

LRD represents light rocky desertification; MRD represents moderate rocky desertification and SRD represents severe rocky desertification.

At least three representative plots were sampled from the LRD, MRD, and SRD area under the same landform position, resulting in 51 soil samples. The distance between sites was beyond 100 m under the same rocky desertification grade. At each site, 5 plots (1 m × 1 m) were randomly chosen at 20 m intervals. Soils were obtained from the 0 to 15 cm layer after litter removal in each plot and all subsamples were mixed into one composite sample for each site. Fresh soil was passed through a 2 mm sieve, and stones and roots were removed to improve soil homogeneity and were air-dried for measurement of the soil's basic properties and nutrient element concentrations.

2.3. Methods

Soil pH was determined at a 1:2.5 (w:v) soil:water ratio by a DMP-2 mV/pH detector (Quark Ltd., Nanjing, China). SOC was measured using the $K_2Cr_2O_7$-H_2SO_4 oxidation method; total N concentration was measured with the Semi-Micro Kjeldahl method; total P (TP) was determined using $HClO_4$–H_2SO_4 digestion followed by a Mo–Sb colorimetric assay; and total potassium (TK) concentration was measured with the HF-HClO4 flame photometric method [23,24]. Available P (AvP) was determined by the $NaHCO_3$-extraction method [25]. Soil Ca, Mg, copper (Cu), iron (Fe), manganese (Mn), and zinc (Zn) were extracted by HNO_3-HF-$HClO_4$ and analyzed by Inductively Coupled Plasma-Atomic Emission Spectrometry (ICP-AES). Three replicates were performed for each soil sample.

2.4. Data Analysis

Soil nutrient stoichiometry was reported as a molar ratio because it could accurately reflect the amount of elements in the soil [19,26]. The SOC, TN, TP, and AvP concentrations (g/kg) were transformed to mol/kg. The C:N, C:P, C:AvP, N:P, and N:AvP ratios of each soil sample were then calculated as molar ratios (atomic ratios) using SOC:TN, SOC:TP, SOC:AvP, TN:TP, and TN:AvP data, respectively.

Multiple comparisons were conducted by the Duncan method when the variance was homogeneous or the T2 Tamhane test when the variance was not homogeneous. The correlations between the stoichiometric characteristics and the environmental factors studied were analyzed by the Pearson correlation test.

3. Results

3.1. General Patterns of Soil C, N, and P in the Karst Graben Basin

In total, the average values of the C:N, C:P, and N:P ratios in the studied region were lower than those in China. However, both C:AvP and N:AvP were far higher than those in China (Table 2).

Table 2. Soil C, N, and P molar ratios in the karst graben basin.

Landform	C:N	C:P	N:P	C:AvP	N:AvP
Basin	13.4 ± 3.5 a	65.8 ± 18.6 a	5.0 ± 1.3 a	42,429 ± 28,020 a	3292 ± 2181 a
Slope	15.4 ± 3.2 b	116.0 ± 26.2 b	7.8 ± 2.6 b	81,067 ± 36,628 b	5600 ± 3079 b
Plateau	13.2 ± 1.7 a	96.3 ± 39.9 b	7.2 ± 2.5 b	46,285 ± 37,982 a	3399 ± 2589 a
Average	13.6 ± 2.6	92.6 ± 37.3	6.8 ± 2.5	51,516 ± 37,650	3762 ± 2682
China [27]	14.4 ± 0.4	136 ± 11	9.3 ± 0.7	15,810 ± 1832	1114 ± 115

SOC represents soil organic carbon; TN represents total nitrogen; TP represents total phosphorus; AvP represents available phosphorus; C:N represents the molar ratio of SOC:TN; C:P represents the molar ratio of SOC:TP; N:P represents the molar ratio of TN:TP. C:AvP represents the molar ratio of SOC:AvP; N:AvP represents the molar ratio of TN:AvP. Identical letters indicate no significant differences in the average values among soils under different landforms at the 0.05 level.

Both SOC and TN concentrations in the basin were significantly lower than those in the slope and plateau, but no significant differences were found between the slope and plateau ($p < 0.05$, Figure 2). Soil TP concentration in the plateau was significantly higher than that in the slope, but the differences in soil TP concentration between the basin and slope and between the slope and plateau was not significant ($p > 0.05$).

The soil C:N ratio in the basin was significantly lower than that in the slope, while there was no significant difference between the basin and plateau ($p < 0.05$). Both the soil C:P and N:P ratios in the basin were much lower than those in the slope and plateau ($p < 0.05$), while no significant differences were found in the slope and plateau ($p > 0.05$, Figure 2).

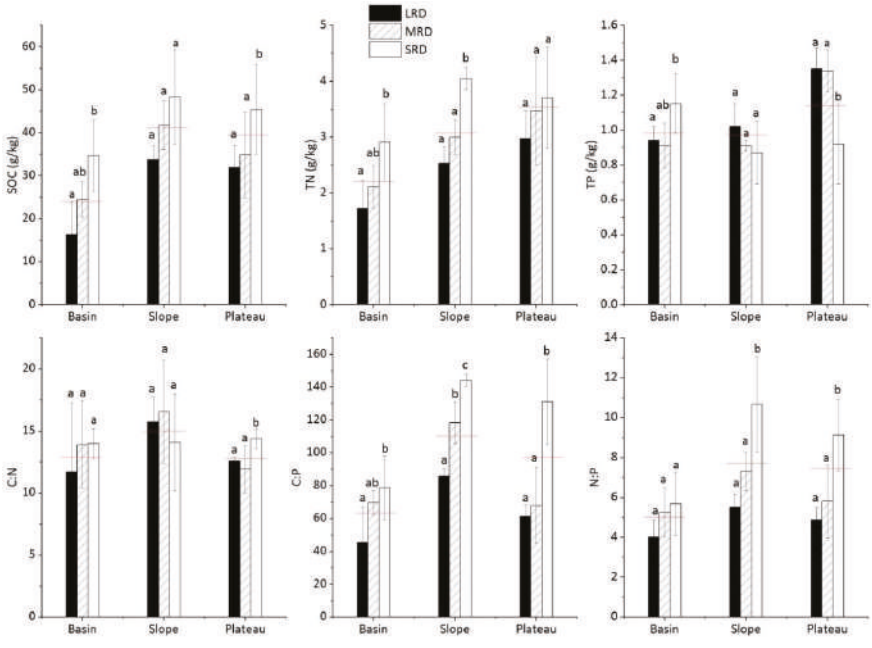

Figure 2. Soil nutrient concentrations and their stoichiometry. The red short line indicates the average value of different rocky desertification degrees in the same geomorphological location. SOC represents soil organic carbon; TN represents total nitrogen; TP represents total phosphorus; C:N represents the molar ratio of SOC:TN; C:P represents the molar ratio of SOC:TP; N:P represents the molar ratio of TN:TP. LRD represents light rocky desertification; MRD represents moderate rocky desertification and SRD represents severe rocky desertification. Identical letters indicate no significant differences in the average values among soils under different rocky desertification in the same landform at the 0.05 level.

3.2. Soil Nutrient Concentrations and their Stoichiometry under Different Rocky Desertification

Both SOC and TN concentrations increased with the aggravation of rocky desertification among the three landforms, while the TP concentration decreased with the aggravation of rocky desertification in the slope and plateau and there was no obvious regularity with the aggravation of rocky desertification in the basin (Figure 2).

The C:N ratios had no consistent regularity with the aggravation of rocky desertification among the three landforms, and there were no significant differences among rocky desertification in the same landform. The C:P and N:P ratios increased with the aggravation of rocky desertification among the three landforms.

3.3. Correlations among Geochemical Variables and C, N, and P Stoichiometry

The correlation between both of SOC and TN and Ca was significant under the condition of zero-order or with the pH value as the controlling factor. There was a simple negative correlation between the Ca and AvP concentration (zero-order in Figure 3). However, the Pearson correlation coefficient between the Ca and AvP concentration decreased significantly when pH was the controlling factor. Soil pH was positively correlated with SOC and TN (zero-order), but under the condition that Ca was the controlling factor, the partial correlation between both of SOC and TN and pH was significantly negative. Hence, Ca was the core element affecting SOC and TN concentrations. Although there was a negative partial correlation between Mg and SOC and TN when Ca was the controlling factor, the correlation between Mg and the stoichiometry of C, N, and P was not significant.

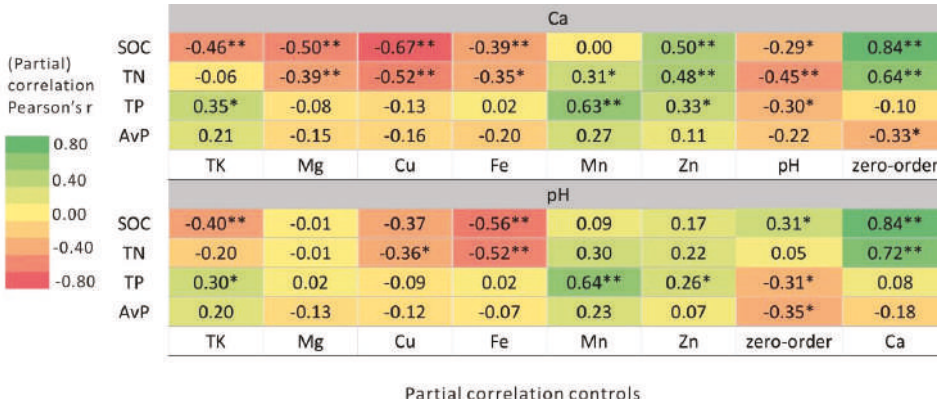

Figure 3. Partial correlation between C, N, and P and geochemical variables. Ca, Mg, Cu, Fe, Mn and Zn represents calcium, magnesium, copper, iron, manganese, and zinc respectively; TK represents total potassium; The color and numbers shown indicate the strength and sign of the correlation. No change in color between controlled and zero-order = no dependency; increase/decrease of color intensity = gain of /loss of correlation. Significance levels are denoted as follows: *, $p < 0.05$; **, $p < 0.01$.

Undoubtedly, both Ca and pH directly influenced the C, N, and P stoichiometry (Figure 4 and zero-order correlations in Figure 5). Both Ca and pH were positively correlated with C:N and C:P ($p < 0.01$). However, the relationship between Ca and N:P was extremely significant and positive ($p < 0.01$), while the correlation between pH and N:P was not significant ($p > 0.05$). Similarly, the correlations between Ca and C:AvP, Ca and N:AvP, and pH and C:AvP were very significant ($p < 0.01$). A significant positive correlation was found between pH and N:AvP ($p < 0.05$).

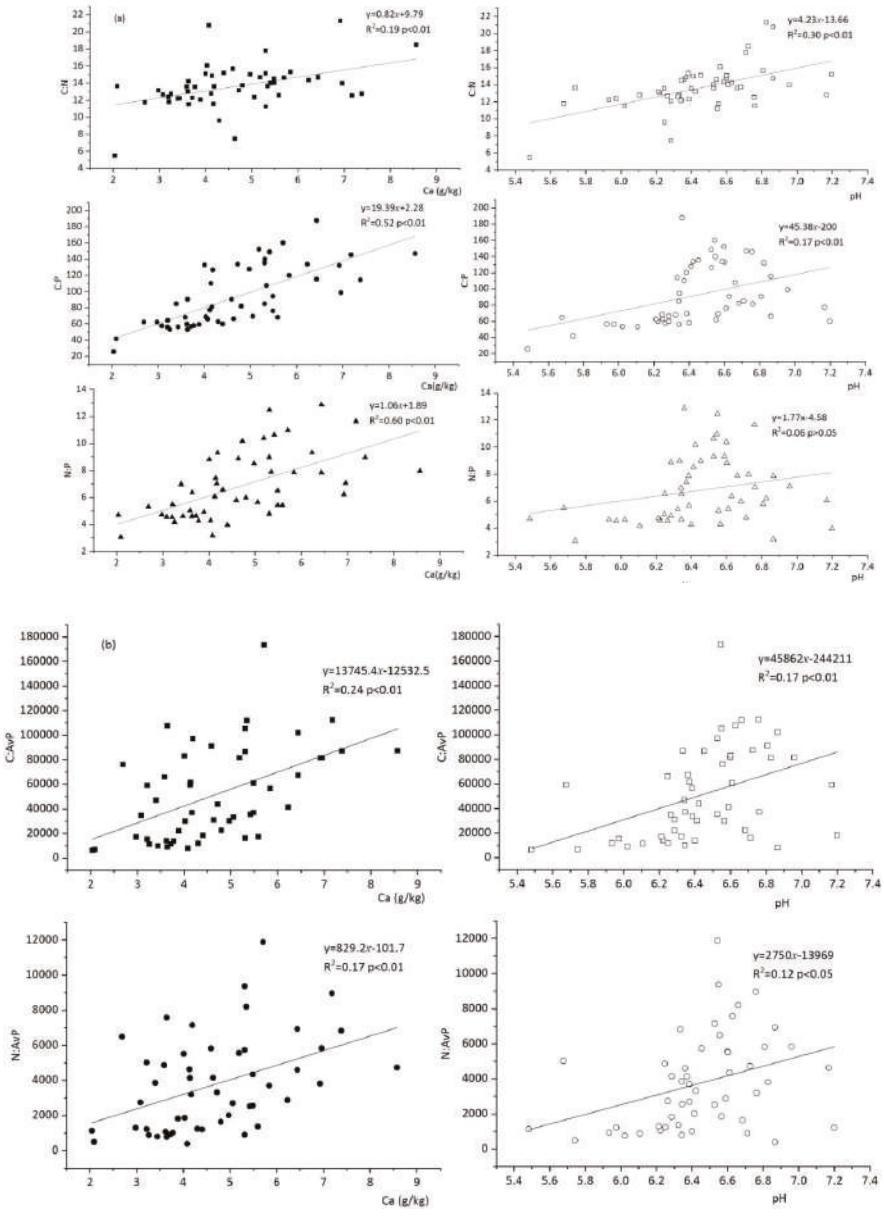

Figure 4. The relationship between Ca, pH, and C, N, and P stoichiometry. (**a**): The relationship between Ca, pH, and C:N, C:P and N:P; (**b**): The relationship between Ca, pH, and C:AvP, N:AvP.

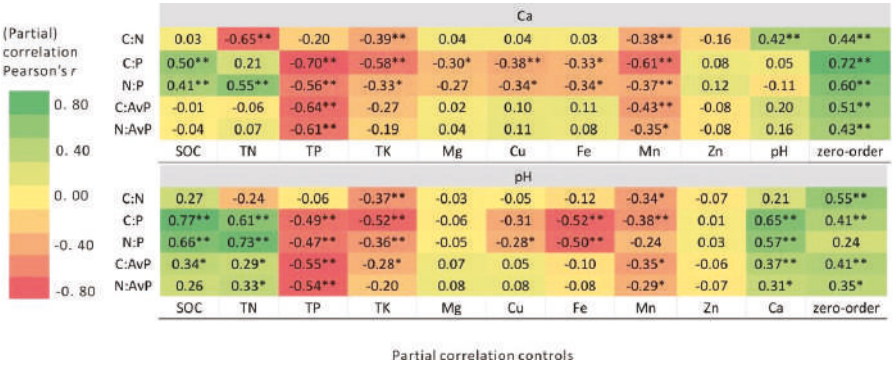

Figure 5. Partial correlation between C, N, and P stoichiometry and geochemical variables. Significance levels are denoted as follows: *, $p < 0.05$; **, $p < 0.01$.

4. Discussion

4.1. Spatial Pattern of Eco-Stoichiometric Characteristics of C, N, and P and Analysis of Influencing Factors

It has been widely accepted that SOC in calcareous soils in the karst region of Southwest China is significantly higher than that in other zonal soils in the same latitude [28,29], which is mainly attributed to the shallow soil layer, high bareness rate, and low soil quantity in the karst area [16]. Most researchers also found that an increased SOC concentration is closely related to the geological background of Ca-rich and pH-alkaline soils in the karst area [30–33]. Calcium in different forms plays an important role in SOC protection through a chemical bonding mechanism and chemical structure stability [34–38]. In this study, Ca was positively correlated with SOC concentration (Figure 3), indicating the important role of Ca in maintaining the SOC pool. Furthermore, SOC and TN had a significant positive correlation, suggesting the co-evolution process of the C and N cycle in calcareous soil. However, the P pool was not basically affected by the changes in the C and N pools, which resulted in the weak correlation between soil TP and SOC and TN. This indicates that P is mainly derived from the weathering release of soil minerals, rather than from the short-term biological cycle in this study [39]. Soil C:N, C:P, and N:P in the studied region were all lower than the average value of China, but the values of C:AvP and N:AvP were much higher than the average value of China (Table 1), which may be attributed to a high total P concentration but low AvP concentration in the karst soil [40].

The spatial distribution of C:N in the studied area is relatively stable, and no significant difference was found among the three rocky desertification lands in different geomorphological locations, suggesting that the vegetation type and rocky desertification degree have little significant effect on the C:N ratio. This was in agreement with a previous result that the C:N ratio was relatively stable and was insignificantly affected by climate, although C and N concentrations had great spatial variability [38,39]. Previous studies found that soil C:P and N:P ratios decreased with increasing disturbance, because the loss of soil C and N pools was faster than the P pool. However, in this study, N:P and C:P ratios increased with the aggravation of rocky desertification, more noticeably in the severe rocky desertification rock region with strong disturbance. Possibly, this could be attributed to increased SOC and TN concentrations with the aggravation of rocky desertification but the soil P concentration at a relatively stable level (Figure 2). Some studies found that soil physical and chemical properties do not always deteriorate with an increasing rocky desertification grade, but the degradation process initially decreases and improves after a certain stage [16,40,41]. This may be related to the "aggregation effect" of bare rocks in a rocky desertification environment [16], which refers to bare rock aggregated nutrients and the karst process from atmospheric subsidence into the surrounding soil. With the grade of rocky desertification, the aggregation effect of bare rock increases gradually. In the intensive rocky desertification environment, this aggregation effect becomes more obvious, coupled with the

weakening of soil erosion, and subsequently results in the improvement of soil nutrients and physical properties, such as SOC, TN, and Ca.

4.2. Soil Ca and pH Controls on Soil C, N, and P Stoichiometry

Due to high Ca concentrations, calcareous soils developed by carbonate bedrock are characterized by high pH [42]. Soil pH can affect the forms and transformation of C, N, and P elements in the soil by changing the geochemical environment and microbial abundance, community, and activity. In addition, soil with a high Ca concentration in rock desertification areas has become the most important environmental factor affecting the local plant physiological characteristics and distribution [1]. In this study, although the correlations between pH and C, N, and P stoichiometry were highly significant (zero-order correlations in Figure 5), the Pearson correlation coefficients between pH and C:P, N:P, C:AvP, and N:AvP decreased significantly when Ca was used as a control variable (Figure 5). In sharp contrast, both zero-order correlations and the Pearson correlations between Ca and C, N, and P stoichiometry were highly significant, when pH was used as a control variable (Figure 5).

Calcium greatly impacted soil C, N, and P stoichiometry in this study. The dominant role of Ca in soil C, N, and P stoichiometry is intriguing, and Ca can supply several possible alternative explanations. Firstly, Ca is the necessary metabolic component of microbial growth, and fungal and bacterial heterotrophs may access and accumulate root Ca to form oxalates, which can be used to maintain microbial metabolism under unfavorable soil conditions [43]. Similar results were reported that Ca-rich species exhibited more rapid decomposition [44]. Secondly, Ca can combine with humus to form Ca humate, which is difficult to mineralize and decompose [28], and thereby lowers the active organic matter.

5. Conclusions

In this work, we analyzed the C, N, and P stoichiometry under different rocky desertification grades from a basin, slope, and plateau in the karst graben basin. Our results showed that the influence of the rocky desertification degree on soil C:N was not significant in the same landform, but soil C:P and N:P increased with the increase of rocky desertification, which was attributed to increased SOC and TN concentrations in the same geomorphic location along with the intensification of rocky desertification, while the difference of P concentration in the same geomorphic location was not significant. This indicates that the soil quality is not deteriorating with the aggravation of rocky desertification, but has a trend of improvement. In addition, we also found that the correlations between pH and C, N, and P stoichiometry decreased significantly when Ca was used as a control variable. In sharp contrast, the correlations between Ca and C, N, and P stoichiometry were highly significant no matter whether pH was used as a control variable, indicating the important role of Ca in soil C, N, and P stoichiometry in karst graben basins. This result provides expanded guidance on the practice of ecological restoration and agricultural cultivation in karst rocky desertification regi ns. Forexample, when conducting ecological restoration of rocky desertification in karst graben basins, we should consider not only the impacts of altitude and vertical climate, but also the tolerance of species to Ca. Selecting suitable species according to local conditions are of great significance for the promotion of ecological restoration in rocky desertification areas.

Supplementary Materials: The following are available online at http://www.mdpi.com/1999-4907/10/7/601/s1, Figure S1: Agricultural planting patterns in rocky desertification areas, Figure S2: Vegetation and rocky desertification in three sampling sites.

Author Contributions: Conceptualization, T.Z.; writing—original draft preparation, H.Y.; investigation, P.Z. and Q.L.; writing—review and editing, T.Z. and J.C.

Funding: This study was supported by the National Key Research and Development Program of China (No. 2016YFC0502501), Guangxi Natural Science Foundation (2017GXNSFAA198153) and Guangxi Scientific Research and Technology Development Project (Guikeneng 1598023-1).

Acknowledgments: Special thanks to the anonymous referees for their valuable comments and suggestions. We also thank Junbing Pu, Manfu Hou, and his team for assistance with collecting soil samples and surveying plant diversity at sampling points.

Conflicts of Interest: The authors declare no conflict of interest.

References

1. Wei, X.; Deng, X.; Xiang, W.; Lei, P.; Ouyang, S.; Wen, H.; Chen, L. Calcium content and high calcium adaptation of plants in karst areas of southwestern Hunan, China. *Biogeosciences* **2018**, *15*, 2991–3002. [CrossRef]
2. Jiang, Z.; Lian, Y.; Qin, X. Rocky desertification in Southwest China: Impacts, causes, and restoration. *Earth Sci. Rev.* **2014**, *132*, 1–12. [CrossRef]
3. Yuan, D.X. Rock desertification in the subtropical Karst of South China. *Z. Geomorphol.* **1997**, *108*, 81–90.
4. Li, Q.; Pu, J.B.; Huang, N.; Du, H.M.; Qi, X.K.; Wang, L.; Yang, H. A research approach for ecological, environmental and geological differentiation of rocky desertification and its driving mechanism in karst graben basin. *Adv. Earth Sci.* **2017**, *32*, 899–907. (In Chinese)
5. Cao, J.H.; Deng, Y.; Yang, H.; Pu, J.B.; Zhu, T.B.; Lan, F.N.; Huang, F.; Liang, J.H. Rocky desertification evolution, treatment technology and demonstration in Karst faulted basins, Southwest China. *Acta Ecol. Sin.* **2016**, *36*, 7103–7108. (In Chinese)
6. Müller, M.; Oelmann, Y.; Schickhoff, U.; Böhner, J.; Scholten, T. Himalayan treeline soil and foliar C:N:P stoichiometry indicate nutrient shortage with elevation. *Geoderma* **2017**, *291*, 21–32. [CrossRef]
7. Hu, C.; Li, F.; Xie, Y.H.; Deng, Z.M.; Chen, X.S. Soil carbon, nitrogen, and phosphorus stoichiometry of three dominant plant communities distributed along a small-scale elevation gradient in the East Dongting Lake. *Phys. Chem. Earth* **2018**, *103*, 28–34. [CrossRef]
8. Mooney, H.A.; Vitousek, P.M.; Matson, P.A. Exchange of Materials Between Terrestrial Ecosystems and the Atmosphere. *Science* **1987**, *238*, 926. [CrossRef]
9. Mooshammer, M.; Hofhansl, F.; Frank, A.H.; Wanek, W.; Hämmerle, I.; Leitner, S.; Schnecker, J.; Wild, B.; Watzka, M.; Keiblinger, K.M.; et al. Decoupling of microbial carbon, nitrogen, and phosphorus cycling in response to extreme temperature events. *Sci. Adv.* **2017**, *3*, e1602781. [CrossRef]
10. Finzi, A.C.; Austin, A.T.; Cleland, E.E.; Frey, S.D.; Houlton, B.Z.; Wallenstein, M.D. Responses and feedbacks of coupled biogeochemical cycles to climate change: Examples from terrestrial ecosystems. *Front. Ecol. Environ.* **2011**, *9*, 61–67. [CrossRef]
11. Jacques Agra Bezerra da Silva, Y.; Williams Araújo do Nascimento, C.; Jacques Agra Bezerra da Silva, Y.; Miranda Biondi, C.; Cordeiro Atanázio Cruz Silva, C.M. Rare Earth Element Concentrations in Brazilian Benchmark Soils. *Rev. Bras. Ciênc. Solo.* **2016**, *40*, 1–13.
12. Wang, S.Q.; Yu, G.R. Ecological stoichiometry characteristics of ecosystem carbon, nitrogen and phosphorus elements. *Acta Ecol. Sin.* **2008**, *28*, 3937–3947. (In Chinese)
13. Li, Y.B.; Shao, J.A.; Yang, H.; Bai, X.Y. The relations between land use and karst rocky desertification in a typical karst area, China. *Environ. Geol.* **2009**, *57*, 621–627. [CrossRef]
14. Luo, G.J.; Li, Y.B.; Wang, S.J.; Cheng, A.Y.; Dan, W.L. Comparison of ecological significance of landscape diversity changes in karst mountains: A case study of 4 typical karst area in Guizhou Province. *Acta Ecol. Sin.* **2011**, *31*, 3882–3889. (In Chinese)
15. Song, T.Q.; Peng, W.X.; Du, H.; Wang, K.L.; Zeng, F.P. Occurrence, spatial-temporal dynamics and regulation strategies of karst rocky desertification in southwest China. *Acta Ecol. Sin.* **2014**, *34*, 5328–5341. (In Chinese)
16. Sheng, M.Y.; Liu, Y.; Xiong, K.N. Response of soil physical-chemical properties to rocky desertification succession in South China Karst. *Acta Ecol. Sin.* **2013**, *33*, 6303–6313. (In Chinese) [CrossRef]
17. Liu, F.; Wang, S.J.; Liu, Y.S.; He, T.B.; Luo, H.B.; Long, J. Changes of soil quality in the process of karst rocky desertification and evaluation of impact on ecological environment. *Acta Ecol. Sin.* **2005**, *25*, 639–644. (In Chinese)
18. Pang, D.; Wang, G.; Li, G.; Sun, Y.; Liu, Y.; Zhou, J. Ecological Stoichiometric Characteristics of Two Typical Plantations in the Karst Ecosystem of Southwestern China. *Forests* **2018**, *9*, 56. [CrossRef]
19. Tian, H.; Chen, G.; Zhang, C.; Melillo, J.M.; Hall, C.A.S. Pattern and variation of C:N:P ratios in China's soils: A synthesis of observational data. *Biogeochemistry* **2010**, *98*, 139–151. [CrossRef]

20. Alfaro, M.R.; Nascimento, C.W.A.; Biondi, C.M.; Silva, Y.J.A.B.; Accioly, A.M.; Montero, A.; Ugarte, O.M.; Estevez, J. Rare-earth-element geochemistry in soils developed in different geological settings of Cuba. *Catena* **2018**, *162*, 317–324. [CrossRef]
21. Li, G.P. Progress and propects in research of mountain meteorogy in China during the past 25 years. *Adv. Meteorol. Sci. Technol.* **2016**, *6*, 115–122. (In Chinese)
22. Wang, S.N.; Pu, J.B.; Li, J.H.; Zhang, T.; Huo, W.J.; Yuan, D.X. Climatic chararacteristics under the influence of basin-mountain coupled topography and its influence on the ecological restoration of rocky desertification in a Mengzi karst graben basin, Southwest China. *Carsol. Sin.* **2019**, *38*, 50–59. (In Chinese)
23. Tyler, G.L.; Olsson, T. Conditions related to solubility of rare and minor elements in forest soils. *J. Plant Nutr. Soil Sci.* **2002**, *165*, 594–601. [CrossRef]
24. Bao, S.D. *Soil Agricultural Chemistry Analysis*; China Agricultural Publishing House: Beijing, China, 2000. (In Chinese)
25. Olsen, S.R. *Estimation of Available Phosphorus in Soils by Extraction with Sodium Bicarbonate*; United States Department of Agriculture: Washington, DC, USA, 1954.
26. Cleveland, C.; Liptzin, D. C:N:P stoichiometry in soil: Is there a "Redfield ratio" for the microbial biomass? *Biogeochemistry* **2007**, *85*, 235–252. [CrossRef]
27. Wei, F.S.; Chen, J.S.; Wu, Y.Y.; Zheng, C.J. Study on the background contents on elements of soils in China. *Chin. J. Environ. Sci.* **1991**, *12*, 12–19.
28. Zhu, T.; Zeng, S.; Qin, H.; Zhou, K.; Yang, H.; Lan, F.; Huang, F.; Cao, J.; Müller, C. Low nitrate retention capacity in calcareous soil under woodland in the karst region of southwestern China. *Soil Biol. Biochem.* **2016**, *97*, 99–101. [CrossRef]
29. Yang, H.; Zhang, L.K.; Yu, S.; Cao, J.H. Effects of different land-uses on the features of water-stable aggregates in karst and clasolite areas in Maocun, Guilin. *Carsol. Sin.* **2012**, *31*, 265–271. (In Chinese)
30. Hu, L.N.; Su, Y.R.; He, X.Y.; Li, Y.; Li, L.; Wang, Y.H.; Wu, J.S. The speciation and content of calcium in karst soils, and its effects on soil organic carbon in karst region of Southwest China. *Sci. Agric. Sin.* **2012**, *45*, 1946–1953.
31. Cao, J.H.; Yuan, D.X.; Pan, G.X. Some soil features in karst ecosystem. *Adv. Earth Sci.* **2003**, *18*, 37–44. (In Chinese)
32. Duan, Z.F.; Fu, W.L.; Zen, X.J.; Du, F.Z. Correlation between soil organic carbon and water-stable aggregate in karst area-A case study in Zhongliangshan karst valley, Chongqing. *Carsol. Sin.* **2009**, *28*, 75–79. (In Chinese)
33. Yang, H.; Zhang, L.K.; Cao, J.H.; Yu, S. Comparison of mineralization and chemical structure of the soil organic carbon under different land uses in Maocun karst area, Guilin. *Carsol. Sin.* **2011**, *30*, 410–416. (In Chinese)
34. Shen, Y.; Fu, W.L.; Lan, J.C.; Cheng, H.; Zhang, S.Q.; Wu, L.Z. Distribution characteristics of soil particulate organic carbon and mineral-associated organic carbon of different land use in karst mountain. *Res. Soil Water Conserv.* **2012**, *19*, 1–6.
35. Chen, X.B.; He, X.Y.; Hu, Y.J.; Su, Y.R. Characteristics and mechanisms of soil organic carbon accumulation and stability in typical karst ecosystems. *Res. Agric. Mod.* **2018**, *39*, 907–915. (In Chinese)
36. Yang, H.; Liang, Y.; Xu, J.M.; Cao, J.H. Research progress of the relationship between soil calcium and soil organic carbon in karst area. *Guangxi Sci.* **2018**, *25*, 505–514. (In Chinese)
37. Yang, H.; Chen, J.R.; Liang, J.H.; Cao, J.H. Preliminary study on the relationship between soil organic carbon and pH value and calcium species in Yaji karst region, Giulin. *Geol. Rev.* **2017**, *63*, 1117–1126. (In Chinese)
38. Yang, H.; Cao, J.H.; Sun, L.; Luan, H.N.; Hou, Y.L. Fractions and distribution of inorganic phosphorus in different land use types of karst area. *J. Soil Water Conserv.* **2010**, *24*, 135–140. (In Chinese)
39. Wen, J.; Ji, H.; Sun, N.; Tao, H.; Du, B.; Hui, D.; Liu, C. Imbalanced plant stoichiometry at contrasting geologic-derived phosphorus sites in subtropics: The role of microelements and plant functional group. *Plant Soil* **2018**, *430*, 113–125. [CrossRef]
40. Yang, H.; Zhu, T.B.; Wang, X.H.; Pu, J.B.; Li, J.H.; Zhang, T.; Cao, J.H. Soil element contents of typical small watershed in the plateau area of karst fault basin, Yunnan. *Ecol. Environ. Sci.* **2018**, *27*, 859–865. (In Chinese)
41. Sheng, M.Y.; Xiong, K.N.; Cui, G.Y.; Liu, Y. Plant diversity and soil physical-chemical properties in karst rocky desertification ecosystem of Guizhou, China. *Acta Ecol. Sin.* **2015**, *35*, 434–448. (In Chinese)
42. Bárcenas-Moreno, G.; Rousk, J.; Bååth, E. Fungal and bacterial recolonisation of acid and alkaline forest soils following artificial heat treatments. *Soil Biol. Biochem.* **2011**, *43*, 1023–1033. [CrossRef]

43. Grabovich, M.Y.D.G.; Churikova, V.V.; Churikov, S.N.; Korovina, T.I. Mechanisms of synthesis and utilization of oxalate inclusions in the colorless sulfur bacterium Macromonas bipunctata. *Mikrobiology* **1995**, *64*, 630–636.
44. Silver, W.L.; Miya, R.K. Global patterns in root decomposition: Comparisons of climate and litter quality effects. *Oecologia* **2001**, *129*, 407–419. [CrossRef]

forests

MDPI

Article

Differential Responses and Controls of Soil CO_2 and N_2O Fluxes to Experimental Warming and Nitrogen Fertilization in a Subalpine Coniferous Spruce (*Picea asperata* Mast.) Plantation Forest

Dandan Li [1], Qing Liu [1,*], Huajun Yin [1], Yiqi Luo [2] and Dafeng Hui [3]

[1] Key Laboratory of Mountain Ecological Restoration and Bioresource Utilization & Ecological Restoration Biodiversity Conservation Key Laboratory of Sichuan Province, Chengdu Institute of Biology, Chinese Academy of Sciences, Chengdu 610041, China; ddli1984@hotmail.com (D.L.); yinhj@cib.ac.cn (H.Y.)
[2] Department of Biological Sciences, Northern Arizona University, Flagstaff, AZ 86001, USA; Yiqi.Luo@nau.edu
[3] Department of Biological Sciences, Tennessee State University, Nashville, TN 37209, USA; dhui@tnstate.edu
* Correspondence: liuqing@cib.ac.cn

Received: 13 August 2019; Accepted: 15 September 2019; Published: 17 September 2019

Abstract: Emissions of greenhouse gases (GHG) such as CO_2 and N_2O from soils are affected by many factors such as climate change, soil carbon content, and soil nutrient conditions. However, the response patterns and controls of soil CO_2 and N_2O fluxes to global warming and nitrogen (N) fertilization are still not clear in subalpine forests. To address this issue, we conducted an eight-year field experiment with warming and N fertilization treatments in a subalpine coniferous spruce (*Picea asperata* Mast.) plantation forest in China. Soil CO_2 and N_2O fluxes were measured using a static chamber method, and soils were sampled to analyze soil carbon and N contents, soil microbial substrate utilization (MSU) patterns, and microbial functional diversity. Results showed that the mean annual CO_2 and N_2O fluxes were 36.04 ± 3.77 mg C m^{-2} h^{-1} and 0.51 ± 0.11 μg N m^{-2} h^{-1}, respectively. Soil CO_2 flux was only affected by warming while soil N_2O flux was significantly enhanced by N fertilization and its interaction with warming. Warming enhanced dissolve organic carbon (DOC) and MSU, reduced soil organic carbon (SOC) and microbial biomass carbon (MBC), and constrained the microbial metabolic activity and microbial functional diversity, resulting in a decrease in soil CO_2 emission. The analysis of structural equation model indicated that MSU had dominant direct negative effect on soil CO_2 flux but had direct positive effect on soil N_2O flux. DOC and MBC had indirect positive effects on soil CO_2 flux while soil NH_4^+-N had direct negative effect on soil CO_2 and N_2O fluxes. This study revealed different response patterns and controlling factors of soil CO_2 and N_2O fluxes in the subalpine plantation forest, and highlighted the importance of soil microbial contributions to GHG fluxes under climate warming and N deposition.

Keywords: warming; nitrogen; greenhouse gas; soil characteristics; microbial properties

1. Introduction

Due to fossil fuel combustion and land use change, global air temperature has been increasing over the past decades [1]. The Qinghai–Tibet Plateau region (QTP) of China is experiencing a larger increase in temperature than other regions with an increasing rate of 0.2 °C per decade [2]. Accompanied with climate warming, nitrogen (N) deposition is increasing in many places on the Earth [3]. China has the third highest rate of nitrogen deposition, followed by North America and Western Europe due to the industrialization and intensive agricultural activities [3,4]. Additionally, in the QTP region, N deposition continues to increase. The climate warming and N deposition are likely to have significant

impacts on greenhouse gases (GHG) emissions in QTP ecosystems because the high-latitude regions are very sensitive to global change with large soil C pool, low inorganic N availability, and higher temperature sensitivity [3].

Carbon dioxide (CO_2) and nitrous oxide (N_2O) are two important GHGs, which contribute to about 60% and 6% of the global warming potential, respectively [2,5]. Many studies have investigated the effects of warming and N deposition on soil GHG fluxes, but large uncertainties still remain. For example, some studies found that warming leads to increase in soil CO_2 emission because it accelerates the decomposition of soil organic C (SOC) [6], but others reported that warming decreases or has no effect on soil CO_2 emission due to the loss of SOC in a long-term warming experiment [7]. Climate warming generally increases soil N_2O flux by enhancing decomposition and N mineralization [8,9], however, it may not influence soil N_2O flux or decrease it depending on the soil conditions [10]. Studies on the effect of N fertilization or deposition on GHG fluxes also showed various results. For example, Jassal et al. [11] found that the N application increases soil CO_2 and N_2O emissions in the first year, but shifts to soil N_2O uptake has no effect on soil CO_2 emission in the second year. Geng et al. [12] reported that the N addition at a low rate of 10 kg N ha^{-1} $year^{-1}$ significantly stimulated soil CO_2 emission, whereas the high rate of N addition (140 kg N ha^{-1} $year^{-1}$) significantly inhibits soil CO_2 emission in a temperate mixed forest.

The different responses of soil CO_2 and N_2O fluxes to global warming and N fertilization in different environments could be determined by soil physical–chemical properties such as soil temperature, soil inorganic nitrogen availability, and soil carbon content [13,14]. One study showed that soil CO_2 flux is positively related to soil dissolve organic carbon (DOC) and NO_3^--N, and soil N_2O flux is positively correlated with soil NH_4^+-N [14]. Another study found that soil CO_2 efflux is positively correlated with soil NH_4^+-N and negatively with soil NO_3^--N [12]. Thus, any changes in these soil properties caused by warming and N fertilization could have different impacts on GHG fluxes [15]. Indeed, Geng et al. [12] found high N addition enhances soil NO_3^--N and inhibits soil CO_2 emission, while low N addition does not affect soil NO_3^--N but stimulates soil CO_2 emission. Seo et al. [16] found warming increases the labile C pool, causes a loss of soil C, and increases soil CO_2 emission. Yin et al. [7] reported that warming decreases SOC and decreases soil CO_2 emission.

The influences of warming and N deposition on soil microbial activity and composition may have significant impacts on soil CO_2 and N_2O fluxes. Soil microorganisms are the major drivers in the biogeochemical processes such as soil C decomposition and N mineralization [17,18]. Any changes in soil microbial diversity and community structure may alter the C and N cycling [17]. For instance, the fungi to bacteria ratio is negatively correlated to soil N mineralization [19]. Furthermore, soil microorganisms can be affected by multiply factors such as climate, soil physical, and chemical properties, and substrate quantity and quality [20,21]. Several studies reported that soil microbial community structure and diversity are strongly impacted by warming and N fertilization, and play an important role on controlling soil CO_2 and N_2O fluxes [17,22,23]. However, convincing data about the direct link of soil GHG fluxes and soil microbial characteristics under warming and N fertilization are still scarce.

The subalpine and alpine forest ecosystems in Eastern Tibetan Plateau, located at the high latitude of the transition zone from the QTP to Sichuan basin, constitute the second largest biome in China and are the main forest ecosystems in southwest China [24]. Spruce (*Picea asperata* Mast.) is the dominant tree species of the plantation, which is the major forest ecosystem in this region after deforestation in the 1950s. Past studies on climate warming and N fertilization in forests in this region mostly focused on the soil C pool and N pool and associated processes [7,25,26]. Although soil GHG fluxes are highly related to the soil C and N pool, these data are not directly reflecting the GHG magnitude. Direct evidence of variations of the responses of soil CO_2 and N_2O fluxes and their controls is needed.

We took advantage of an eight-year field experiment with warming and N fertilization in subalpine spruce plantation forest, and measured soil CO_2 and N_2O fluxes over one year using the static chamber method. We also analyzed soil C and N contents, microbial substrate utilization patterns, and microbial

functional diversity using BIOLOG microplates. We aimed to quantify the magnitude of soil CO_2, N_2O fluxes in the plantation forest and the effects of climate warming and applying N fertilization on the gas fluxes, and reveal influential factors that control soil CO_2 and N_2O fluxes.

2. Materials and Methods

2.1. Experimental Site

The experimental site is located at the Maoxian Ecological Station of the Chinese Academy of Sciences, Sichuan Province, China (31°41′ N, 103°53′ E, 1820 m a.s.l.). The site is in a subalpine canyon zone at the transition region from Qinghai–Tibet Plateau (QTP) to Sichuan basin, with the mean annual temperature, total annual precipitation, and evaporation of 8.9 °C, 920 mm, and 796 mm, respectively. The experiment started in March 2007 with warming and N fertilization treatments and ended in 2015. Soil CO_2 and N_2O fluxes were measured for one year from 14 June 2014 to 25 June 2015, eight years after the treatments were applied.

2.2. Experimental Set-Up and Design

To avoid the potential effects of soil heterogeneity on soil GHG fluxes, we collected the top 50 cm soil from a nearby spruce plantation forest and replaced the indigenous soil in all plots. In March 2007, 40 healthy four-year-old seedlings of spruce were randomly planted in each plot (2 m × 2 m). The seedlings were collected from a local nursery. The experiment included four treatments: Control, warming, N fertilization, and warming and N fertilization. A randomized block design with four replicates (blocks) was used in this study. Artificial warming and N application started in April 2007 and continued to the end of the experiment. The heating method were described in detail in published papers of our research team [27,28]. Ammonium nitrate solution (25 g N m^{-2} $year^{-1}$) was added weekly to the soil surface of fertilization treatment. The equivalent amount of water was added to the other four pairs of plots for unfertilized treatments. In order to eliminate the potential effects of difference in soil water on soil processes between the warmed and un-warmed plots, the warmed plots were watered as frequently as needed and were monitored with a hand-held probe (IMKO, Ettlingen, Germany).

2.3. Microclimate Measurements

Air temperature (20 cm above soil surface) and soil temperature (5 cm depth) were measured using the DS1923G temperature sensor with iButton data loggers (Maxim/Dallas Semiconductor Inc., Dallas, TX, USA) at 60 min intervals. The warming effect decreased with the trees growth and plant coverage. The monthly air temperature in the warmed plots was increased by an average of 2.1, 1.9, 0.3 °C in 2007, 2011, and 2014, respectively. The monthly soil temperature in the warmed plots was increased by an average of 2.6, 3.6, and 0.6 °C in 2007, 2011, and in 2014, respectively.

2.4. Soil CO_2 and N_2O Fluxes Measurements

Soil CO_2 and N_2O fluxes were measured monthly using the static chamber method and gas chromatography technique from 14 June 2014 to 25 June 2015 according to Cai et al. [29]. One PVC tube base with a groove outside but without top and bottom (20 cm inside diameter, and 15 cm height) was inserted into a 10 cm-depth soil in each plot. The removable chamber with a small silicon-sealed bent for gas sampling and a port for measuring chamber temperature at the top of the chamber (without bottom, 21 cm in diameter and 30 cm in height) was placed into the PVC tube base during sampling and removed afterwards. Litter and plants were removed around the tube base before fixing it and four replicates were set in each treatment.

Samples were taken between 10:00 a.m. and 1:00 p.m. in order to minimize diurnal variation in fluxes. Each time, four air samples of each chamber were manually pulled into 100 mL pre-evacuated gas collecting bags (made in Dalian, China) at 0, 15, 30, and 45 min after enclosure of the chamber, and

were taken to the laboratory for analysis using gas chromatography (Agilent 7890A, Santa Clara, CA, USA) within two weeks. Air temperature inside the chamber was measured with a mercury-in-glass thermometer at the time of gas sampling. Soil temperature and moisture were measured outside of each chamber with the DS1923G temperature sensor with iButton data loggers (Maxim/Dallas Semiconductor Inc., Dallas, TX, USA).

Soil CO_2 and N_2O fluxes were calculated as the slope of linear regression between gases concentration and time with an average chamber temperature [30]. All the coefficients of the linear regression (r^2) were greater than 0.80 in this study. Flux was calculated as:

$$\mathrm{F} = \frac{dc}{dt} \times \frac{\mathrm{p}}{0.082\mathrm{T}} \times \mathrm{M} \times \frac{\mathrm{V}}{\mathrm{A}} \quad (1)$$

where F is the gas flux (μg N m^{-2} h^{-1} for N_2O and mg C m^{-2} h^{-1} for CO_2), $\frac{dc}{dt}$ is the rate of change in gas concentration inside the chamber, p is barometric pressure at temperature T (atm), T is the air temperature inside the chamber in K, M is the molecular weight of the gas, 0.082 is the universal gas constant, V is the chamber volume (m^3) and A is the chamber area (m^2).

2.5. Soil Samples and Analysis

Soil samples (n = 4) in each treatment were collected in August and November of 2014, and February and May of 2015. At each sampling date, we took five topsoil (0–15 cm) cores (2.5 cm diameter) close to each chamber and then combined into one composite sample. Soil samples were sieved through 2 mm mesh to remove visible living plant and rock, stored in an icebox at 4 °C, and delivered to the laboratory for analysis.

Soil organic C (SOC) was determined using the $K_2Cr_2O_7$-H_2SO_4 wet digestion method [31]. After digestion with $K_2Cr_2O_7$-H_2SO_4, $FeSO_4$ was used to titrate the remaining $K_2Cr_2O_7$ in the digestion solution and SOC was calculated based on the consumptions of the $K_2Cr_2O_7$. The dissolve organic C (DOC) was measured using the $K_2Cr_2O_7$-H_2SO_4 wet digestion method after extracted by deionized water [32]. Total soil N (TN) was determined by semi-micro Kjeldahl digestion using Se, $CuSO_4$, and K_2SO_4 as catalysts [33]. Soil ammonium (NH_4^+), nitrate (NO_3^-), and nitrite (NO_2^-)-N concentrations were determined using Auto Analyzer 3 (AA3, Bran Luebbe, Norderstedt, Germany) after being extracted with 2 M KCl solution (soil:water = 1:5) for 1 h [34]. Microbial biomass C (MBC) and N (MBN) concentrations were measured with the chloroform fumigation extraction method [35]. MBC and MBN were calculated as the difference between the C and N concentrations extracted with 2 M K_2SO_4 solution of the fumigated and non-fumigated soil, respectively, and then divided an efficiency factor K = 0.45. All the concentrations were calculated based on soil dry weight.

Microbial substrate utilization (MSU) patterns were analyzed using BIOLOG ECO plates (Biolog, Inc., Hayward, CA, USA). Equivalent to 1.0 g dry soil from each fresh sample was first added into 99 mL distilled autoclaved water and was shaken for 20 min to ensure that all the fungal spores are well mixed. Then, the soil solutions were settled for 30 min at 4 °C to remove suspended clay particles. 150 μL supernatant was transferred to the plates and then was incubated at 25 °C for up to 168 h. The OD values (absorbance at 590 nm and 750 nm, respectively) were measured at each 24 h from 48 to 168 h with a microtiter-plate reader (Biolog GenIII Microstation, Biolog company, Hayward, CA, USA). The OD value at 590 nm subtracting the OD value at 750 nm, and then the difference in the control was subtracted from each well's OD to correct for background activity. To minimize the effects of different inoculation densities, data from the 96 h reading were normalized by h dividing the absorbency of each well by the average absorbency for the whole plate (average well color development, AWCD) [17]. AWCD reflect the metabolic activity of soil microbes. Moreover, the Shannon diversity index (H) and diversity index (U) were calculated to represent the diversity and uniformity of the microbial communities.

$$H = -\sum p_i ln p_i \quad (2)$$

$$U = \sqrt{\left(n_i^2\right)} \quad (3)$$

where $p_i = \frac{OD(i,j,t)}{\sum OD(i,j,t)}$; and $n_{i=OD(i,j,t)}$

2.6. Data Analysis

The exponential model was used to determine the sensitivity of soil GHG fluxes to soil temperature (T):

$$F = ae^{bT} \quad (4)$$

where F is the GHG flux, a is the value of flux at 0 °C, and b is the sensitivity of flux to temperature.

The flux sensitivity to temperature (Q_{10}) was calculated as:

$$Q_{10} = e^{10b} \quad (5)$$

The cumulative global warming potential (GWP, kg CO_2 hm^{-2}) was calculated by adding cumulative soil CO_2 flux, and the cumulative GWP from N_2O (cumulative N_2O flux multiplied by 298) [36].

The repeated measure-ANOVA was used to analyze the effects of warming and N fertilization on soil CO_2 and N_2O fluxes. A three-way analysis of variance (ANOVA) was used to test the effects of warming, N fertilization, and sample time (season) on TOC, DOC, TN, inorganic N, AWCD, H, and U. The ECO plates contained 31 types of carbon substrates. The microbial substrates utilization patterns were analyzed to identify the effects of treatments and soil environment factors such as soil water, temperature, soil DOC, SOC, and inorganic nitrogen using Canonical Correspondence Analysis (CCA) in the CANOCO 4.5 software (Microcomputer Power, Ithaca, NY, USA).

Structural equation modelling (SEM) was performed to determine the relative importance of soil variables to soil CO_2 and N_2O fluxes using the Amos 24.0 software package (IBM, New York, NY, USA). We first tested the relationships between the CO_2 and N_2O fluxes and soil properties before the SEM analysis. If the correlation was significant, that variable was put into the SEM. As microbial substrate utilization patterns included 31 types of carbon source utilization, we selected the significant correlations of the carbon source utilization with soil CO_2 and N_2O fluxes, and then used the Principal Component Analysis (PCA) to create a multivariate functional index. The best-fit model was derived using maximum likelihood and a chi-square test (χ^2), P-values, df, and root mean square errors of approximation (RSMEA) were used to evaluate model fitting.

3. Results

3.1. Soil Carbon, Nitrogen and Microbial Properties

Warming significantly increased soil NO_3^--N, NO_2^--N, DOC, and the ratio of MBC/MBN, but decreased TN, SOC, MBC, and MBN (Table 1). Nitrogen fertilization significantly increased soil NO_3^--N, TN, TOC, and the ratio of MBC/MBN, but decreased soil NO_2^--N, DOC, MBC, and MBN. The metabolic activity of soil microbes measured as the average absorbency for the whole BIOLOG ECO plate (AWCD), the Shannon diversity index (H), and uniformity index (U) varied seasonally (Table 1). Warming decreased AWCD and U. Nitrogen fertilization alone had no effect on AWCD and U but significantly affected these variables with warming. The CCA analysis identified 21 substrates that were the most important variables in separating plots along the environmental axes among the 31 carbon substrates (Figure 1). Most of these MSU patterns were correlated with temperature, soil DOC, and soil water. The correlation coefficient were 0.68, 0.72, −0.72 in CCA1 and −0.62, −0.18, 0.32 in CCA2 for temperature, soil DOC, and soil water, respectively.

Table 1. Factorial ANOVA results (p-values) of the effects of season, warming, nitrogen fertilization, as well as their interactions on the soil properties and microbial function diversity. MBC: Microbial biomass C, MBN: Microbial biomass N, SOC: Soil organic C, DOC: Dissolved organic C, TN: Total N, AWCD: Average well color development, H: Shannon diversity index, U: Uniformity.

Treatments	NO_3^--N	NH_4^+-N	NO_2^--N	TN	SOC	DOC	MBC	MBN	MBC/MBN	AWCD	H	U
Season (S)	<0.001	<0.001	<0.001	<0.001	<0.001	<0.001	<0.001	<0.001	<0.001	0.001	<0.001	0.010
Warming (W)	<0.001	0.756	<0.001	<0.001	<0.001	<0.001	<0.001	<0.001	<0.001	0.009	0.461	0.006
Nitrogen (N)	<0.001	0.103	<0.001	0.009	<0.001	<0.001	<0.001	<0.001	<0.001	0.237	0.953	0.276
S × W	<0.001	0.322	<0.001	<0.001	<0.001	<0.001	<0.001	<0.001	<0.001	<0.001	0.032	<0.001
S × N	<0.001	0.008	0.040	0.365	<0.001	<0.001	<0.001	<0.001	<0.001	0.002	0.013	0.006
W ×N	0.565	0.011	0.059	0.015	<0.001	0.002	0.003	<0.001	<0.001	0.016	0.115	0.032
S × W × N	<0.001	0.209	<0.001	0.080	<0.001	<0.001	<0.001	<0.001	<0.001	0.001	0.002	0.004

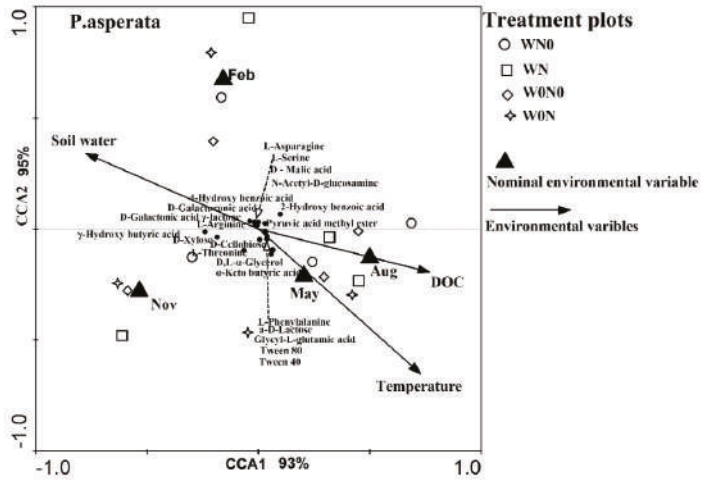

Figure 1. Canonical correspondence analysis (CCA) ordination biplot of treatment plot scores, Biolog substrates, and significant environmental variables. Arrows indicate the direction and relative importance (arrow length) of the environmental variable. Substrates with approximate correlation coefficient >0.20 to the environmental variables are labelled. W_0N_0: Ambient temperature without nitrogen fertilization; W_0N: Ambient temperature with nitrogen fertilization; WN0: Warming without nitrogen fertilization; WN: Warming with nitrogen fertilization. Environmental variables in CCA1 and CCA2 explain 93% and 95%, respectively.

3.2. Soil CO_2 and N_2O Fluxes

The highest soil CO_2 and N_2O fluxes occurred in August and the lowest in January (Figure 2). The mean annual CO_2 and N_2O fluxes were 36.04 ± 3.77 mg C m^{-2} h^{-1} and 0.51 ± 0.11 μg N m^{-2} h^{-1}, respectively (Table 2). Compared to the control (W_0N_0), the annual soil CO_2 flux was slightly decreased in the WN_0 and WN treatments but was increased by 27.8% in the W_0N treatment. Annual soil N_2O flux was increased by 8.2 times and 3.0 times in the W_0N and WN treatments. Soil CO_2 flux was mainly affected by warming, while soil N_2O flux was mainly affected by N fertilization and its interaction with warming. The cumulative GWP from CO_2 and N_2O were 9984 ± 321 and 20.31 ± 3.02 kg CO_2 hm^{-2}, respectively (Table 2).

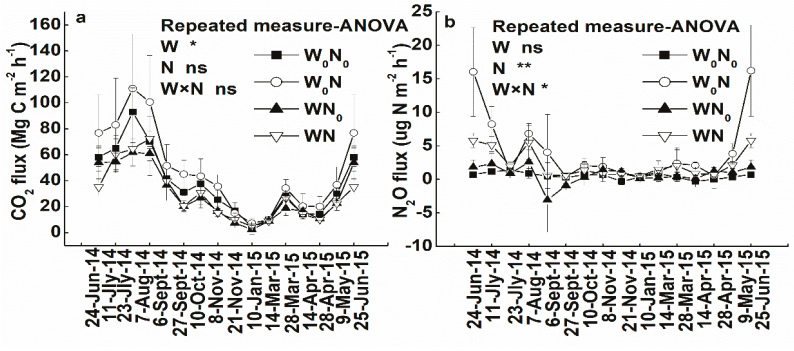

Figure 2. Seasonal changes of soil CO_2 (**a**) and N_2O fluxes (**b**) affected by warming and nitrogen fertilization. W_0N_0: Ambient temperature without nitrogen fertilization; W_0N: Ambient temperature with nitrogen fertilization; WN_0: Warming without nitrogen fertilization; WN: Warming with nitrogen fertilization.

Table 2. Mean annual fluxes of CO_2 (mg m^{-2} h^{-1}), N_2O (μg N m^{-2} h^{-1}) (means + SE) and the cumulative global warming potential (GWP) from CO_2 and N_2O fluxes (kg CO_2 hm^{-2} $year^{-1}$) as affected by treatments.

Variables	Treatment	CO_2	N_2O
Fluxes	W_0N_0	36.04 ± 3.77 ^{ab}	0.51 ± 0.11 ^{a}
	WN_0	27.90 ± 3.14 ^{a}	0.65 ± 0.27 ^{a}
	W_0N	46.08 ± 5.39 ^{b}	4.68 ± 1.61 ^{b}
	WN	29.07 ± 3.29 ^{a}	2.02 ± 0.32 ^{b}
GWP	W_0N_0	9984 ± 321 ^{ab}	20.31 ± 3.02 ^{a}
	WN_0	7800 ± 844 ^{a}	25.63 ± 10.33 ^{a}
	W_0N	12748 ± 2110 ^{b}	208.8 ± 56.37 ^{b}
	WN	8002 ± 282 ^{a}	79.88 ± 8.90 ^{b}
ANOVA (F values)	Warming	8.97 *	4.52
	N fertilization	1.64	17.47 **
	Warming * N fertilization	1.27	5.34 *

Different lowercase letters represent significant differences ($p < 0.05$) between the treatments analyzed by least-significant difference (LSD). Significant * $p < 0.05$, ** $p < 0.01$, *** $p < 0.001$.

3.3. Relationship between the Soil CO_2 and N_2O Fluxes and Environmental Factors

Soil CO_2 and N_2O fluxes increased exponentially with soil temperature across all treatments (Figure 3). The Q_{10} values for CO_2 flux were not significantly different among the control, W_0N, and WN_0 treatments, while Q_{10} in the WN treatment was increased to 5.54 compared to the control (3.94). The Q_{10} values for soil N_2O flux was increased by N fertilization without warming but was decreased by N fertilization with warming.

Soil CO_2 flux was positively correlated with soil MBC, DOC and the microbial substrates utilization, and negatively correlated with soil NH_4^+-N. Soil N_2O flux was positively correlated with the MSU and negatively correlated with soil NH_4^+-N (Figure 3).

3.4. Contributions of Soil Variables to Soil CO_2 and N_2O Fluxes

To quantify the relative importance of the different controlling factors on soil CO_2 and N_2O fluxes, two structural equation modellings (SEMs) were constructed based on the known relationships between soil CO_2 and N_2O fluxes and their key drivers in soil. The SEM showed a better fit to our hypothesized causal relationships ($\chi^2 = 2.82$, $p = 0.59$, RMSEA) = 0.000, Figure 4a; $\chi^2 = 0.81$, $p = 0.94$, RMSEA = 0.000, Figure 4b). The models accounted for 63% and 22% of the variance of soil CO_2 and N_2O fluxes, respectively. Microbial substrates utilization patterns had dominant direct negative effect on soil CO_2 flux and positive effect on N_2O (Figure 5). Soil NH_4^+-N had negative effects on soil CO_2 and N_2O fluxes. DOC and MBC had indirect positive effects on soil CO_2. In addition, soil NO_3^--N and NO_2^--N had indirect effects on soil N_2O.

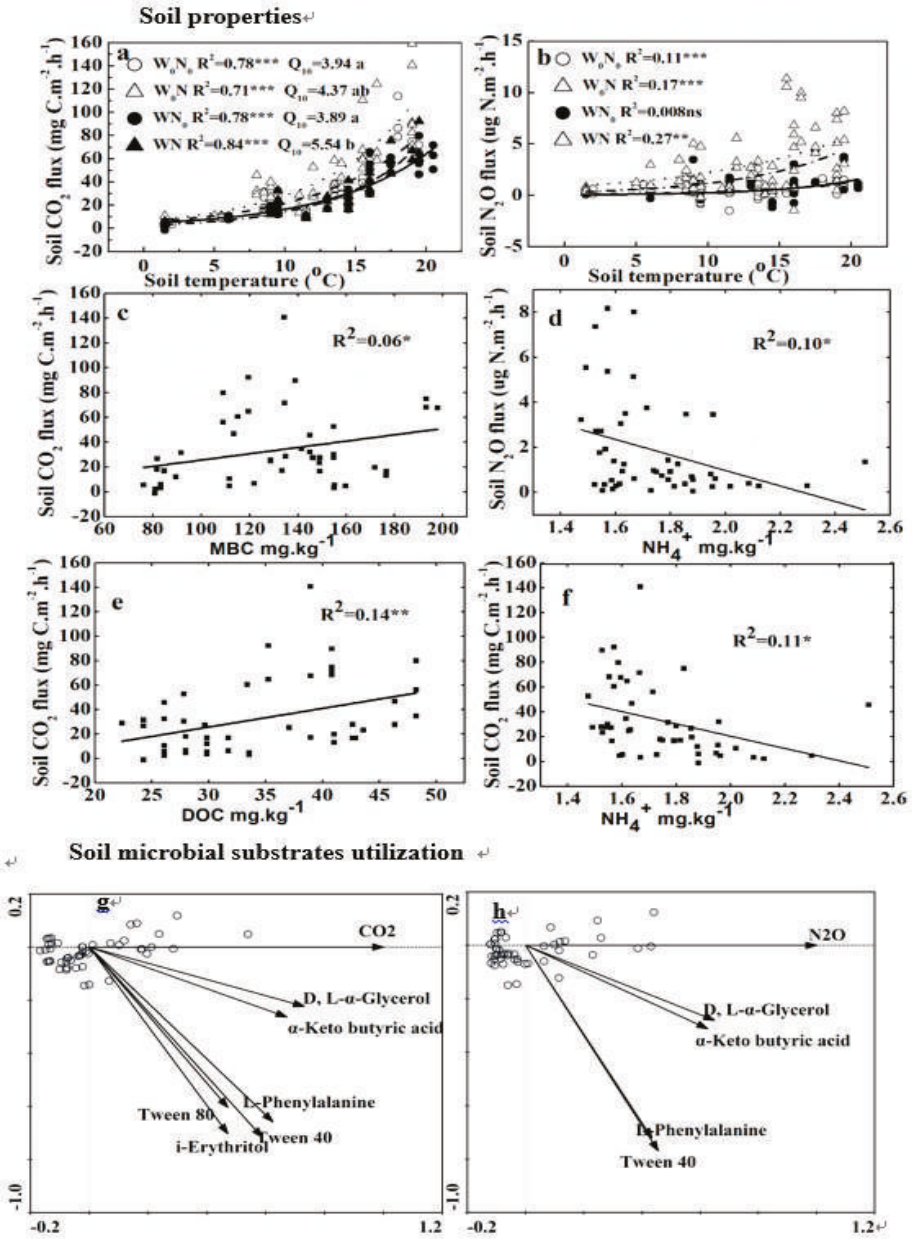

Figure 3. Relationships between the fluxes of soil CO_2 and soil temperature (**a**), MBC (**c**), DOC (**e**), soil NH_4^+ (**f**) and soil microbial substrates utilization (**g**), and between the fluxes of soil N_2O and soil temperature (**b**), soil NH_4^+ (**d**), and carbon utilization of microbial communities (**h**) in the different treatments. Q_{10} values with different lowercase letters indicate significant difference at $p < 0.05$. W_0N_0: Ambient temperature without nitrogen fertilization; W_0N: Ambient temperature with nitrogen fertilization; WN_0: Warming without nitrogen fertilization; WN: Warming with nitrogen fertilization. Different lowercase letters in Figure 3a represent significant differences ($p < 0.05$) between the treatments using least square difference (LSD) method. Significant * $p < 0.05$, ** $p < 0.01$, *** $p < 0.001$.

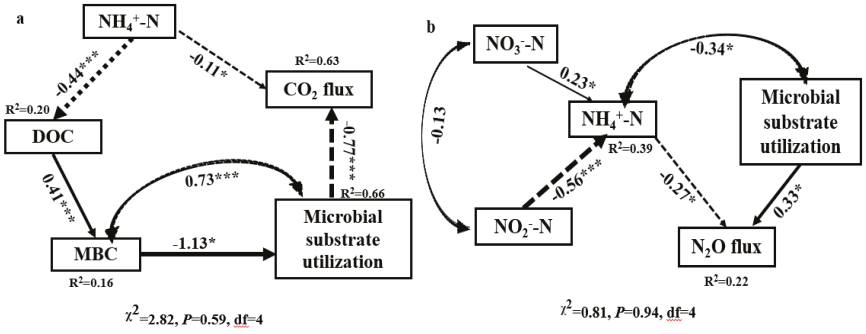

Figure 4. Result of structural equation modelling (SEM) to assess the direct and indirect effects of soil carbon, nitrogen, and microbial properties on soil CO_2 (**a**) and N_2O fluxes (**b**). Single-headed arrows indicate the hypothesized direction of causation. Double-headed arrows represent covariance between related variables. Arrow width is proportional to the strength of the relationship. The numbers adjacent to arrows are standardized path coefficient, which reflect the effect size of the relationship. R^2 value represent the proportion of variance explained for each endogenous variable. Significant * $p < 0.05$, ** $p < 0.01$, *** $p < 0.001$.

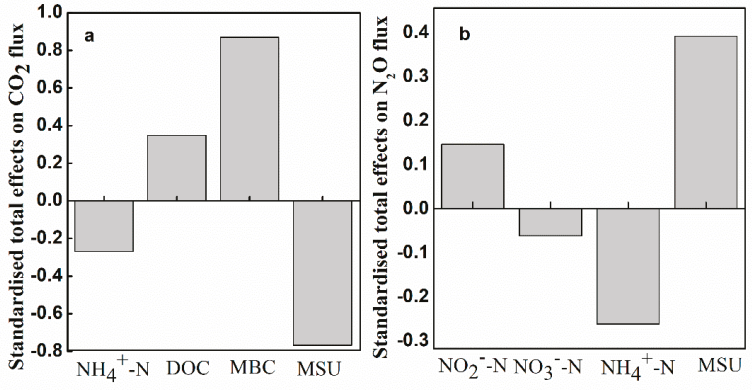

Figure 5. Standardized total effects of soil variables on soil CO_2 (**a**) and N_2O fluxes (**b**) derived from structural equation modelling (SEM). MSU: Microbial substrate utilizations; DOC: Dissolved organic C; MBC: Microbial biomass C.

4. Discussion

4.1. Effects of Warming and Nitrogen Fertilization on Soil CO_2 Flux

We found that warming decreased soil CO_2 flux, while the N fertilization and its interaction with warming had no significant effect on soil CO_2 flux (Figure 2a, Table 2). These results were quite different to some previous studies. For example, Zou et al. [5] and Xu et al. [37] found warming increases soil CO_2 flux in spruce forests, and the effect of N fertilization on soil CO_2 flux varied in forest plantations [12,38,39]. These differences were a consequence of the different soil properties and experimental conditions among these sites, as the interactions among climate, soil organisms, and vegetation, and the duration of experiment could influence soil CO_2 flux [40].

Carbon quality and quantity could regulate the responses of soil CO_2 flux to temperature. The decrease in soil respiration could be due to the consuming of labile C [41,42]. In this study, the experimental plots were filled with forest soil and spruce seedlings were planted in the plots. There was very limited C input compared to the forest plantation with mature trees. Consequently, the CO_2

emission could be restricted by less carbon in the soil [7]. Indeed, SOC and MBC at the site were lower after eight years of warming, although soil DOC was enhanced in this study. Bossio et al. [43] also found similar results. Although SEM analysis showed that soil DOC had a positive effect on soil CO_2 emission, the decreases in MBC had larger effect on soil CO_2 emission than the increases in DOC (Figures 4a and 5a). Overall, warming decreased soil CO_2 emission.

Climate warming and N fertilization studies have mostly focused on the changes of microbial processes (respiration and N mineralization) [25,26]. Few studies have investigated the direct link of soil microbial community with soil CO_2 flux. In this study, we found that microbial substrate utilization patterns had a direct negative effect on soil CO_2 flux (Figures 4a and 5a). This result suggested that there is an association of soil microbial community composition with the response of soil CO_2 flux to warming and N fertilization, as different microbial communities had different sole substrate utilization patterns in the BIOLOG ECO-plate analysis [44]. The CCA analysis further showed that the MSU patterns were positively correlated with soil DOC and soil temperature in the CCA1 although they had contrast effects in the CCA2 (Figure 3). It suggested that climate warming could enhance the activity of the microbial community and the DOC, then reduce the quantity of SOC, and finally decrease soil CO_2 emission. A similar result was reported by Walker et al. [43] who found that permanent warming accelerates microbial activity and causes more carbon loss from soil, and the soil carbon loss in return reduces soil microbial biomass and constrains the influence of microbes on the ecosystem. In this study, warming decreased the microbial metabolic activity represented by AWCD and uniformity of microbial community. The result further suggested that warming induced a shift of microbial community structure from bacteria to fungi. Since fungi have lower growth rates than bacteria on BIOLOG plates, higher fungal dominance may have lower color development rate, resulting in lower AWCD [17]. Consistently, the higher ratio of MBC/MBN in the warmed plots indicated that warming enhanced the fungi as the microbial biomass C/N ratio has been used as an indicator of changes in microbial community structure [45]. Since fungi have greater C assimilation efficiency compared to bacteria, warming decreased the CO_2 release [17,46]. These findings highlighted the important contribution of soil microbial community to soil CO_2 emission.

Moreover, soil carbon quality and quantity and microbes, soil N had a significant effect on soil CO_2 flux. Previous studies showed that the soil N availability affects the soil C turnover by modifying microbial composition and activity or through its limitation on plant growth [47,48]. With sufficient C supply, an increase in N availability could stimulate the microbial activity, and accelerate SOC mineralization [49]. In this study, there was relatively a lack of soil C and no effect on microbial community induced by N fertilization. As a result, N fertilization did not affect the soil CO_2 flux. One surprising finding was that soil NH_4^+-N had a negative effect on soil CO_2 flux in this study (Figure 4a). The positive effect of soil NH_4^+ on soil CO_2 flux had been reported in temperate and subtropical forests [12,50]. The difference between our study and the previous studies may be attributed to the following two reasons. One reason was that spruce prefers to absorb soil NO_3^--N than soil NH_4^+-N [51]. As NH_4^+ was strongly absorbed and held to cation exchange sites of SOC and clay minerals, it would lead to declines in labile C compounds and increases in complex C compounds [50,52]. Thus, soil NH_4^+ had a negative effect on soil DOC as shown in the SEM (Figure 4a). The second reason was that soil NH_4^+ had a negative relationship with the microbial substrate utilization (Figure 4), tended to inhibit soil microbial activity and community composition, and resulted in a decrease in the decomposition of SOC [50]. Therefore, soil NH_4^+ had a negative effect on soil CO_2 flux in this study.

4.2. Effects of Warming and Nitrogen Fertilization on Soil N_2O Flux

Previous studies showed strong positive correlations between soil temperature and N_2O emission in temperate forests [53,54], but quite weak correlations in tropical forests [55,56]. In this study, we found that the soil N_2O emission was slightly positively correlated with the soil temperature and warming did not significantly affect soil N_2O flux in the subalpine plantation forest. However, applying N fertilization had a positive effect on soil N_2O emission. These results suggested that the soil N

condition rather than the temperature controls soil N_2O emission. Consistent with our study, other studies also found that soil N_2O emission increased with N addition in forests [57,58]. The reasons could be that high NO_3^- deposition provided additional N for denitrification and thus increased soil N_2O emission. In this study, the fertilizer as NH_4NO_3 was added into the soil and resulted in an increase in soil NO_3^-, but the SEM indicated that the soil NH_4^+ and NO_2^- were the key factors controlling soil N_2O emission and soil NO_3^- had little effect on soil N_2O. Furthermore, N fertilization had no effect on soil NH_4^+ and decreased soil NO_2^- which may result from enhanced nitrification of soil NH_4^+ and denitrification of soil NO_2^- by nitrifier. The resulting increase in soil N_2O emission, with the depletion of soil NH_4^+, was probably not due to plant uptake as spruce prefers to uptake soil NO_3^- than NH_4^+ [51]. In theory, inorganic N, as the substrate for nitrification and denitrification processes, should be positively correlated with soil N_2O emission regardless of N forms [14,57]. However, more soil NH_4^+ decreased the soil DOC (Figure 4a) and inhibited the soil microbiomes activity (Figure 4b). Since soil N_2O emission was positively correlated with soil CO_2 flux, soil NH_4^+ had the negative effect on soil N_2O emission.

Soil microbe is another factor controlling soil N_2O emission (Figure 4b). The analysis of SEM showed that the soil microbial substrate utilization pattern had a positive effect on soil N_2O emission, which provided direct information that the soil microbial activity controls the soil N_2O emission under global change. Several previous studies showed that climate change can impact N transformations and N_2O emissions via indirect effects on the abundance of different microbial populations and microbial community structure [9,59]. For instance, Cantarel et al. [9] showed a stronger correlation of N_2O fluxes with the soil denitrification activity and the nirK denitrifiers community. In this study, the method of the BIOLOG ECO plates identified soil microbial community and functional diversity mainly through carbon substrates, which may not be sensitive to N addition and may not directly reflect N transformation. Thus, MSU patterns was not affected by N fertilization in this study. Future study is needed to determine the relative importance of the specific microbial activities in nitrification and denitrification.

Furthermore, N condition and microbes, many other soil environmental factors such as soil moisture and soil pH may influence soil N_2O emission [60]. In this study, soil moisture was not influenced by treatments as plots were monitored and watered as frequently as needed to eliminate the effects of soil moisture induced by warming. Seasonal variation of soil N_2O flux could be influenced by soil moisture change. Soil pH varied slightly seasonally and among different treatments, and might not have a large influence on soil N_2O emission. In addition, soil moisture and soil pH mainly affect the soil N availability and soil microbial activity and then indirectly influence soil N_2O emission [60]. Thus, soil N condition and soil microbes were the main factors controlling soil N_2O emission.

5. Conclusions

Eight years after continuous warming and N fertilization in a subalpine spruce plantation forest, we found that soil CO_2 flux was decreased by warming while soil N_2O flux was significantly increased by N fertilization and its interaction with warming. Warming enhanced the DOC and MSU pattern, reduced SOC and MBC, and further constrained the metabolic potential of soil microbes, uniformity index of microbial communities, and finally resulted in a decrease in soil CO_2 emission. For soil N_2O emission, the MSU pattern and soil NO_2^- had positive effects on soil N_2O flux, while the soil NH_4^+ had a negative effect on soil N_2O emission. Both for soil CO_2 flux and N_2O flux, the microbes played a more important role than other factors. This study revealed different response patterns and controls of soil CO_2 and N_2O fluxes in the subalpine plantation forest under climate warming and N deposition, and further highlighted the important contributions of soil microbes to GHG fluxes.

Author Contributions: Conceptualization, D.L. and Q.L.; Methodology, H.Y.; Software, Y.L.; Validation, D.L., Q.L., H.Y., Y.L., and D.H.; Formal analysis, Y.L. and D.H.; Investigation, D.L. and H.Y.; Resources, Q.L.; Data curation, D.L.; Writing—original draft preparation, D.L.; Writing—review and editing, D.L., Q.L., and D.H; Supervision, H.Y.; Project administration, D.L.; Funding acquisition, D.L. and Q.L.

Funding: This research was funded by the National Key R&D Program of China, 2017YFC0505002 and the China Scholarship Council, CSC201804910053.

Acknowledgments: We would like to express our gratitude to the Maoxian Ecological Station of the Chinese Academy of Sciences, Sichuan Province, China, who gave permission to conduct the experiment in this study.

Conflicts of Interest: The authors declare no conflict of interest.

References

1. Trenberth, K.E. Stronger evidence of human influences on climate—The 2001 IPCC assessment. *Environment* **2001**, *43*, 8–19. [CrossRef]
2. IPCC. *Climate Change 2013: The Physical Science Basis*; Cambridge University Press: Cambridge, UK; New York, NY, USA, 2013.
3. Chen, X.P.; Wang, G.X.; Zhang, T.; Mao, T.X.; Wei, D.; Hu, Z.Y.; Song, C.L. Effects of warming and nitrogen fertilization on GHG flux in the permafrost region of an alpine meadow. *Atmos. Environ.* **2017**, *157*, 111–124. [CrossRef]
4. Galloway, J.N.; Cowling, E.B. Reactive nitrogen and the world: 200 years of change. *Ambio* **2002**, *31*, 64–71. [CrossRef]
5. Zou, J.L.; Tobin, B.; Luo, Y.Q.; Osborne, B. Differential responses of soil CO_2 and N_2O fluxes to experimental warming. *Agric. For. Meteorol.* **2018**, *259*, 11–22. [CrossRef]
6. Wu, Z.T.; Dijkstra, P.; Koch, G.W.; Penuelas, J.; Hungate, B.A. Responses of terrestrial ecosystems to temperature and precipitation change: A meta-analysis of experimental manipulation. *Glob. Chang. Biol.* **2011**, *17*, 927–942. [CrossRef]
7. Yin, H.J.; Xiao, J.; Li, Y.F.; Chen, Z.; Cheng, X.Y.; Zhao, C.Z.; Liu, Q. Warming effects on root morphological and physiological traits: The potential consequences on soil C dynamics as altered root exudation. *Agric. For. Meteorol.* **2013**, *180*, 287–296. [CrossRef]
8. Bijoor, N.S.; Czimczik, C.I.; Pataki, D.E.; Billings, S.A. Effects of temperature and fertilization on nitrogen cycling and community composition of an urban lawn. *Glob. Chang. Biol.* **2008**, *14*, 2119–2131. [CrossRef]
9. Cantarel, A.A.M.; Bloor, J.M.G.; Pommier, T.; Guillaumaud, N.; Moirot, C.; Soussana, J.F.; Poly, F. Four years of experimental climate change modifies the microbial drivers of N_2O fluxes in an upland grassland ecosystem. *Glob. Chang. Biol.* **2012**, *18*, 2520–2531. [CrossRef]
10. Hu, Y.G.; Chang, X.F.; Lin, X.W.; Wang, Y.F.; Wang, S.P.; Duan, J.C.; Zhang, Z.H.; Yang, X.X.; Luo, C.Y.; Xu, G.P.; et al. Effects of warming and grazing on N_2O fluxes in an alpine meadow ecosystem on the Tibetan plateau. *Soil Biol. Biochem.* **2010**, *42*, 944–952. [CrossRef]
11. Jassal, R.S.; Black, T.A.; Trofymow, J.A.; Roy, R.; Nesic, Z. Soil CO_2 and N_2O flux dynamics in a nitrogen-fertilized Pacific Northwest Douglas-fir stand. *Geoderma* **2010**, *157*, 118–125. [CrossRef]
12. Geng, J.; Cheng, S.L.; Fang, H.J.; Yu, G.R.; Li, X.Y.; Si, G.Y.; He, S.; Yu, G.X. Soil nitrate accumulation explains the nonlinear responses of soil CO_2 and CH4 fluxes to nitrogen addition in a temperate needle-broadleaved mixed forest. *Ecol. Indic.* **2017**, *79*, 28–36. [CrossRef]
13. Huang, R.; Wang, Y.; Liu, J.; Li, J.; Xu, G.; Luo, M.; Xu, C.; Ci, E.; Gao, M. Variation in N_2O emission and N_2O related microbial functional genes in straw- and biochar-amended and non-amended soils. *Appl. Soil Ecol.* **2019**, *137*, 57–68. [CrossRef]
14. Zhang, J.J.; Peng, C.H.; Zhu, Q.A.; Xue, W.; Shen, Y.; Yang, Y.Z.; Shi, G.H.; Shi, S.W.; Wang, M. Temperature sensitivity of soil carbon dioxide and nitrous oxide emissions in mountain forest and meadow ecosystems in China. *Atmos. Environ.* **2016**, *142*, 340–350. [CrossRef]
15. Shrestha, R.K.; Strahm, B.D.; Sucre, E.B. Greenhouse gas emissions in response to nitrogen fertilization in managed forest ecosystems. *New For.* **2015**, *46*, 167–193. [CrossRef]
16. Seo, J.; Jang, I.; Jung, J.Y.; Lee, Y.K.; Kang, H. Warming and increased precipitation enhance phenol oxidase activity in soil while warming induces drought stress in vegetation of an Arctic ecosystem. *Geoderma* **2015**, *259*, 347–353. [CrossRef]
17. Zhang, W.; Parker, K.M.; Luo, Y.; Wan, S.; Wallace, L.L.; Hu, S. Soil microbial responses to experimental warming and clipping in a tallgrass prairie. *Glob. Chang. Biol.* **2005**, *11*, 266–277. [CrossRef]

18. Qin, H.L.; Xing, X.Y.; Tang, Y.F.; Hou, H.J.; Yang, J.; Shen, R.; Zhang, W.Z.; Liu, Y.; Wei, W.X. Linking soil N_2O emissions with soil microbial community abundance and structure related to nitrogen cycle in two acid forest soils. *Plant Soil* **2019**, *435*, 95–109. [CrossRef]
19. Hogberg, P.; Hogberg, M.N.; Gottlicher, S.G.; Betson, N.R.; Keel, S.G.; Metcalfe, D.B.; Campbell, C.; Schindlbacher, A.; Hurry, V.; Lundmark, T.; et al. High temporal resolution tracing of photosynthate carbon from the tree canopy to forest soil microorganisms. *New Phytol.* **2008**, *177*, 220–228. [CrossRef]
20. Djukic, I.; Zehetner, F.; Watzinger, A.; Horacek, M.; Gerzabek, M.H. In situ carbon turnover dynamics and the role of soil microorganisms therein: A climate warming study in an Alpine ecosystem. *FEMS Microbiol. Ecol.* **2013**, *83*, 112–124. [CrossRef]
21. Gholz, H.L.; Wedin, D.A.; Smitherman, S.M.; Harmon, M.E.; Parton, W.J. Long-term dynamics of pine and hardwood litter in contrasting environments: Toward a global model of decomposition. *Glob. Chang. Biol.* **2000**, *6*, 751–765. [CrossRef]
22. Wang, Y.S.; Cheng, S.L.; Fang, H.J.; Yu, G.R.; Yang, X.M.; Xu, M.J.; Dang, X.S.; Li, L.S.; Wang, L. Relationships between ammonia-oxidizing communities, soil methane uptake and nitrous oxide fluxes in a subtropical plantation soil with nitrogen enrichment. *Eur. J. Soil Biol.* **2016**, *73*, 84–92. [CrossRef]
23. Martins, C.S.C.; Macdonald, C.A.; Anderson, I.C.; Singh, B.K. Feedback responses of soil greenhouse gas emissions to climate change are modulated by soil characteristics in dryland ecosystems. *Soil Biol. Biochem.* **2016**, *100*, 21–32. [CrossRef]
24. Xu, Z.F.; Yin, H.J.; Xiong, P.; Wan, C.; Liu, Q. Short-term responses of Picea asperata seedlings of different ages grown in two contrasting forest ecosystems to experimental warming. *Environ. Exp. Bot.* **2012**, *77*, 1–11. [CrossRef]
25. Zhao, C.; Zhu, L.; Liang, J.; Yin, H.; Yin, C.; Li, D.; Zhang, N.; Liu, Q. Effects of experimental warming and nitrogen fertilization on soil microbial communities and processes of two subalpine coniferous species in Eastern Tibetan Plateau, China. *Plant Soil* **2014**, *382*, 189–201. [CrossRef]
26. Yin, H.J.; Li, Y.F.; Xiao, J.; Xu, Z.F.; Cheng, X.Y.; Liu, Q. Enhanced root exudation stimulates soil nitrogen transformations in a subalpine coniferous forest under experimental warming. *Glob. Chang. Biol.* **2013**, *19*, 2158–2167. [CrossRef]
27. Zhang, Z.L.; Qiao, M.F.; Li, D.D.; Yin, H.J.; Liu, Q. Do warming-induced changes in quantity and stoichiometry of root exudation promote soil N transformations via stimulation of soil nitrifiers, denitrifiers and ammonifiers? *Eur. J. Soil Biol.* **2016**, *74*, 60–68. [CrossRef]
28. Yin, H.J.; Chen, Z.; Liu, Q. Effects of experimental warming on soil N transformations of two coniferous species, Eastern Tibetan Plateau, China. *Soil Biol. Biochem.* **2012**, *50*, 77–84. [CrossRef]
29. Cai, Y.J.; Wang, X.D.; Tian, L.L.; Zhao, H.; Lu, X.Y.; Yan, Y. The impact of excretal returns from yak and Tibetan sheep dung on nitrous oxide emissions in an alpine steppe on the Qinghai-Tibetan Plateau. *Soil Biol. Biochem.* **2014**, *76*, 90–99. [CrossRef]
30. Liu, H.; Zhao, P.; Lu, P.; Wang, Y.S.; Lin, Y.B.; Rao, X.Q. Greenhouse gas fluxes from soils of different land-use types in a hilly area of South China. *Agric. Ecosyst. Environ.* **2008**, *124*, 125–135. [CrossRef]
31. Walkley, A.; Black, L.A. An examination of the Dgtjareff method for determining soil organic matter, and a proposed modification of the chromic acid titration method. *Soil Sci.* **1934**, *37*, 29–38. [CrossRef]
32. Li, Y.Q.; Qing, Y.X.; Lyu, M.K.; Chen, S.D.; Yang, Z.J.; Lin, C.F.; Yang, Y.S. Effects of artificial warming on different soil organic carbon and nitrogen pools in a subtropical plantation. *Soil Biol. Biochem.* **2018**, *124*, 161–167. [CrossRef]
33. Cohen, J.B. *Practical Organic Chemistry*; Macmillan Collection Library: London, UK, 1910.
34. Maynard, D.G.; Kalra, Y.P. Nitrate and exchangeable ammonium nitrogen. In *Soil Sampling and Methods of Analysis*; Carter, M.R., Ed.; Lewis: Edmonton, AB, Canada, 1993.
35. Vance, E.D.; Brookes, P.C.; Jenkinson, D.S. An Extraction Method for Measuring Soil Microbial Biomass-C. *Soil Biol. Biochem.* **1987**, *19*, 703–707. [CrossRef]
36. Dijkstra, F.A.; Morgan, J.A.; Follett, R.F.; Lecain, D.R. Climate change reduces the net sink of CH4 and N_2O in a semiarid grassland. *Glob. Chang. Biol.* **2013**, *19*, 1816–1826. [CrossRef]
37. Xu, Z.F.; Wan, C.A.; Xiong, P.; Tang, Z.; Hu, R.; Cao, G.; Liu, Q. Initial responses of soil CO_2 efflux and C, N pools to experimental warming in two contrasting forest ecosystems, Eastern Tibetan Plateau, China. *Plant Soil* **2010**, *336*, 183–195. [CrossRef]

38. Zhang, J.J.; Li, Y.F.; Chang, S.X.; Qin, H.; Fu, S.L.; Jiang, P.K. Understory management and fertilization affected soil greenhouse gas emissions and labile organic carbon pools in a Chinese chestnut plantation. *For. Ecol. Manag.* **2015**, *337*, 126–134. [CrossRef]
39. Deng, Q.; Zhou, G.; Liu, J.; Liu, S.; Duan, H.; Zhang, D. Responses of soil respiration to elevated carbon dioxide and nitrogen addition in young subtropical forest ecosystems in China. *Biogeosciences* **2010**, *7*, 315–328. [CrossRef]
40. Barrena, I.; Menéndez, S.; Duñabeitia, M.; Merino, P.; Stange, C.F.; Spott, O.; González-Murua, C.; Estavillo, J.M. Greenhouse gas fluxes (CO_2, N_2O and CH_4) from forest soils in the Basque Country: Comparison of different tree species and growth stages. *For. Ecol. Manag.* **2013**, *310*, 600–611. [CrossRef]
41. Luo, Y.Q.; Wan, S.Q.; Hui, D.F.; Wallace, L.L. Acclimatization of soil respiration to warming in a tall grass prairie. *Nature* **2001**, *413*, 622–625. [CrossRef]
42. Oechel, W.C.; Vourlitis, G.L.; Hastings, S.J.; Zulueta, R.C.; Hinzman, L.; Kane, D. Acclimation of ecosystem CO_2 exchange in the Alaskan Arctic in response to decadal climate warming. *Nature* **2000**, *406*, 978–981. [CrossRef]
43. Walker, T.W.N.; Kaiser, C.; Strasser, F.; Herbold, C.W.; Leblans, N.I.W.; Woebken, D.; Janssens, I.A.; Sigurdsson, B.D.; Richter, A. Microbial temperature sensitivity and biomass change explain soil carbon loss with warming. *Nat. Clim. Chang.* **2018**, *8*. [CrossRef]
44. Bossio, D.A.; Scow, K.M. Impact of Carbon and Flooding on the Metabolic Diversity of Microbial Communities in Soils. *Appl. Environ. Microb.* **1995**, *61*, 4043–4050.
45. Paul, E.A.; Clark, F.E. *Soil Microbiology and Biochemistry*; Academic Press: San Diego, CA, USA, 1989.
46. Sakamoto, K.; Oba, Y. Effect of Fungal to Bacterial Biomass Ratio on the Relationship between CO_2 Evolution and Total Soil Microbial Biomass. *Biol. Fert. Soils* **1994**, *17*, 39–44. [CrossRef]
47. Chen, R.R.; Senbayram, M.; Blagodatsky, S.; Myachina, O.; Dittert, K.; Lin, X.G.; Blagodatskaya, E.; Kuzyakov, Y. Soil C and N availability determine the priming effect: Microbial N mining and stoichiometric decomposition theories. *Glob. Chang. Biol.* **2014**, *20*, 2356–2367. [CrossRef]
48. Fisk, M.; Santangelo, S.; Minick, K. Carbon mineralization is promoted by phosphorus and reduced by nitrogen addition in the organic horizon of northern hardwood forests. *Soil Biol. Biochem.* **2015**, *81*, 212–218. [CrossRef]
49. Qiu, Q.Y.; Wu, L.F.; Ouyang, Z.; Li, B.B.; Xu, Y.Y.; Wu, S.S.; Gregorich, E.G. Priming effect of maize residue and urea N on soil organic matter changes with time. *Appl. Soil Ecol.* **2016**, *100*, 65–74. [CrossRef]
50. Wang, Y.S.; Cheng, S.L.; Fang, H.J.; Yu, G.R.; Xu, X.F.; Xu, M.J.; Wang, L.; Li, X.Y.; Si, G.Y.; Geng, J.; et al. Contrasting effects of ammonium and nitrate inputs on soil CO_2 emission in a subtropical coniferous plantation of southern China. *Biol. Fert. Soils* **2015**, *51*, 815–825. [CrossRef]
51. TingTing, Z.; ZILiang, Z.; Na, L.; YuanShuang, Y.; DongHui, Z.; Qin, L.; HuaJun, Y. Differential uptakes of different forms of soil nitrogen among major tree species in subalpine coniferous forests of western Sichuan, China. *Chin. J. Plant Ecol.* **2017**, *41*, 1051–1059.
52. Fang, H.J.; Cheng, S.L.; Yu, G.R.; Xu, M.J.; Wang, Y.S.; Li, L.S.; Dang, X.S.; Wang, L.; Li, Y.N. Experimental nitrogen deposition alters the quantity and quality of soil dissolved organic carbon in an alpine meadow on the Qinghai-Tibetan Plateau. *Appl. Soil Ecol.* **2014**, *81*, 1–11. [CrossRef]
53. Schindlbacher, A.; Zechmeister-Boltenstern, S.; Butterbach-Bahl, K. Effects of soil moisture and temperature on NO, NO_2, and N_2O emissions from European forest soils. *J. Geophys. Res.-Atmos.* **2004**, *109*. [CrossRef]
54. Wu, X.; Bruggemann, N.; Gasche, R.; Shen, Z.Y.; Wolf, B.; Butterbach-Bahl, K. Environmental controls over soil-atmosphere exchange of N_2O, NO, and CO_2 in a temperate Norway spruce forest. *Glob. Biogeochem. Cycles* **2010**, *24*, 45. [CrossRef]
55. Kiese, R.; Butterbach-Bahl, K. N_2O and CO_2 emissions from three different tropical forest sites in the wet tropics of Queensland, Australia. *Soil Biol. Biochem.* **2002**, *34*, 975–987. [CrossRef]
56. Werner, C.; Kiese, R.; Butterbach-Bahl, K. Soil-atmosphere exchange of N_2O, CH_4, and CO_2 and controlling environmental factors for tropical rain forest sites in western Kenya. *J. Geophys. Res.-Atmos.* **2007**, *112*, 71. [CrossRef]
57. Yan, J.H.; Zhang, W.; Wang, K.Y.; Qin, F.; Wang, W.T.; Dai, H.T.; Li, P.X. Responses of CO_2, N_2O and CH4 fluxes between atmosphere and forest soil to changes in multiple environmental conditions. *Glob. Chang. Biol.* **2014**, *20*, 300–312. [CrossRef]

58. Venterea, R.T.; Groffman, P.M.; Verchot, L.V.; Magill, A.H.; Aber, J.D.; Steudler, P.A. Nitrogen oxide gas emissions from temperate forest soils receiving long-term nitrogen inputs. *Glob. Chang. Biol.* **2003**, *9*, 346–357. [CrossRef]
59. Barnard, R.; Leadley, P.W.; Hungate, B.A. Global change, nitrification, and denitrification: A review. *Glob. Biogeochem. Cycles* **2005**, *19*, 152. [CrossRef]
60. Signor, D.; Cerri, C.E.P. Nitrous oxide emissions in agricultural soils: A review. *Pesq. Agropec. Trop.* **2013**, *43*, 322–338. [CrossRef]

forests

MDPI

Article

Nitrogen Addition Affects Soil Respiration Primarily through Changes in Microbial Community Structure and Biomass in a Subtropical Natural Forest

Jiacong Zhou [1,2], Xiaofei Liu [1,2], Jinsheng Xie [1,2,3], Maokui Lyu [1,2], Yong Zheng [1,2], Zhangtian You [1,2], Yuexin Fan [1,2], Chengfang Lin [1,2,3], Guangshui Chen [1,2,3], Yuehmin Chen [1,2,3,*] and Yusheng Yang [1,2,3]

1 State Key Laboratory for Subtropical Mountain Ecology of the Ministry of Science and Technology and Fujian Province, Fujian Normal University, Fuzhou 350007, China; zhoujiacong522@163.com (J.Z.); xfliu@fjnu.edu.cn (X.L.); jshxie@163.com (J.X.); 228lmk@163.com (M.L.); 18059046619@163.com (Y.Z.); allentime@126.com (Z.Y.); yxfan@fjnu.edu.cn (Y.F.); Tonylcf99@163.com (C.L.); gschen@fjnu.edu.cn (G.C.); geoyys@fjnu.edu.cn (Y.Y.)

2 School of Geographical Sciences, Fujian Normal University, Fuzhou 350007, China

3 Institute of Geography, Fujian Normal University, Fuzhou 350007, China

* Correspondence: ymchen@fjnu.edu.cn; Tel.: +86-591-83465013; Fax: +86-591-83465397

Received: 31 March 2019; Accepted: 19 May 2019; Published: 20 May 2019

Abstract: Forest soil respiration plays an important role in global carbon (C) cycling. Owing to the high degree of C and nitrogen (N) cycle coupling, N deposition rates may greatly influence forest soil respiration, and possibly even global C cycling. Soil microbes play a crucial role in regulating the biosphere–atmosphere C exchange; however, how microbes respond to N addition remains uncertain. To better understand this process, the experiment was performed in the *Castanopsis kawakamii* Hayata Nature Reserve, in the subtropical zone of China. Treatments involved applying different levels of N (0, 40, and 80 kg ha^{-2} $year^{-1}$) over a three-year period (January 2013–December 2015) to explore how soil physicochemical properties, respiration rate, phospholipid fatty acid (PLFA) concentration, and solid state ^{13}C nuclear magnetic resonance responded to various N addition rate. Results showed that high levels of N addition significantly decreased soil respiration; however, low levels of N addition significantly increased soil respiration. High levels of N reduced soil pH and enhanced P and C co-limitation of microorganisms, leading to significant reductions in total PLFA and changes in the structure of microbial communities. Significant linear relationships were observed between annual cumulative respiration and the concentration of microbial biomass (total PLFA, gram-positive bacteria (G^+), gram-negative bacteria (G^-), total bacteria, and fungi) and the microbial community structure (G^+: G^- ratio). Taken together, increasing N deposition changed microbial community structure and suppressed microbial biomass, ultimately leading to recalcitrant C accumulation and soil C emissions decrease in subtropical forest.

Keywords: N addition; soil respiration; microbe; subtropical forest

1. Introduction

Anthropogenic reactive nitrogen (N) production originated primarily from agricultural activities, fossil fuel combustion, and the growing popularity of biofuels, and has increased three- to five-fold over the past century [1]. By 2050, N deposition is projected to reach 200 Tg N $year^{-1}$, especially in forest ecosystems [1,2]. Approximately twice as much C is stored in soils compared to that in the atmosphere. Soil respiration (*Rs*) is the primary pathway through which C is released from the soil system into the atmosphere [3]. Thus, even minor changes in *Rs* would have significant effects on C

cycling. Given the nature of the relationship between the C and N cycles, which are highly coupled in terrestrial ecosystems [4,5], it is likely that increasing N deposition will greatly influence *Rs*.

N addition affects *Rs* through regulating forest productivity, microbial biomass, and activities that are directly related to CO_2 production [6]. Meta-analyses have revealed that N addition can increase aboveground and belowground plant growth by 29% and 35.5%, respectively [7,8]. Additionally, N addition reduced microbial biomass by 20% at the global scale [9]. However, how *Rs* responds to rapid N addition remains unclear and previous results have been inconclusive, including acceleration [10], deceleration [11], and no change [9,12]. The conclusions mentioned above are largely dependent on N-limited regions and there is a lack of subtropical studies. Subtropical systems have high rates of CO_2 exchange [13] and relatively high levels of available N in forest soils. Sun et al. [14] suggested that the main factor driving the reduction in *Rs* is different in N-enriched (microbe-mediated) and N-limited (plant-mediated) forests. However, Lee and Jose [15] also found that fine root production is the main factor affecting *Rs* in tropical forests. In our previous study, N addition promoted root biomass to utilize higher levels of P (Figure S1) [16]; however, the microbial response has not yet been described.

Large uncertainties exist in terms of belowground C cycling because soil C dynamics are often regulated by complicated microbial processes. N addition directly increases soil N availability and promotes substrate utilization for microbial decomposition [17–19]. However, co-limitation with other elements, such as P, may occur in subtropical forests. Moreover, N addition could elicit changes in the availability of substrates, which could accentuate C limitation of soil microbes. Although N addition increased the quantity of litter input to the soil [7,8], the quality of soil organic matter (SOM) may decline via increasing lignin content in litter and polymerization of polyphenols [20–22]. Furthermore, chronic N addition could enhance nitrification rates, increase inorganic N concentration, and leach base cations, eventually causing soil acidification to accompany an increase in Al^{3+}, Mn^{2+}, and Fe^{3+} [23,24], thereby suppressing microbial activity. Therefore, the magnitude of these processes determines the direction of *Rs* in response to N addition.

Previous studies have shown that the response of microbial activity to N addition gradients is not linear, with the highest levels of microbial activity occurring at moderate N concentration, and decreasing as N levels increase [25–27]. This tendency was observed not only in *Rs* but also in forest respiration, ectomycorrhizal fungal sporocarp production, and fungal mineralization [28–30]. Different magnitudes of N addition may have different effects on *Rs*.

In our study, we performed a manipulative experiment designed to test the effects of N addition on soil CO_2 emissions in a subtropical forest. The response factors assessed consisted of *Rs* rates, soil microbial biomass, microbial community structure, and soil C structure. Investigating the responses of *Rs* and microbial traits (biomass and community structure) to N addition is critical to develop our understanding of C cycling in subtropical forests. Hence, we hypothesized that: (1) changes in *Rs* would coincide with changes in microbial traits; (2) the effects of N addition on *Rs* are mainly mediated by microbial traits, rather than roots.

2. Materials and Methods

2.1. Study Site

The experiment was carried out in the *Castanopsis kawakamii* Hayata Nature Reserve, which is in central Fujian Province, China (117°28′ E, 26°11′ N), over an almost three-year period (January 2013–December 2015). The study site was composed of an approximately 200-year-old undisturbed mixed stand dominated by *Castanopsis carlesii* Hayata and *Schima superba* Gardn. et Champ., with other less abundant species. Stand density and canopy coverage were approximately 1955 trees ha^{-1} and 89%, respectively.

The climate is classified as a subtropical monsoon, with mean annual precipitation of 1552 mm, 2141 mm, and 2025 mm in 2013, 2014, and 2015, respectively. It has distinct seasons, with most

rain falling between March and August. Mean annual temperature, potential evapotranspiration, and relative humidity in this region were 18.7 °C, 1585 mm, and 79%, respectively [31]. Regional soils are Oxisols, formed from sandstone (based on the United States Department of Agriculture Soil Taxonomy), and are about 30–70 cm deep [32].

2.2. Experimental Design

Three N addition treatments (with four replicates each) were established in this forest, consisting of 0 kg ha^{-2} $year^{-1}$ (control, CT), 40 kg ha^{-2} $year^{-1}$ (low N, LN), and 80 kg ha^{-2} $year^{-1}$ (high N, HN). Treatment levels were based on known background atmospheric N deposition rates in subtropical regions of China (18–53 kg ha^{-2} $year^{-1}$), with an average deposition rate of ~40 kg ha^{-2} $year^{-1}$ [33]. A total of 12 plots (20 m × 20 m) were established, each surrounded by a 10-m wide buffer zone and unshielded from natural atmospheric N deposition. The plots and treatments were set randomly. Beginning in November 2012, a solution of ammonium nitrate (NH_4NO_3), and 20 L of deionized water was distributed monthly below the canopy with a backpack sprayer, totaling 12 applications of equal volume annually, and an equivalent volume of deionized water was sprayed on the control plots.

2.3. Soil Sample Collection

Five soil cores were collected from each subplot with a 3.5-cm-diameter corer in January 2016. We removed the surface litterfall and collected soil samples from the A horizon (0–10 cm). Soil cores were then kept in portable refrigerated box until being processed in the laboratory. After removal of plant roots and stones, soil samples were sieved through a 2-mm mesh and stored at 4 °C prior to the analysis of inorganic N, dissolved organic C, and N and microbial phospholipid fatty acid (PLFA) content. Part of the soil was air-dried for measuring its pH. The remaining soil was air-dried and ground (<150 μm) for determination of total C and total N.

2.4. Soil Respiration Rate Measurement

Soil respiration rate (R_s) was measured using an automated CO_2 efflux system (LI-8100, LI-COR Inc., Lincoln, NE, USA). Eight polyvinyl chloride (PVC) collars (diameter: 20 cm; height: 10 cm) were fixed in each plot in August 2011. Living plants inside the collars were removed and kept for almost 1.5 years to minimize disruption. Soil respiration was assessed once every two weeks over the course of the experimental period. Measurements were taken between 09:00 and 12:00, as soil flux over these hours has been shown to represent the mean of the whole day [34]. Soil temperatures and moisture were simultaneously monitored using a hand-held long-stem thermometer (Model SK-250WP, Sato Keiryoki Mfg. Co. Ltd, Tokyo, Japan) and a time-domain reflectometer (TDR) (Model TDR300, Spectrum Technologies Inc., Plainfield, IL, USA), respectively. The data of monthly soil temperature and annual moisture during study period are shown in Figures S2 and S3.

To examine the effects of N addition rate on R_s in sub/tropical forests, data were obtained from 15 peer-reviewed articles (Table S4) by searching Web of Science. The searched key words were combinations of, "nitrogen (N) addition," "nitrogen (N) deposition," "soil respiration," "subtropical forest" and "tropical forest". Data were selected based on the following criteria: (1) from a field study (data from incubation studies were excluded); (2) from control and simulated N addition treatments in multifactorial studies. Response ratios of R_s to N addition rate (RRs) were calculated using the following equation:

$$RRs = \ln (R_T/R_C) \quad (1)$$

where R_T is the treatment mean and R_C is the control mean. Here, $RRs > 0$ means N addition increased soil respiration; $RRs = 0$, means N addition has no effect on soil respiration; $RRs < 0$ means N addition reduced soil respiration.

2.5. Phospholipid Fatty Acid Analysis

The soil microbial community was characterized using a phospholipid fatty acid (PLFA) analysis, as previously described by Wan et al. [35]. In brief, a solvent consisting of a 2:1:0.8 mixture of methanol (CH_3OH), chloroform ($CHCl_3$), and phosphate buffer (pH 7.4) was used to extract 10 g of freeze-dried soil by shaking for 2 h. The samples were centrifuged at 3500 g for 10 min, and then the supernatant was transferred to a new tube. The remaining soil was re-extracted as described above. The extracted solvents from both steps were combined and then evaporated to 1 mL under N_2 gas. Then, neutral glycolipids, glycolipids-, and polar lipids were separated over a silicon hydroxide column eluted with chloroform, acetone, and methanol, respectively. Polar lipids were methylated to form fatty acid methyl esters (FAMEs) by subjecting them to 0.2 M methanolic KOH. Individual FAMEs were identified by Hewlett Packard 5890 gas chromatography, equipped with a 6890 series injector, a flame ionization detector, and an Ultra 2 capillary column (25 m × 0.2 mm inner diameter, film thickness, 0.33 μm) based on their retention times and in combination with the MIDI Sherlock Microbial Identification System (MIDI Inc., Newark, DE, USA).

Although more than 70 PLFAs, ranging from C_{10}–C_{24}, were identified in this experiment, only the 23 PLFAs found to be consistently present in each sample were included in the analysis. PLFAs identified as being derived from gram-positive bacteria (G^+) included i14:0, i15:0, a15:0, i16:0, i17:0, and a17:0, whereas those identified as being derived from gram-negative bacteria (G^-) included 16:1ω9c, 16:1ω7c, cy17:0, 18:1ω7c, 18:1ω5c, and cy19:0 [36,37]. The sum of the PLFAs from G^+ and G^- bacteria was used to as a measure of total bacteria, and those of 10Me16:0, 10Me17:0, and 10Me18:0 were selected to measure actinomycetes. We selected 18:2ω6c and 18:1ω9c as fungi markers [38]. The PLFAs 14:0, 15:0, 16:0, 16:1ω5c, 17:0, and 18:0 were detected in both bacteria and fungi; thus, they were used to assess the unclassified markers [39–41]. The sum of all selected phospholipids was used to estimate the total microbial biomass and for the analysis of microbial community structure. The G^+:G^- ratio was used to estimate the G^+ to G^- bacterial biomass (G^+:G^-), and the fungal: bacterial PLFA ratio was used to estimate the ratio of fungi to bacteria (F:B).

2.6. Solid-State ^{13}C Nuclear Magnetic Resonance Spectroscopy Analysis

Soil samples for solid state ^{13}C cross polarization magic angle spinning (CP-MAS) nuclear magnetic resonance (NMR) analysis were repeatedly treated with 2% hydrofluoric acid, then rinsed with deionized water, freeze-dried, and ground into powder [42]. The powdered samples were packed into 4-mm zirconium rotors. Solid state ^{13}C NMR spectra were acquired on a 500 MHz Bruker BioSpin Avance III spectrometer (Bruker BioSpin, Rheinstetten, Germany) equipped with a 4-mm probe. The parameters used to obtain the spectra consisted of a 13 kHz spinning rate, 1 ms ramp-CP contact time, 1 s recycle delay, and 4096 scans. Glycine was used as the external reference for chemical shift. NMR spectra were processed using a zero filling factor of 2 and 75 Hz line broadening. The NMR spectra were divided into seven regions representing the different chemical environments of the ^{13}C nucleus (Table S1). The ratios were calculated using percentage intensity values as follows [43,44]:

$$\text{A/O-A ratio} = \text{alkyl C/O} - \text{alkyl C} \quad (2)$$

$$\text{aromaticity} = \text{aromatic C}/(\text{alkyl C} + \text{methoxyl and N-alkyl C} + \text{O-alkyl C} + \text{Di-O-alkyl} + \text{phenolic C} + \text{aromatic C}) \quad (3)$$

2.7. Additional Soil Analysis

Soil inorganic N was treated with 2 M KCl and analyzed using a Continuous Flow Analytic System (Skalar san++, Skalar, Breda, Netherlands); soil organic C (SOC) and total N (TN) were determined with an elemental analyzer (Elementar Vario EL III, Elementar, Langenselbold, Germany). Dissolved organic C (DOC) and N (DON) were extracted from 10 g of field-moist soil by mixing the soil with 40 mL deionized water at 20 °C and shaking for 30 min, then filtering the supernatant through a 0.45-μm

filter membrane [45]. Soil pH was determined with a pH meter (STARTER 300, OHAUS, Pine Brook, NJ, USA) in a 1:2.5 soil: water solution. Soil moisture content was measured gravimetrically by drying for 48 h at 105 °C.

2.8. Statistical Analyses

Daily cumulative respiration (R_c) was calculated from R_s as follows:

$$R_c\ (\text{g C m}^{-2}\ \text{d}^{-1}) = R_s\ (\mu\text{mol m}^{-2}\ \text{s}^{-1}) \times 3600\ (\text{s h}^{-1}) \times 24\ (\text{h d}^{-1}) \times 12/1{,}000{,}000\ (\text{g mol}^{-1}) \quad (4)$$

Soil respiration was measured every two weeks with a total of 24 samplings/year. Annual cumulative respiration was calculated by daily R_c multiplied by the number of sampling interval days. Equation used was as follows:

$$\textit{Annual cumulative respiration} = \sum_{i=1}^{24} \text{daily } R_c\ (\text{i})\ \times 15 \quad (5)$$

The relationship between the R_s and soil temperatures was performed using following widely exponential regression model [46]:

$$R_s = \text{ae}^{\text{bt}} \quad (6)$$

where R_s is the soil respiration rate, t is the soil temperature at 5 cm depth, a and b are the model coefficients.

The apparent temperature sensitively (Q_{10}) was calculated as follows:

$$Q_{10} = \text{e}^{10\text{b}} \quad (7)$$

All statistical analyses were performed using SPSS v.21.0 (SPSS Inc., Chicago, IL, USA). All response variables were tested for normality and homoscedasticity prior to statistical analyses, and data were log-transformed when the assumptions were not met (DON, ammonium nitrogen [NH_4^+-N]). One-way analysis of variance (ANOVA) with the Tukey's HSD test was used to evaluate the differences in soil physicochemical properties, annual cumulative respiration, Q_{10}, and PLFA in response to different N-addition treatments. Linear regression model analyses were conducted to explore the relationships among PLFA and annual cumulative respiration.

3. Results

3.1. Response of Soil Physicochemical Properties to N Deposition

No significant differences in SOC, TN, ammonium N (NH_4^+-N), or nitrate N (NO_3^--N) were detected after three years of N deposition (Table 1). Soil pH decreased with increasing N, with pH significantly reduced (by 0.13 units) in the HN treatment. Soil DOC was significantly higher in the LN treatment, and soil DON increased with higher N addition, with levels in the HN treatment being significantly higher than those in the CT and LN treatments.

Table 1. Effects of N deposition on soil physicochemical properties.

Properties	CT	LN	HN	Contrast Test
SOC ($g \cdot kg^{-1}$)	36.61(7.47)	39.18(13.03)	33.32(7.99)	0.709
Total N ($g \cdot kg^{-1}$)	2.67(0.27)	2.70(0.53)	2.54(0.32)	0.838
pH	4.08(0.06)a	3.97(0.09)ab	3.95(0.09)b	0.096
NH_4^+-N ($mg \cdot kg^{-1}$)	10.79(2.50)	7.21(0.96)	9.57(4.21)	0.053
NO_3^--N ($mg \cdot kg^{-1}$)	1.37(0.32)	1.62(0.53)	1.59(0.57)	0.070
DOC ($mg \cdot kg^{-1}$)	41.93(12.36)b	66.80(3.43)a	39.88(8.03)b	0.003
DON ($mg \cdot kg^{-1}$)	49.95(5.32)b	58.66(6.98)b	132.32(12.93)a	<0.001

The different letters indicate significant differences between treatments at $p < 0.05$. Contrast test (ANOVA) was conducted between N treatments and the controls. Values are expressed as (mean ± standard deviation; $n = 4$). CT: control treatments; LN: low N; HN: high N; SOC: soil organic carbon; TN: total N; NH_4^+-N: ammonium N; NO_3^--N: nitrate N; DOC: dissolved organic carbon; DON: dissolved organic N.

3.2. Response of Soil Respiration Rate and Temperature Sensitivity to N Addition

Monthly dynamics of *Rs* rate showed a strong seasonal pattern, with the highest rate observed in July–August and the lowest in January–February for all treatments (Figure 1). Annual cumulative *Rs* in the LN treatment was 15.62%, 19.16%, and 23.29% higher than in the CT treatment in 2013, 2014, and 2015, respectively, while annual cumulative *Rs* in the HN treatment was 11.86% and 16.68% lower relative to the CT treatment in 2014 and 2015, respectively (Figure 2). However, during the period of 2013 to 2015, the sensitivities of *Rs* to soil temperature were not significantly different among N-addition treatments (Table 2 and Table S2).

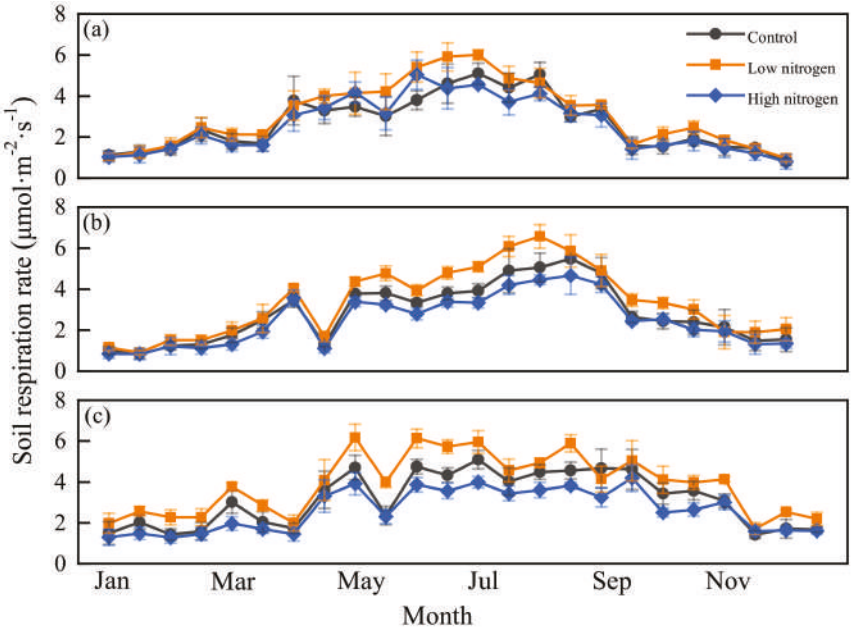

Figure 1. Monthly dynamics of soil respiration rate under different N treatments in 2013 (**a**), 2014 (**b**), and 2015 (**c**). Error bars represent standard deviation ($n = 4$).

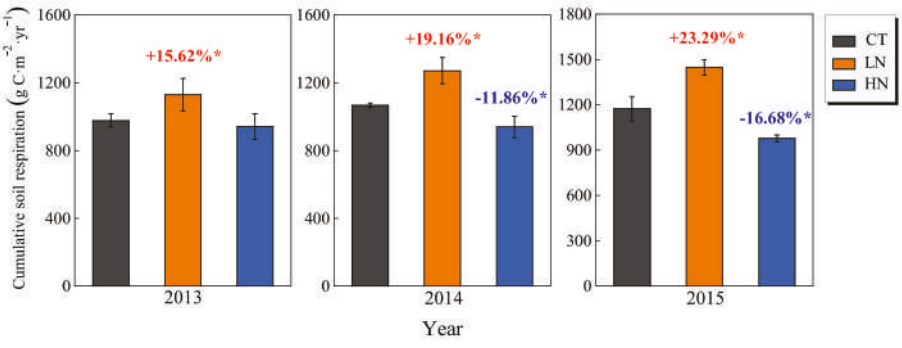

Figure 2. Annual cumulative soil respiration under different N treatments for the period of 2013–2015. * indicates statistically significant difference at $p < 0.05$.

Table 2. The soil respiration sensitivities to soil temperature for the period of 2013–2015.

Treatments	Q_{10}
CT	2.07(0.11)
LN	2.09(0.36)
HN	2.00(0.12)

3.3. Response of Microbial Community to N Addition

The concentrations of G^+, G^-, fungi, and total PLFA were significantly decreased in the HN treatment, but no significant differences were observed for any of the PLFA between the LN and CT treatments (Figure 3; Table S3). The ratio of G^+: G^- was significantly higher in the HN treatment than in the CT treatment (1.5 and 1.1, respectively), but no significant difference in F:B ratio was observed among the treatments.

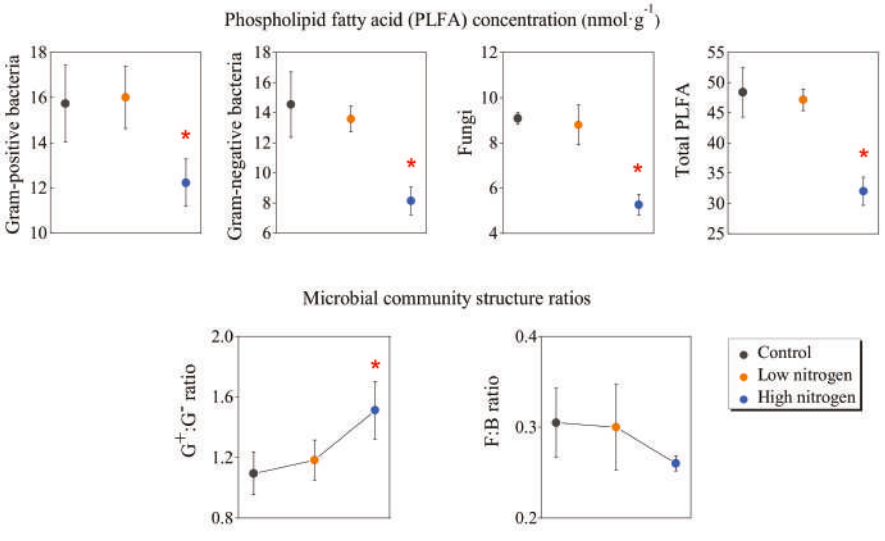

Figure 3. Phospholipid fatty acid (PLFA) concentrations and microbial community structure ratios under different N addition treatments. Error bars represent standard deviation ($n = 4$). * indicates significant difference between the treatment and control at $p < 0.05$.

3.4. Response of Soil Chemical Characteristics to N Addition

The most dominant component was the alkyl C region (Figure 4; Table S1). Alkyl C, aromatic C, phenolic C, and carboxyl/carbonyl C exhibited major differences in the HN treatment. Thus, differences in these chemical shift regions caused a 9% reduction in A/O-A and a 5% increase in aromaticity.

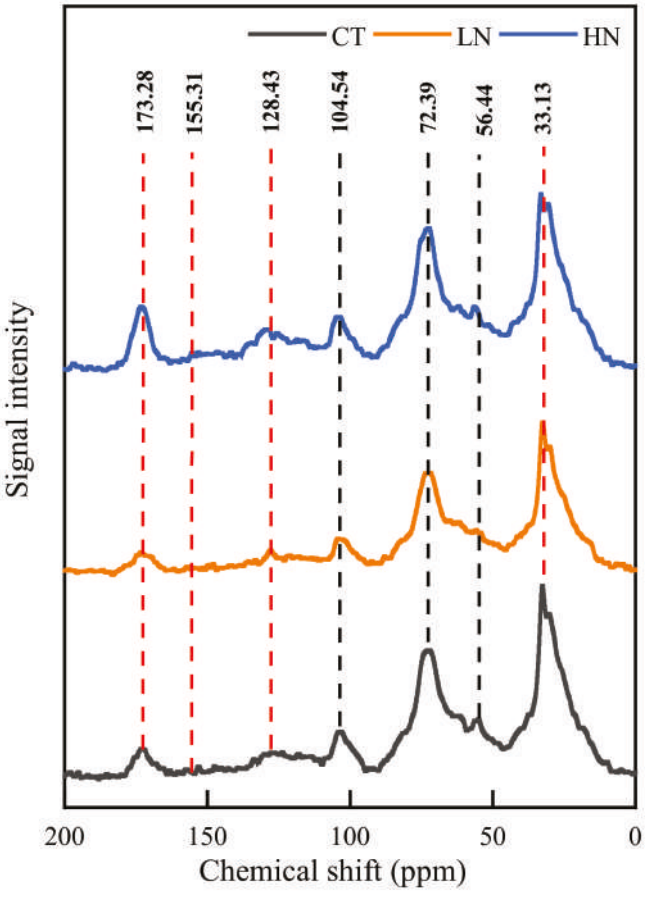

Figure 4. Solid-state ^{13}C nuclear magnetic resonance spectra of soil under different N addition treatments. The red dashed line indicates changes in the chemical shift regions.

3.5. Correlation between Annual Cumulative Soil Respiration and Microbial Biomass, Root Biomass and Microbial Community Structure Ratio

Significant linear relationships were found between annual cumulative *Rs* and the concentration of microbial biomass (total PLFA, G^+, G^-, total bacteria, and fungi) and the G^+: G^- ratio according to linear regression. However, neither root biomass nor the F:B ratio was significantly correlated with annual cumulative *Rs* in 2015 (Figure 5).

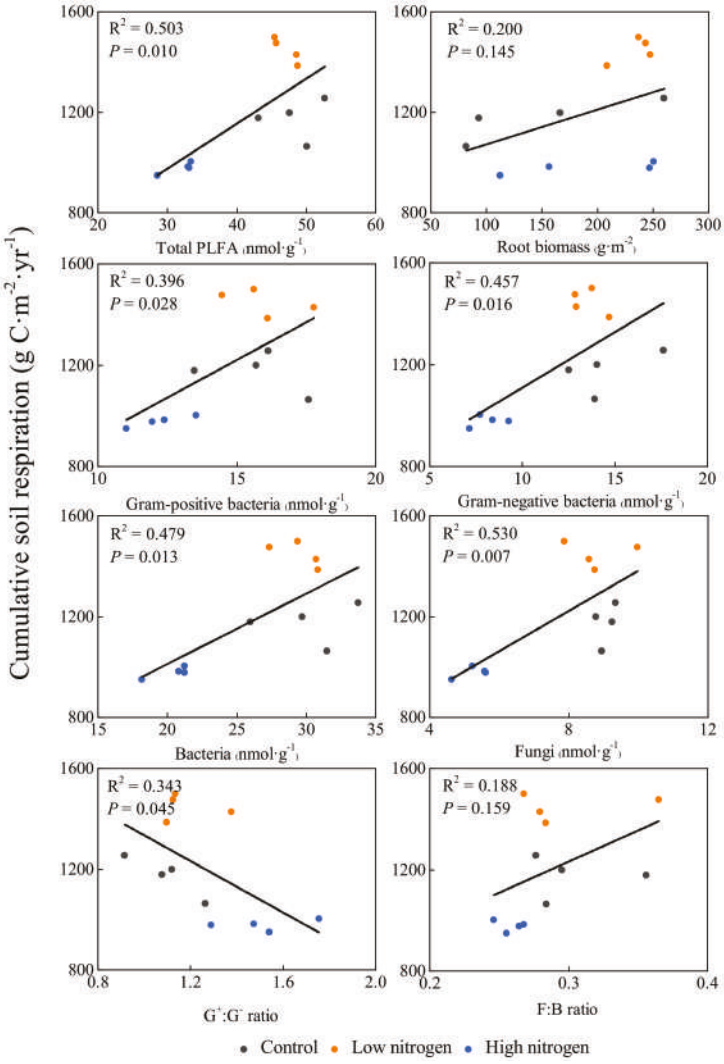

Figure 5. Linear relationships between annual cumulative respiration in 2015 and concentrations of PLFA, microbial community structure ratios, and root biomass.

4. Discussion

4.1. Effects of N Addition on Soil Respiration

Nitrogen deposition did not affect the seasonal patterns of *Rs* rates, with the highest rate observed in July–August and the lowest in January–February (Figure 1). This seasonal pattern has been reported in previous studies and can be ascribed to differences in mean temperature [47,48]. N addition induced significant changes in *Rs* rates ($p < 0.05$); however, the different rates of N addition exhibited distinct trends in terms of their effect on *Rs*. This discrepancy in annual cumulative respiration among the treatments continued to diverge over time, which was consistent with results reported by Allison et al. [28], Hasselquist et al. [30], Bowden et al. [48], and Maaroufi et al. [49]. This is because a certain threshold for N addition exists. For instance, in a subtropical Moso bamboo forest ecosystem,

Li et al. [6] found that a N addition rate of 60 kg N ha^{-1} $year^{-1}$ may reflect a N saturation threshold. When N addition rate exceed 60 kg N ha^{-1} $year^{-1}$, N addition still increased *Rs*, but the positive effects diminished. However, in our study, a significant decrease in *Rs* was observed in 2014 and 2015 when N addition rate exceed 60 kg N ha^{-1} $year^{-1}$, possibly because the bamboo plantation was N-limited and had a high demand for N [50], unlike the natural forests examined in previous research.

Previously, there have been six meta-analyses with regard to the effects of N addition on *Rs* [9–12,51,52]. However, these studies paid little attention to subtropical forests owing to the smaller sample sizes reported. With the increasing attention paid to subtropical forests in recent years, several studies have been carried out. We recollected a series of data from 16 study sites (including this study) and defined <60 kg N ha^{-1} $year^{-1}$ as a low N addition rate according to a N saturation threshold of 50–60 kg N ha^{-1} $year^{-1}$ for global aboveground net primary production [53]. We found strong evidence to indicate that N addition significantly reduces *Rs* in subtropical forests as observed in all examined studies (n = 58, p = 0.011; Figure 6, Table S4). However, the magnitude of N addition rate also affected the response of *Rs*, which mainly showed as a high N addition rate reducing *Rs* (n = 37, p = 0.046), while the response of *Rs* to low N addition rate varied (n = 21, p = 0.052). It is noteworthy that N addition rate is a dominant factor affecting soil acidification and total microbial biomass; however, Zhou et al. [54] indicated that the effect of N addition rate was ignored in several of the previous meta-analyses, such as Janssens et al. [11], Treseder [51], and Lu et al. [52]. In particular, in subtropical forest ecosystems, rapid N addition exacerbates the loss of NO_3^- combined base cations (K^+, Na^+, Ca^{2+}, and Mg^{2+}) through leaching, which in turn causes nutrient cations to be lost at a faster rate than minerals can be replenished [55]. A lack of base cations can be harmful to vegetative and microbial growth in subtropical forest ecosystems [56,57] leading to lower *Rs*.

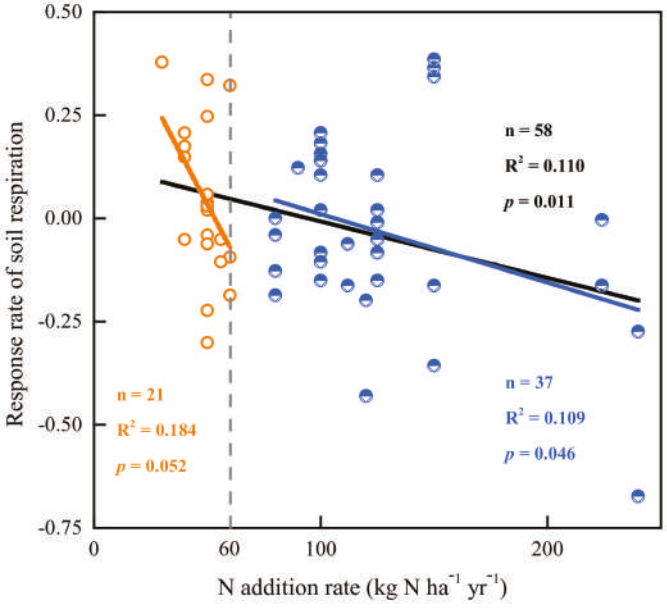

Figure 6. Linear relationship between N addition rate and response ratios of soil respiration (*RRs*) in subtropical systems of the present study and other regions of the world. Orange hollow points indicate relatively low N addition (N addition rate < 60 kg N ha^{-1} $year^{-1}$); blue points indicate relatively high N addition (N addition rate > 60 kg N ha^{-1} $year^{-1}$); orange line indicates linear regression between relatively low N addition rate and *RRs*; blue line indicates linear regression between relatively high N addition rate and *RRs*; black line indicates linear regression between N addition rate and *RRs*.

In our control treatment, the Q_{10} value (2.07) was similar to that reported from a subtropical rehabilitated forest (2.1) [58], but lower than those from a subtropical disturbed forest (2.3) [58], a Moso bamboo forest (2.29) [6], a sweetgum forest (2.73) [59], and a larch forest (3.24) [14] across the temperate zone. This is in line with the observations of Wang et al. [60], in which Q_{10} showed a positive relationship with latitude in forest ecosystems. In addition, the C:N ratio is a dominant factor for regulating Q_{10}, owing to the shift from C limitation to nutrient limitation with increasing latitude [60,61]. This result may support the microbial N mining theory, which suggests that microbes decompose more SOM to obtain sufficient N at high temperature in high latitude forests with low N availability [62].

4.2. Microbial Community and Carbon Structure under N Addition

In accordance with our first hypothesis, we found that the HN treatment reduced the concentration of bacteria, fungi, actinomycetes, and unclassified biomarkers (Figure 3; Table S3), leading to a significant reduction in total PLFA. Both incubation and field studies have definitively shown that *Rs* and microbial biomass are consistently suppressed following N addition [11,51,63]. However, a recent meta-analysis by Zhou et al. [54] revealed that a decrease in microbial biomass is not always associated with N addition suppressing microbial activity. Interestingly, the companion study reported that the C:N:P stoichiometry in microbial biomass was significantly altered in the HN treatments and enhanced microbial P limitation [32]. Additionally, high N addition significantly reduced soil pH. Therefore, these results collectively demonstrate that high N addition inhibits microbial growth.

Ramirez et al. [63] suggested that understanding how N addition induces change in soil microbial communities is imperative for better understanding soil C storage dynamics. High availability of N could alter the microbial process of SOC that is controlled by the microbial community [64,65]. In our study, the HN treatments not only inhibited microbial biomass but also shifted microbial composition (increased G^+:G^- ratio). The two different groups of Gram-stained bacteria, classified by their cell wall compositions, have been shown to differ in their preferences regarding substrate conditions and living strategies in a changing environment [66]. G^+ are well-adapted to low SOM substrates, while G^- prefer conditions with high organic matter availability [67,68]. Increase in the G^+:G^- ratio under the high N addition treatment not only indicated a low quality substrate but also an acclimation of microbes to changes in substrate and nutrient availability.

Undoubtedly, the inhibition in microbial biomass and shift in soil microbial community structure affected the soil C structure, to an extent. The results of the solid state ^{13}C NMR spectroscopy analysis showed that the relative proportions of aromatic C and phenolic C, which originate from lignin and amino acids of peptides [43,69], increased under the HN treatment (Figure 4; Table S1). Wang et al. [65] also observed that lignin-derived phenols accumulated in soil with long-term N addition (22 years). There are two plausible reasons for this observation. First, that N addition significantly increased the lignin content of the plant and litter [21], leading to lower substrate decomposition rates with higher lignin content [70]. Second, phenolic compounds are highly resistant to degradation, being susceptible only to a handful of fungal species that are more efficient at lignin decomposition [71]. Thus, non-preferred microbial substrates would accumulate under high N addition.

4.3. Correlation between Soil Respiration and Microbial Biomass, Root Biomass, and Microbial Community Structure Ratio under N Addition

A significant correlation was observed between microbial traits (biomass and community structure) and cumulative *Rs* rather than root biomass (Figure 5). These results supported our second hypothesis, that microbial traits are primary factors affecting *Rs* under N addition, which is to say that the decrease in *Rs* is mainly due to microbes. A reasonable explanation is that microbes may be subject to co-limiting factors in subtropical forests, such as C and P, rather than N [65,72,73]. This pattern of *Rs* under N addition is different in N limited ecosystems, which have often been reported to increase *Rs* via root products and biomass [74]. Importantly, heterotrophic respiration dominates *Rs* (almost

72%) [75], and the positive relationships were observed between root/fine root biomass and autotrophic respiration [15,76] and microbial biomass and heterotrophic respiration [77]. Additionally, N addition significantly increased root biomass (Figure S1) and decreased microbial biomass, which collectively suggested that heterotrophic respiration may have decreased even further under N addition.

Decreasing microbial biomass is always accompanied by decreasing microbial diversity [78]. Microbial diversity is a vital determinant of ecological function that cannot be obtained using the PLFA method [79]. Thus, it is necessary to employ nucleic-acid-based methods to link microbial diversity to function. In this study, N addition inhibited microbial biomass and shifted microbial community structure, which disrupted the microbial process of SOM, leading to a decrease in *Rs* and an increase in recalcitrant C accumulation, but was also beneficial to an increase in forest soil C sequestration. However, nutrient release from microbial decomposition will slow down as SOC storage increases. Especially in natural forests without intensive management practices (such as fertilization), shifts in biogeochemical cycling will alter the productivity of ecosystems.

5. Conclusions

The effects of N addition on *Rs* are subject to an N saturation threshold, which triggered low N addition to increase *Rs* and high N addition to decrease *Rs* in the subtropical *C. carlesii* forest investigated. High N addition increased P limitation and decreased pH. Additionally, high N addition led to recalcitrant C accumulation, restricting microbial utilization. These processes collectively reduced the total PLFA concentration and shifted microbial community structure (G^+: G^- ratio). Our results suggest that microbial traits are dominant factors affecting *Rs*. As such, additional research on the transformations in soil microbial traits in response to increasing rates of N deposition may provide further insights into soil C emission dynamics in subtropical forests.

Supplementary Materials: The following are available online at http://www.mdpi.com/1999-4907/10/5/435/s1, Figure S1. Changes in root biomass under different N addition treatments. Values are means ± standard error ($n = 4$). * indicates statistically significant differences at $p < 0.05$. CT: control, LN: low nitrogen, HN: high nitrogen, Figure S2. Monthly soil temperature dynamics in 2013 (a), 2014 (b), and 2015 (c), Figure S3. Soil moisture under N addition from 2013 to 2015, Table S1. Relative carbon (C) distribution (%) in different chemical shift regions in ^{13}C cross-polarization magic-angle spinning of soil under different nitrogen addition treatments, Table S2. The exponential relationship between soil CO_2 emission rate and soil temperature in each subplots under different nitrogen addition treatments, Table S3 Effects of N addition on the phospholipid fatty acid biomarker concentration (nmol g^{-1} soil). Error bars represent standard deviation ($n = 4$). The different letters indicate significant differences between treatments at $p < 0.05$. G^+: gram-positive bacteria; G^-: gram-negative bacteria; Bacteria: sum of G^+ and G^-; Unclassified: unclassified biomarkers; ACT: actinomycetes; Total: total PLFA, Table S4 Characteristics of 16 studies site. RRs: Response ratio of soil respiration.

Author Contributions: Conceptualization, J.Z., X.L., Y.C. and Y.Y.; Formal analysis, J.X.; Funding acquisition, Y.C. and Y.Y.; Investigation, J.Z., X.L., M.L., Y.Z. and Z.Y.; Methodology, J.X., M.L., Y.Z., Z.Y., Y.F., C.L. and G.C.; Supervision, Y.C. and Y.Y.; Writing—original draft, J.Z.; Writing—review & editing, J.Z. and Y.C.

Funding: This research was funded in part through the National Natural Science Foundation of China (No. U1505233, No. 31670620) and the National Key Basic Research Program of China (973 Program) (No. 2014CB954003).

Acknowledgments: We would like to thank Wei Zheng, Yuhuang Ji and Guoyu Li for their help in field work and laboratory analyses.

Conflicts of Interest: The authors declare no conflict of interest.

References

1. Galloway, J.N.; Townsend, A.R.; Erisman, J.W.; Bekunda, M.; Cai, Z.; Freney, J.R.; Martinelli, L.A.; Seitzinger, S.P.; Sutton, M.A. Transformation of the nitrogen cycle: Recent trends, questions, and potential solutions. *Science* **2008**, *320*, 889–892. [CrossRef]
2. Sutton, M.A.; Nemitz, E.; Erisman, J.W.; Beier, C.; Bahl, K.B.; Cellier, P.; de Vries, W.; Cotrufo, F.; Skiba, U.; Di Marco, C.; et al. Challenges in quantifying biosphere-atmosphere exchange of nitrogen species. *Environ. Pollut.* **2007**, *150*, 125–139. [CrossRef] [PubMed]

3. Bond-Lamberty, B.; Thomson, A. Temperature-associated increases in the global soil respiration record. *Nature* **2010**, *464*, 579–582. [CrossRef]
4. Tateno, M.; Chapin, F.S. The logic of carbon and nitrogen interactions in terrestrial ecosystems. *Am. Nat.* **1997**, *149*, 723–744. [CrossRef]
5. Cleveland, C.C.; Liptzin, D. C:N:P stoichiometry in soil: Is there a "Redfield ratio" for the microbial biomass? *Biochemistry* **2007**, *85*, 235–252. [CrossRef]
6. Li, Q.; Song, X.; Chang, S.X.; Peng, C.; Xiao, W.; Zhang, J.; Xiang, W.; Li, Y.; Wang, W. Nitrogen depositions increase soil respiration and decrease temperature sensitivity in a Moso bamboo forest. *Agric. For. Meteorol.* **2019**, *268*, 48–54. [CrossRef]
7. Lebauer, D.S.; Treseder, K.K. Nitrogen limitation of net primary productivity in terrestrial ecosystems is globally distributed. *Ecology* **2008**, *89*, 371–379. [CrossRef]
8. Xia, J.; Wan, S. Global response patterns of terrestrial plant species to nitrogen addition. *New Phytol.* **2008**, *179*, 428–439. [CrossRef]
9. Liu, L.; Greaver, T.L. A global perspective on belowground carbon dynamics under nitrogen enrichment. *Ecol. Lett.* **2010**, *13*, 819–828. [CrossRef] [PubMed]
10. Zhou, L.; Zhou, X.; Zhang, B.; Lu, M.; Luo, Y.; Liu, L.; Li, B. Different responses of soil respiration and its components to nitrogen addition among biomes: a meta-analysis. *Glob. Chang. Biol.* **2014**, *20*, 2332–2343. [CrossRef]
11. Janssens, I.A.; Dieleman, W.; Luyssaert, S.; Subke, J.A.; Reichstein, M.; Ceulemans, R.; Ciais, P.; Dolman, A.J.; Grace, J.; Matteucci, G. Reduction of forest soil respiration in response to nitrogen deposition. *Nat. Geosci.* **2010**, *3*, 315–322. [CrossRef]
12. Yue, K.; Peng, Y.; Peng, C.; Yang, W.; Peng, X.; Wu, F. Stimulation of terrestrial ecosystem carbon storage by nitrogen addition: a meta-analysis. *Sci. Rep.* **2016**, *6*, 19895. [CrossRef] [PubMed]
13. Townsend, A.R.; Cleveland, C.C.; Houlton, B.Z.; Alden, C.B.; White, J.W.C. Multi-element regulation of the tropical forest carbon cycle. *Front. Ecol. Environ.* **2011**, *9*, 9–17. [CrossRef]
14. Sun, Z.; Liu, L.; Ma, Y.; Yin, G.; Zhao, C.; Zhang, Y.; Piao, S. The effect of nitrogen addition on soil respiration from a nitrogen-limited forest soil. *Agric. For. Meteorol.* **2014**, *197*, 103–110. [CrossRef]
15. Lee, K.H.; Jose, S. Soil respiration, fine root production, and microbial biomass in cottonwood and loblolly pine plantations along a nitrogen fertilization gradient. *For. Ecol. Manag.* **2003**, *185*, 263–273. [CrossRef]
16. Fan, Y.; Zhong, X.; Lin, F.; Liu, C.; Yang, L.; Wang, M.; Chen, G.; Chen, Y.; Yang, Y. Responses of soil phosphorus fractions after nitrogen addition in a subtropical forest ecosystem: Insights from decreased Fe and Al oxides and increased plant roots. *Geoderma* **2019**, *337*, 246–255. [CrossRef]
17. Vivanco, L.; Austin, A.T. Intrinsic effects of species on leaf litter and root decomposition: A comparison of temperate grasses from North and South America. *Oecologia* **2006**, *150*, 97–107. [CrossRef]
18. Parton, W.; Silver, W.L.; Burke, I.C.; Grassens, L.; Harmon, M.E.; Currie, W.S.; King, J.Y.; Adair, E.C.; Brandt, L.A.; Hart, S.C. Global-Scale Similarities in Nitrogen Release Patterns during Long-Term Decomposition. *Science* **2007**, *315*, 361. [CrossRef]
19. Schimel, J.P.; Weintraub, M.N. The implication of exoenzyme activity on microbial carbon and nitrogen limitation in soil: a theoretical model. *Soil Biol. Biochem.* **2003**, *35*, 549–563. [CrossRef]
20. Wu, N.; Filley, T.R.; Bai, E.; Han, S.; Jiang, P. Incipient changes of lignin and substituted fatty acids under N addition in a Chinese forest soil. *Org. Geochem.* **2015**, *79*, 14–20. [CrossRef]
21. Liu, J.; Wu, N.; Wang, H.; Sun, J.; Peng, B.; Jiang, P.; Bai, E. Nitrogen addition affects chemical compositions of plant tissues, litter and soil organic matter. *Ecology* **2016**, *97*, 1796–1806. [CrossRef]
22. Haider, K.; Martin, J.P. Synthesis and Transformation of Phenolic Compounds by Epicoccum nigrum in Relation to Humic Acid Formation1. *Soil Sci. Soc. Am. J.* **1967**, *31*, 766. [CrossRef]
23. Bouwman, A.F.; van Vuuren, D.P.; Derwent, R.G.; Posch, M. A global analysis of acidification and eutrophication of terrestrial ecosystems. *Water Air Soil Pollut.* **2002**, *141*, 349–382. [CrossRef]
24. Tian, D.; Niu, S. A global analysis of soil acidification caused by nitrogen addition. *Environ. Res. Lett.* **2015**, *10*, 024019. [CrossRef]
25. Enrique, A.G.; Bruno, C.; Christopher, A.; Virgile, C.; Stéven, C. Effects of nitrogen availability on microbial activities, densities and functional diversities involved in the degradation of a Mediterranean evergreen oak litter (*Quercus ilex* L.). *Soil Biol. Biochem.* **2008**, *40*, 1654–1661. [CrossRef]

26. Zhang, N.; Wan, S.; Li, L.; Bi, J.; Zhao, M.; Ma, K. Impacts of urea N addition on soil microbial community in a semi-arid temperate steppe in northern China. *Plant Soil* **2008**, *311*, 19–28. [CrossRef]
27. Zhou, X.; Zhang, Y.; Downing, A. Non-linear response of microbial activity across a gradient of nitrogen addition to a soil from the Gurbantunggut Desert, northwestern China. *Soil Biol. Biochem.* **2012**, *47*, 67–77. [CrossRef]
28. Allison, S.D.; LeBauer, D.S.; Ofrecio, M.R.; Reyes, R.; Ta, A.M.; Tran, T.M. Low levels of nitrogen addition stimulate decomposition by boreal forest fungi. *Soil Biol. Biochem.* **2009**, *41*, 293–302. [CrossRef]
29. Ouyang, X.; Zhou, G.; Huang, Z.; Zhou, C.; Li, J.; Shi, J.; Zhang, D. Effect of N and P addition on soil organic C potential mineralization in forest soils in South China. *J. Environ. Sci.* **2008**, *20*, 1082–1089. [CrossRef]
30. Hasselquist, N.J.; Metcalfe, D.B.; Högberg, P. Contrasting effects of low and high nitrogen additions on soil CO2flux components and ectomycorrhizal fungal sporocarp production in a boreal forest. *Glob. Chang. Biol.* **2012**, *18*, 3596–3605. [CrossRef]
31. Liu, X.; Yang, Z.; Lin, C.; Giardina, C.P.; Xiong, D.; Lin, W.; Chen, S.; Xu, C.; Chen, G.; Xie, J. Will nitrogen deposition mitigate warming-increased soil respiration in a young subtropical plantation? *Agric. For. Meteorol.* **2017**, *246*, 78–85. [CrossRef]
32. Fan, Y.; Lin, F.; Yang, L.; Zhong, X.; Wang, M.; Zhou, J.; Chen, Y.; Yang, Y. Decreased soil organic P fraction associated with ectomycorrhizal fungal activity to meet increased P demand under N application in a subtropical forest ecosystem. *Biol. Fertil. Soils* **2017**, *54*, 149–161. [CrossRef]
33. Liu, X.; Lei, D.; Mo, J.; Du, E.; Shen, J.; Lu, X.; Ying, Z.; Zhou, X.; He, C.; Zhang, F. Nitrogen deposition and its ecological impact in China: An overview. *Environ. Pollut.* **2011**, *159*, 2251–2264. [CrossRef]
34. Sheng, H.; Yang, Y.; Yang, Z.; Chen, G.; Xie, J.; Guo, J.; Zou, S. The dynamic response of soil respiration to land-use changes in subtropical China. *Glob. Chang. Biolog.* **2010**, *16*, 1107–1121. [CrossRef]
35. Wan, X.; Huang, Z.; He, Z.; Yu, Z.; Wang, M.; Davis, M.R.; Yang, Y. Soil C:N ratio is the major determinant of soil microbial community structure in subtropical coniferous and broadleaf forest plantations. *Plant Soil* **2015**, *387*, 103–116. [CrossRef]
36. Frostegård, Å.; Tunlid, A.; Bååth, E. Use and misuse of PLFA measurements in soils. *Soil Biol. Biochem.* **2011**, *43*, 1621–1625. [CrossRef]
37. Ushio, M.; Balser, T.C.; Kitayama, K. Effects of condensed tannins in conifer leaves on the composition and activity of the soil microbial community in a tropical montane forest. *Plant Soil* **2013**, *365*, 157–170. [CrossRef]
38. Swallow, M.; Quideau, S.A.; MacKenzie, M.D.; Kishchuk, B.E. Microbial community structure and function: The effect of silvicultural burning and topographic variability in northern Alberta. *Soil Biol. Biochem.* **2009**, *41*, 770–777. [CrossRef]
39. Olsson, P.A. Signature fatty acids provide tools for determination of the distribution and interactions of mycorrhizal fungi in soil. *Fems Microbiol. Ecol.* **1999**, *29*, 303–310. [CrossRef]
40. Fierer, N.; Schimel, J.P.; Holden, P.A. Variations in microbial community composition through two soil depth profiles. *Soil Biol. Biochem.* **2003**, *35*, 167–176. [CrossRef]
41. Tornberg, K.; Bååth, E.; Olsson, S. Fungal growth and effects of different wood decomposing fungi on the indigenous bacterial community of polluted and unpolluted soils. *Biol. Fertil. Soils* **2003**, *37*, 190–197.
42. Skjemstad, J.O.; Clarke, P.; Taylor, J.A.; Oades, J.M.; Newman, R.H. The removal of magnetic materials from surface soils—A solid state 13 C CP/MAS NMR study. *Aus. J. Soil Res.* **1994**, *32*, 1215–1229. [CrossRef]
43. Preston, C.M.; Nault, J.R.; Trofymow, J.A. Chemical Changes During 6 Years of Decomposition of 11 Litters in Some Canadian Forest Sites. Part 2. ^{13}C Abundance, Solid-State ^{13}C NMR Spectroscopy and the Meaning of "Lignin". *Ecosystems* **2009**, *12*, 1078–1102. [CrossRef]
44. Dai, K.O.H.; Johnson, C.E.; Driscoll, C.T. Organic matter chemistry and dynamics in clear-cut and unmanaged hardwood forest ecosystems. *Biogeochemistry* **2001**, *54*, 51–83. [CrossRef]
45. Jones, D.L.; Willett, V.B. Experimental evaluation of methods to quantify dissolved organic nitrogen (DON) and dissolved organic carbon (DOC) in soil. *Soil Biol. Biochem.* **2006**, *38*, 991–999. [CrossRef]
46. Lloyd, J.; Taylor, J.A. On the Temperature Dependence of Soil Respiration. *Funct. Ecol.* **1994**, *8*, 315–323. [CrossRef]
47. Zhang, X.J.; Hui, X.U.; Chen, G.X. Major factors controlling nitrous oxide emission and methane uptake from forest soil. *J. For. Res.* **2001**, *12*, 239–242.

48. Bowden, R.D.; Davidson, E.; Savage, K.; Arabia, C.; Steudler, P. Chronic nitrogen additions reduce total soil respiration and microbial respiration in temperate forest soils at the Harvard Forest. *For. Ecol. Manag.* **2004**, *196*, 43–56. [CrossRef]
49. Maaroufi, N.I.; Nordin, A.; Hasselquist, N.J.; Bach, L.H.; Palmqvist, K.; Gundale, M.J. Anthropogenic nitrogen deposition enhances carbon sequestration in boreal soils. *Glob. Chang. Biol.* **2015**, *21*, 3169–3180. [CrossRef]
50. Song, X.; Gu, H.; Wang, M.; Zhou, G.; Li, Q. Management practices regulate the response of Moso bamboo foliar stoichiometry to nitrogen deposition. *Sci. Rep.* **2016**, *6*, 24107. [CrossRef]
51. Treseder, K.K. Nitrogen additions and microbial biomass: A meta-analysis of ecosystem studies. *Ecol. Lett.* **2008**, *11*, 1111–1120. [CrossRef] [PubMed]
52. Lu, M.; Zhou, X.; Luo, Y.; Yang, Y.; Fang, C.; Chen, J.; Li, B. Minor stimulation of soil carbon storage by nitrogen addition: A meta-analysis. *Agric. Ecosyst. Environ.* **2011**, *140*, 234–244. [CrossRef]
53. Tian, D.; Hong, W.; Jian, S.; Niu, S. Global evidence on nitrogen saturation of terrestrial ecosystem net primary productivity. *Environ. Res. Lett.* **2016**, *11*, 024012. [CrossRef]
54. Zhou, Z.; Wang, C.; Zheng, M.; Jiang, L.; Luo, Y. Patterns and mechanisms of responses by soil microbial communities to nitrogen addition. *Soil Biol. Biochem.* **2017**, *115*, 433–441. [CrossRef]
55. Driscoll, C.T.; Driscoll, K.M.; Mitchell, M.J.; Raynal, D.J. Effects of acidic deposition on forest and aquatic ecosystems in New York State. *Environ. Pollut.* **2003**, *123*, 327–336. [CrossRef]
56. Mo, J.; Li, D.; Gundersen, P. Seedling growth response of two tropical tree species to nitrogen deposition in southern China. *Eur. J. For. Res.* **2008**, *127*, 275–283. [CrossRef]
57. Lu, X.; Mao, Q.; Gilliam, F.S.; Luo, Y.; Mo, J. Nitrogen deposition contributes to soil acidification in tropical ecosystems. *Glob. Chang. Biol.* **2014**, *20*, 3790–3801. [CrossRef] [PubMed]
58. Mo, J.; Zhang, W.; Zhu, W.; Fang, Y.; Li, D.; Zhao, P. Response of soil respiration to simulated N deposition in a disturbed and a rehabilitated tropical forest in southern China. *Plant Soil* **2007**, *296*, 125–135. [CrossRef]
59. Liu, Q.; Edwards, N.T.; Post, W.M.; Gu, L.; Ledford, J.; Lenhart, S. Temperature-independent diel variation in soil respiration observed from a temperate deciduous forest. *Glob. Chang. Biol.* **2006**, *12*, 2136–2145. [CrossRef]
60. Wang, Q.K.; Zhao, X.C.; Chen, L.C.; Yang, Q.P.; Chen, S.; Zhang, W.D. Global synthesis of temperature sensitivity of soil organic carbon decomposition: Latitudinal patterns and mechanisms. *Funct. Ecol.* **2019**, *33*, 514–523. [CrossRef]
61. Liu, Y.; He, N.P.; Zhu, J.X.; Xu, L.; Yu, G.R.; Niu, S.L.; Sun, X.M.; Wen, X.F. Regional variation in the temperature sensitivity of soil organic matter decomposition in China's forests and grasslands. *Glob. Chang. Biol.* **2017**, *23*, 3393–3402. [CrossRef]
62. Chen, R.; Senbayram, M.; Blagodatsky, S.; Myachina, O.; Dittert, K.; Lin, X.; Blagodatskaya, E.; Kuzyakov, Y. Soil C and N availability determine the priming effect: microbial N mining and stoichiometric decomposition theories. *Glob. Chang. Biol.* **2014**, *20*, 2356–2367. [CrossRef]
63. Ramirez, K.S.; Craine, J.M.; Fierer, N. Consistent effects of nitrogen amendments on soil microbial communities and processes across biomes. *Glob. Chang. Biol.* **2012**, *18*, 1918–1927. [CrossRef]
64. Fatemi, F.R.; Fernandez, I.J.; Simon, K.S.; Dail, D.B. Nitrogen and phosphorus regulation of soil enzyme activities in acid forest soils. *Soil Biol. Biochem.* **2016**, *98*, 171–179. [CrossRef]
65. Wang, J.J.; Bowden, R.D.; Lajtha, K.; Washko, S.E.; Wurzbacher, S.J.; Simpson, M.J. Long-term nitrogen addition suppresses microbial degradation, enhances soil carbon storage, and alters the molecular composition of soil organic matter. *Biogeochemistry* **2019**, *142*, 299–313. [CrossRef]
66. Feng, X.; Simpson, M.J. Temperature and substrate controls on microbial phospholipid fatty acid composition during incubation of grassland soils contrasting in organic matter quality. *Soil Biol. Biochem.* **2009**, *41*, 804–812. [CrossRef]
67. Griffiths, B.S.; Ritz, K.; Ebblewhite, N.; Dobson, G. Soil microbial community structure: effects of substrate loading rates. *Soil Biol. Biochem.* **1999**, *31*, 145–153. [CrossRef]
68. Kramer, C.; Gleixner, G. Variable use of plant- and soil-derived carbon by microorganisms in agricultural soils. *Soil Biol. Biochem.* **2006**, *38*, 3267–3278. [CrossRef]
69. Baldock, J.A.; Oades, J.M.; Waters, A.G.; Peng, X.; Vassallo, A.M.; Wilson, M.A. Aspects of the Chemical Structure of Soil Organic Materials as Revealed by Solid-State ^{13}CNMR Spectroscopy. *Biogeochemistry* **1992**, *16*, 1–42. [CrossRef]
70. Knorr, M.; Frey, S.D.; Curtis, P.S. Nitrogen Additions and Litter Decomposition: A Meta-Analysis. *Ecology* **2005**, *86*, 3252–3257. [CrossRef]

71. Frey, S.D.; Ollinger, S.; Nadelhoffer, K.; Bowden, R.; Brzostek, E.; Burton, A.; Caldwell, B.A.; Crow, S.; Goodale, C.L.; Grandy, A.S.; et al. Chronic nitrogen additions suppress decomposition and sequester soil carbon in temperate forests. *Biogeochemistry* **2014**, *121*, 305–316. [CrossRef]
72. Berg, M.P.; Kniese, J.P.; Zoomer, R.; Verhoef, H.A. Long-term decomposition of successive organic strata in a nitrogen saturated Scots pine forest soil. *For. Ecol. Manag.* **1998**, *107*, 159–172. [CrossRef]
73. Davidson, E.A.; Sabá, R.T. Nitrogen and phosphorus limitation of biomass growth in a tropical secondary forest. *Ecol. Appl.* **2004**, *14*, 150–163. [CrossRef]
74. Zeng, W.; Chen, J.; Liu, H.; Wang, W. Soil respiration and its autotrophic and heterotrophic components in response to nitrogen addition among different degraded temperate grasslands. *Soil Biol. Biochem.* **2018**, *124*, 255–265. [CrossRef]
75. Chambers, J.Q.; Tribuzy, E.S.; Toledo, L.C.; Crispim, B.F.; Higuchi, N.; dos Santos, J.; Araujo, A.C.; Kruijt, B.; Nobre, A.D.; Trumbore, S.E. Respiration from a tropical forest ecosystem: Partitioning of sources and low carbon use efficiency. *Ecol. Appl.* **2004**, *14*, S72–S88. [CrossRef]
76. Zhu, J.; Yan, Q.; Fan, A.N.; Yang, K.; Hu, Z. The role of environmental, root, and microbial biomass characteristics in soil respiration in temperate secondary forests of Northeast China. *Trees* **2009**, *23*, 189–196. [CrossRef]
77. Iqbal, J.; Hu, R.; Feng, M.; Lin, S.; Malghani, S.; Ali, I.M. Microbial biomass, and dissolved organic carbon and nitrogen strongly affect soil respiration in different land uses: A case study at Three Gorges Reservoir Area, South China. Agric. *Ecosyst. Environ.* **2010**, *137*, 294–307. [CrossRef]
78. Wang, C.; Liu, D.; Bai, E. Decreasing soil microbial diversity is associated with decreasing microbial biomass under nitrogen addition. *Soil Biol. Biochem.* **2018**, *120*, 126–133. [CrossRef]
79. Philippot, L.; Spor, A.; Henault, C.; Bru, D.; Bizouard, F.; Jones, C.M.; Sarr, A.; Maron, P.A. Loss in microbial diversity affects nitrogen cycling in soil. *Int. Soc. Microb. Ecol.* **2013**, *7*, 1609–1619.

forests

MDPI

Article

The Influence of Land Use Patterns on Soil Bacterial Community Structure in the Karst Graben Basin of Yunnan Province, China

Jiangmei Qiu [1,2,3], Jianhua Cao [2,3], Gaoyong Lan [2,3], Yueming Liang [2,3], Hua Wang [2,3] and Qiang Li [2,3,*]

1 College of Environmental Science and Engineering, Guilin University of Technology, Guilin 541004, China; 15676217735@163.com

2 Key Laboratory of Karst Dynamics, MNR & GZAR, Institute of Karst Geology, Chinese Academy of Geological Sciences, Guilin 541004, China; jhcaogl@karst.ac.cn (J.C.); langaoyong@karst.ac.cn (G.L.); lym@karst.ac.cn (Y.L.); wanghua@karst.ac.cn (H.W.)

3 International Research Center on Karst under the Auspices of UNESCO, Guilin 541004, China

* Correspondence: liqiang@karst.ac.cn

Received: 21 November 2019; Accepted: 30 December 2019; Published: 31 December 2019

Abstract: Land use patterns can change the structure of soil bacterial communities. However, there are few studies on the effects of land use patterns coupled with soil depth on soil bacterial communities in the karst graben basin of Yunnan province, China. Consequently, to reveal the structure of the soil bacterial community at different soil depths across land use changes in the graben basins of the Yunnan plateau, the relationship between soil bacterial communities and soil physicochemical properties was investigated for a given area containing woodland, shrubland, and grassland in Yunnan province by using next-generation sequencing technologies coupled with soil physicochemical analysis. Our results indicated that the total phosphorus (TP), available potassium (AK), exchangeable magnesium (E-Mg), and electrical conductivity (EC) in the grassland were significantly higher than those in the woodland and shrubland, yet the total nitrogen (TN) and soil organic carbon (SOC) in the woodland were higher than those in the shrubland and grassland. *Proteobacteria*, *Verrucomicrobia*, and *Acidobacteria* were the dominant bacteria, and their relative abundances were different in the three land use types. SOC, TN, and AK were the most important factors affecting soil bacterial communities. Land use exerts strong effects on the soil bacterial community structure in the soil's surface layer, and the effects of land use attenuation decrease with soil depth. The nutrient content of the soil surface layer was higher than that of the deep layer, which was more suitable for the survival and reproduction of bacteria in the surface layer.

Keywords: karst graben basin; land use pattern; bacterial community; next-generation sequencing

1. Introduction

The karst graben basin in the East Yunnan plateau is a special geomorphological formation due to the rifts of the plateau, which were uplifted at the same time [1,2]. This area is also the main area of the "two barriers and three belts" for China's national ecological security. However, due to deforestation of this area over the past several decades, the karst ecosystem has seriously degenerated, thereby affecting soil quality, soil fertility, and ecological conditions, and resulting in abandoned bare land. To fight against this environmental problem, the "Green for Grain" program, or the Natural Forest Protection Project, was launched by the Chinese government in this region [3–5]. Accordingly, the size of the degenerated areas has shrunk with the revegetation process. However, little is known about how vegetation restoration types affect the soil bacterial community's structure in the karst graben basin.

Vegetation restoration can affect soil microorganism communities, which can regulate the soil's biogeochemical cycles and affect the stability of the soil's ecosystem [6–8]. Although many studies have discussed soil microbial community structures with land use pattern changes worldwide, there are few studies on the influence of land use patterns on the soil bacterial community's structure in karst graben basins. For example, Suleiman et al. compared the bacterial community in the original forest-covered area and grassland for eight years and found that the main bacterial community composition showed little difference [9]. Song et al. found that the number and composition of the soil microbial population in the karst peak-cluster depression were different in farmland, grassland, scrubland, forest plantation, secondary forest, and primary forest [10]. Ederson et al. found that there were significant differences in the community composition among crops, pastures, and agroforestry, as well as young secondary forest (up to 5 years old), old secondary forest (5 to 30 years old), and primary forest sites [11]. To better explore the influence of land use patterns on the soil bacterial community structure in the Luxi county in the Yunnan karst graben basin, the woodland, shrubland, and grassland in a given karst area were selected. Our objectives were to (i) gain insight into the difference of soil bacterial community structure with land use changes, (ii) inquire into the effects of land use patterns with soil depth, and (iii) identify the key factors in determining soil bacterial communities. Our findings provide a basis for understanding the influence of land use patterns on soil bacterial community structures in the karst graben basin of Yunnan province, China.

2. Materials and Methods

2.1. Study Sites

Luxi county (103°30′–104°03′ E, 24°15′–24°46′ N) is located in the north Honghe Hani and Yi Autonomous Prefecture in Yunnan province in the subtropical monsoon climate zone, which is rainy in summer and dry in winter. The rainy season extends from May to October, and the dry season runs from March to April. The average annual precipitation is 2026.5 mm. The average annual temperature is 16.3 °C. Moreover, the rocky desertification in Luxi country is serious.

2.2. Soil Sample Collection

Sampling occurred between the wet and dry season, January 2018. Three 20 × 20 m plots were established for each land use pattern. The minimum distance between plots was 400 m to avoid pseudoreplication. Soil samples were collected from the surface soil (0–10 cm), named the A layer, and the other samples were taken from the deep layer (10–20 cm), named B layer, with a split tube auger 5 cm in diameter. At each plot, six soil cores were selected in an S-shaped pattern to form one soil sample. A total of 18 soil samples from woodland (WL), shrubland (SL), and grassland (GL) were collected. Soil samples were named according to the soil sampling sites (such as SL) and soil layer (A: 0–10 cm) in that particular order (e.g., SLA). The three land use patterns were continuously managed for 15 years. All soil samples were transported to the laboratory immediately after collection in sterile plastic bags on dry ice and divided into two uniform portions. One portion was stored at −80 °C for DNA analysis, and the other part was air dried for physicochemical analysis.

2.3. Physicochemical Analysis

Soil moisture content (moisture), soil temperature (T), and EC were measured in situ by soil three-parameter tachometers (Delta-T Devices Ltd., Moisture Meter type HH2, UK). Soil organic carbon (SOC) was determined by wet digestion using the H_2SO_4 and $K_2Cr_2O_7$ method [12]. Total phosphorus (TP) was determined using the molybdenum blue colorimetric method following $HClO_4$ digestion [13]. Available potassium (AK) was extracted with ammonium acetate and analyzed using a flame photometer [14]. Total nitrogen (TN) was determined by an element analyzer [15]. Soil pH was determined by a 1:5 (m:V) soil/water ratio and measured by a corrected desktop pH meter of Maitre-Toledo S470-B Seven Excellence [16]. Exchangeable calcium (E-Ca)

and exchangeable magnesium (E-Mg) were determined by ammonium acetate exchange-atomic absorption spectrophotometry [17].

2.4. DNA Extraction

DNA was extracted using the Powersoil DNA Isolation Kit (Mobio Laboratories, Inc., Carlsbad, CA, USA). For next-generation sequencing, the V3–V4 region of 16S rRNA genes was amplified using PCR primers 338F (ACTCCTACGGGAGGCAGCA) and 806R (GGACTACHVGGGTWTCTA AT). The PCR products targeting the V3–V4 region of the 16S rRNA genes were purified by using the TIANquick Maxi Purification Kit (TIANGEN Biotech (Beijing) Co., Ltd., China). Then, 16S rRNA gene sequencing was performed on the Illumina HiSeq 2500 platform (Illumina Inc., San Diego, CA, USA) at the MAGIENE (Guangzhou, China).

2.5. Bioinformatic Analysis and Statistical Analysis

According to the barcode sequence, the sequencing data were divided into different sample data, and the barcode sequence was truncated. After splicing each sample with FLASH 1.2.11 software [18], the Cutadapt 1.9.1 software was employed to truncate the sequence of PCR amplified primers and remove fragments (less than 200 bp) [19]. Using the SILVA SSURef 123 NR database as the reference database, chimeric sequences were removed by the UCHIME 4.2 software [20,21]. Afterwards, the processed sequences were clustered with the UCLUST 1.2.22 software in operational taxonomic units (OTUs) according to sequences with more than a 97% similarity, and the OTUs were classified by the UCLUST 1.2.22 software alignment against the most recent SILVA (123) database [22]. The QIIME 1.9.1 software was used to perform an alpha diversity (Chao1, Simpson, Shannon, and Observed OTUs) and beta diversity test on the OTU table [23].

SPSS 25 software (SPSS Inc., Chicago, IL, USA) for a one-way ANOVA was used to analyze the difference soil physicochemical properties and bacterial community structure and diversity in different land use patterns [24]. The least significant difference method was used for multiple comparisons, and the Pearson correlation coefficient method was used for a correlation analysis. The Origin 8.5 software was used to map the abundance of bacterial communities at the phyla level. The OTUs whose numbers were more than 0.5% of the total OTUs were defined as the dominant OTUs. RStudio 3.0.3 software was used to draw the heat map of the dominant OTUs and perform a distance-based redundancy analysis (db-RDA) between the soil bacteria and soil physicochemical parameters [25]. The similarity of the OTUs among samples was analyzed by using the Bray–Curtis and weighted UniFrac distance algorithm of principal coordinate analysis (PCoA) [26]. The network maps of dominant OTUs and soil physicochemical factors were drawn via the Gephi 0.9.2 software [27].

3. Results

3.1. Soil Physicochemical Parameters with Land Use Changes

It can be seen that the soil's physicochemical properties were different in the woodland, shrubland, and grassland (Table 1). The TP, AK, E-Mg, EC, and T in grassland were higher than those in the woodland and shrubland. The TN and SOC in the woodland were higher than those in the shrubland and grassland. Moreover, the soil physicochemical properties, except for some physicochemical properties in woodland, decreased by increasing soil depth.

Table 1. The soil physicochemical properties in different land use patterns.

Name	Land Use Pattern	TP	TN	SOC	AK	pH	Moisture	T	EC	E-Ca	E-Mg
		(g/kg)	(g/kg)	(g/kg)	(g/kg)		(%)	(°C)	(ms.m^{-1})	(cmol/kg)	(cmol/kg)
WLA	woodland	0.828 ± 0.020 ab	5.09 ± 0.24 a	61.00 ± 1.96 a	128.47 ± 5.78 b	6.21 ± 0.11 b	37.47 ± 5.04 a	8.60 ± 0.21 c	68.33 ± 4.10 b	5.14 ± 1.15 a	26.82 ± 0.65 c
SLA	Shrubland	0.734 ± 0.025 b	4.11 ± 0.16 b	47.00 ± 2.5 b	124.03 ± 14.05 b	6.72 ± 0.09 a	42.85 ± 2.56 a	11.60 ± 1.12 b	64.33 ± 2.03 b	6.91 ± 0.09 a	36.18 ± 3.48 b
GLA	Grassland	0.941 ± 0.059 a	2.97 ± 0.14 c	33.00 ± 1.47 c	262.17 ± 44.37 a	6.68 ± 0.08 a	40.00 ± 1.42 a	16.53 ± 0.74 a	84.67 ± 2.03 a	6.87 ± 0.08 a	51.56 ± 2.32 a
WLB	woodland	0.640 ± 0.037 a	3.16 ± 0.49 a	35.79 ± 5.32 a	40.40 ± 2.14 b	6.46 ± 0.10 a	36.53 ± 2.98 a	9.37 ± 0.09 c	70.33 ± 6.64 ab	6.64 ± 0.11 a	29.21 ± 0.28 c
SLB	Shrubland	0.595 ± 0.025 a	2.32 ± 0.12 a	24.53 ± 2.13 ab	38.40 ± 3.98 b	6.66 ± 0.08 a	33.07 ± 1.91 a	10.97 ± 0.33 b	56.00 ± 3.00 b	6.85 ± 0.08 a	34.20 ± 1.02 b
GLB	Grassland	0.762 ± 0.084 a	2.34 ± 0.37 a	20.46 ± 3.71 b	127.27 ± 15.21 a	6.55 ± 0.03 a	32.70 ± 1.16 a	12.77 ± 0.34 a	79.33 ± 5.70 a	6.73 ± 0.03 a	39.82 ± 1.05 a

Note: A = 0–10 cm (A layer), B = 10–20 cm (B layer); data are the means ± standard error (means ± SE); different lowercase letters (a, b and c) in the same column represent a significant difference from the different sample points in the same soil layer ($p < 0.05$). TP: total phosphorous, TN: total nitrogen, SOC: soil organic carbon, AK: available potassium, T: temperature, EC: electrical conductivity, E-Ca: exchangeable calcium, E-Mg: exchangeable magnesium.

3.2. Soil Bacterial Community Structure and Diversity

The dominant phyla were different in the three land use types, as well as in the A and B layers, as seen in Figure 1. There were 13 dominant phyla in the A layer (Figure 1a). *Proteobacteria*, *Verrucomicrobia*, and *Acidobacteria* were the most abundant dominant bacteria. The total proportions of the three dominant bacteria in the A layer were woodland (80.22%), shrubland (80.07%), and grassland (59.52%); the *Verrucomicrobia* in grassland were significantly fewer than those in the woodland and shrubland; *Acidobacteria*, *Actinobacteria*, *Bacteroidetes*, and *Chloroflexi* in grassland were significantly higher than those in woodland and shrubland (Table S1). In the B layer, the total proportions of the three most abundant dominant bacteria were woodland (78.61%), shrubland (67.14%), and grassland (56.03%). Among the three different land use patterns, the composition and proportions of the other dominant phyla were different but not significant.

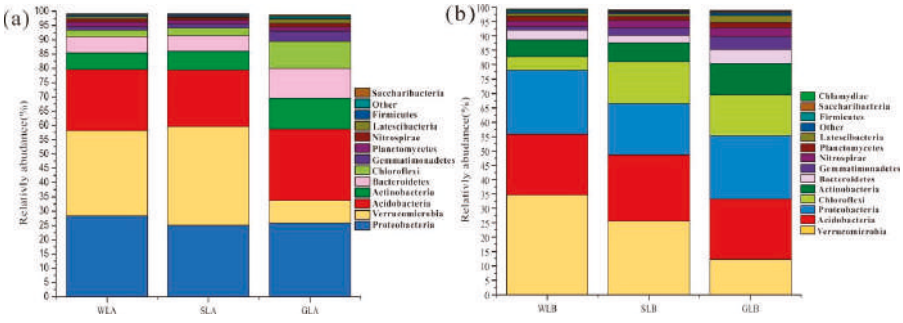

Figure 1. Comparison of the average quantitative contribution of the sequences affiliated with different bacterial phyla from the A layer (**a**) and B layer (**b**). Sequences not classified under any known phylum are included as unassigned bacteria. In each soil sample, the bacterial phylum with relative frequency of less than 1% is included as others.

Moreover, the heat map clearly shows the distribution of the dominant OTUs (Figure 2). In the A layer (Figure 2a), OTU 410 (DA101 soil group) and OTU 24 (*Candidatus Solibacter*) were the dominant OTUs for the woodland; OTUs 238 and 30 (*Candidatus Solibacter*), OTUs 28 and 124 (*Sphingomonas*), OTUs 49, 69, and 27 (subgroup 6), and OTUs 58, 368, 26, and 47 (RB41) were the dominant OTUs for grassland; and OTUs 1, 31, 2312, 9, and 823 (DA101 soil group), and OTU 12 (*Acidobacteria*) were the dominant OTUs for shrubland. In the B layer (Figure 2b), OTUs 163, 823, 2, 1, and 772 (DA101 soil group), and OTUs 10 and 2858 (*Acidobacteriaceae*) were the dominant OTUs in shrubland. OTUs 65 and 16 (0319-6A21) and OTUs 53 and 11 (*Acidobacteriaceae*) were the dominant OTUs in woodland. OTU 21 (*Candidatus Xiphinematobacter*), OTU 71 (*Gemmatimonadaceae*), and OTU 54 (*Pedomicrobium*) were the dominant OTUs in grassland.

The alpha diversities of the soil bacterial communities were different between the three land use types. In the A layer, except for the Simpson index, the alpha diversity indices from grassland were significantly higher than those from shrubland and woodland ($p < 0.05$), as listed in Table 2. Moreover, there was no significant difference between shrubland and woodland ($p > 0.05$). In the B layer, the alpha diversity indices of the three land use patterns were not significantly different, except for the Simpson index. The alpha diversities decreased with an increase in soil depth, except for the Simpson index.

To investigate the effects of land use type and soil depth on soil bacterial communities, we examined the beta diversity (Figure 3). The shrubland and woodland can be accurately clustered together, which shows the similarity of their bacterial communities' compositions. Compared with the A layer, the points in the B layer were more dispersed.

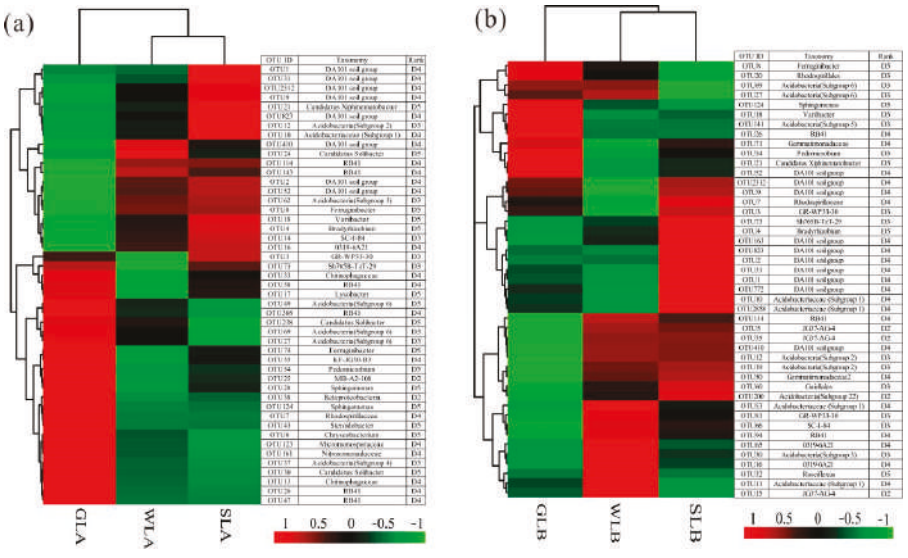

Figure 2. Heat map illustrating the mean relative frequency of the 47 most abundant operational taxonomic units (OTUs) with abundances >0.5% in the A layer with different land uses (**a**). Heat map illustrating the mean relative frequency of the 45 most abundant OTUs with abundances >0.5% in the B layer with different land uses (**b**). Taxonomic assignment of the OTUs is provided at the lowest level of classification possible according to the SILVA 123 database (D1: phylum, D2: class, D3: order, D4: family, and D5: genus).

Table 2. Alpha diversities of the soil bacterial communities with different land use patterns.

Name	Land Use Pattern	Chao1	Shannon	Simpson	Observed OTUs
WLA	Woodland	1656 ± 69 b	8.01 ± 0.23 b	0.985 ± 0.004 a	1162 ± 45 b
SLA	Shrubland	1640 ± 70 b	7.69 ± 0.17 b	0.977 ± 0.004 b	1103 ± 48 b
GLA	Grassland	1935 ± 75 a	8.85 ± 0.10 a	0.993 ± 0.001 a	1409 ± 25 a
WLB	Woodland	1582 ± 89 a	7.80 ± 0.31 a	0.981 ± 0.005 b	1115 ± 67 a
SLB	Shrubland	1565 ± 62 a	7.70 ± 0.07 a	0.982 ± 0.002 a	1030 ± 24 a
GLB	Grassland	1693 ± 119 a	8.54 ± 0.37 a	0.993 ± 0.003 a	1212 ± 106 a

Note: A = 0–10 cm (A layer), B = 10–20 cm (B layer); data are the means ± standard error (means ± SE). Different lowercase letters (a and b) in the same column represent a significant difference from the different sample points in the same soil layer ($p < 0.05$).

3.3. The Relationship between Soil Physicochemical Parameters and Soil Bacteria

To assess the influence of land uses on bacterial community composition, we performed a db-RDA on the dominant bacterial phyla. According to the db-RDA plot and Spearman's correlations between the soil physicochemical parameters and dominant phyla in the land use types, the first two axes accounted for 2.86% of the variability of the bacterial community structure in the A layer. Further, the bacterial communities were positively correlated with six soil physicochemical properties (including SOC, TN, TP, AK, EC, and T) (Figure 4a). *Verrucomicrobia* were negatively correlated with TP, T, E-Mg, AK, and EC, and positively correlated with TN and SOC. *Acidobacteria* were positively correlated with EC, T, and E-Mg; *Actinobacteria* were positively correlated with AK, EC, T, and E-Mg; *Bacteroidetes* were positively correlated with E-Mg, AK, and EC; *Chloroflexi* were positively correlated with T, E-Mg, TP, AK, and EC; and *Actinobacteria*, *Bacteroidetes*, and *Chloroflexi* were negatively correlated with TN and SOC (Figure 5). In the B layer, db-RDA showed that the first two axes accounted for 2.86% of the variability of the bacterial community structure, and bacterial communities were positively

correlated with SOC, TN, AK, and T (Figure 4b). *Verrucomicrobia* were positively correlated with SOC and negatively correlated with AK, T, and E-Mg. *Acidobacteria* were negatively correlated with TP; *Chloroflexi* were negatively correlated with TN and SOC, and positively correlated with T and E-Mg; *Actinobacteria* were positively correlated with AK, TP, T, E-Mg, and EC; and *Bacteroidetes* were positively correlated with AK and TP (Figure 5).

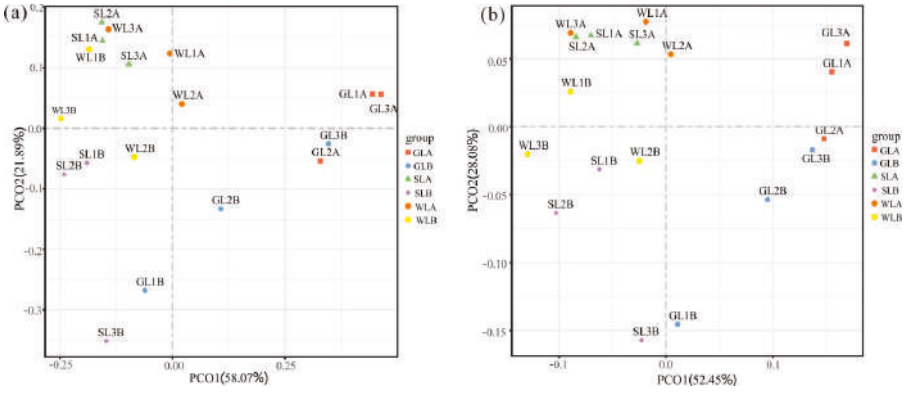

Figure 3. Principal coordinate analysis (PCoA) plots of soil microbial community structures based on the Bray–Curtis and weighted UniFrac results under different land use types in the Yunnan karst graben basin. Bray–Curtis (**a**); weighted UniFrac (**b**).

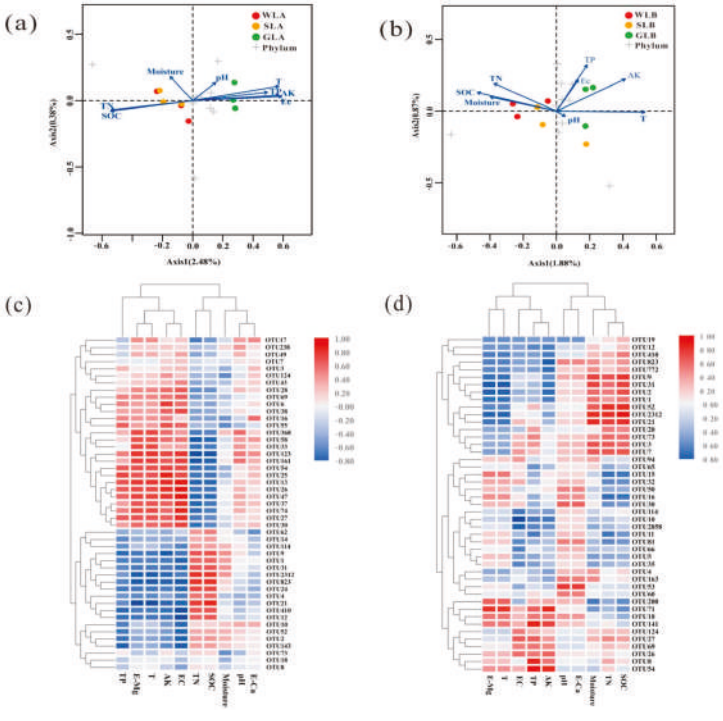

Figure 4. *Cont*.

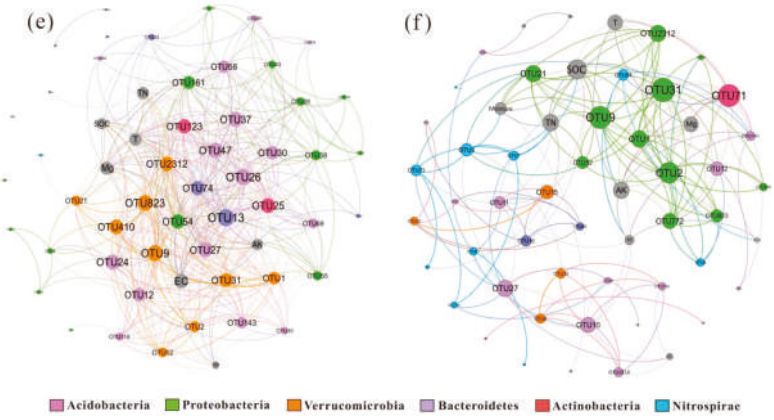

Figure 4. Distance-based redundancy analysis (db-RDA) plots revealing the relationship between the dominant phyla (mean relative frequency >1%) and soil physicochemical parameters in the surface layer (**a**) and deep layer (**b**). Heat map representing the relationship between the soil physicochemical parameters and the most abundant OTUs with abundances >0.5% in the surface layer (**c**) and deep layer (**d**). The networks revealing the co-occurring bacterial OTUs and soil properties in the surface layer (**e**) and deep layer (**f**). The co-occurring networks are colored at the phylum level, and the size of each node is proportional to the number of connections.

A Layer	TP	TN	SOC	AK	pH	T	Moistrue	EC	E-Ca	E-Mg
Proteobacteria	-0.150	0.214	0.283	-0.144	-0.546	-0.395	-0.746*	-0.103	-0.176	-0.395
Verrucomicrobia	-0.691*	0.757*	0.748*	-0.801**	-0.157	-0.775*	0.309	-0.819**	-0.161	-0.775*
Acidobacteria	0.558	-0.611	-0.540	0.565	0.171	0.674*	-0.068	0.777*	-0.089	0.674*
Actinobacteria	0.596	-0.860**	-0.864**	0.820**	0.41	0.830**	-0.132	0.820**	0.327	0.830**
Bacteroidetes	0.666	-0.683*	-0.757*	0.900**	0.114	0.753*	-0.265	0.823**	0.133	0.753*
Chloroflexi	0.739*	-0.776*	-0.816**	0.738*	0.441	0.902**	0.098	0.742*	0.274	0.902**
Planctomycetes	-0.348	0.135	0.254	-0.350	-0.311	-0.180	-0.420	-0.064	-0.439	-0.180
B Layer	**TP**	**TN**	**SOC**	**AK**	**PH**	**T**	**Moisture**	**EC**	**E-Ca**	**E-Mg**
Verrucomicrobia	-0.366	0.581	0.753*	-0.723*	-0.034	-0.845**	0.660	-0.259	-0.028	-0.845**
Acidobacteria	-0.725*	-0.612	-0.423	-0.356	-0.284	0.006	-0.540	-0.568	-0.279	0.006
Proteobacteria	0.472	0.219	0.169	0.354	-0.29	-0.134	0.095	0.503	-0.299	-0.134
Chloroflexi	-0.211	-0.700*	-0.750*	0.193	0.18	0.683*	-0.617	-0.139	0.180	0.683*
Actinobacteria	0.678*	-0.195	-0.406	0.843**	0.239	0.683*	-0.112	0.669*	0.234	0.683*
Bacteroidetes	0.953**	0.437	0.186	0.706	-0.066	0.259	-0.073	0.268	-0.070	0.259
Nitrospirae	-0.386	-0.764*	-0.748*	0.056	0.158	0.534	-0.279	0.143	0.155	0.534
Planctomycetes	0.884**	0.392	0.173	0.641	-0.29	0.153	-0.152	0.251	-0.298	0.153

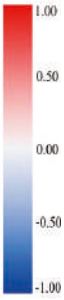

Figure 5. Spearman's correlations showing the relationship between the soil physicochemical parameters and dominant phyla in the three land use types. Significance levels are denoted as follows: $p < 0.05$ (*) and $p < 0.01$ (**).

Heat maps showed that TP, T, E-Mg, AK, EC, TN, and SOC were significantly correlated with most of the dominant OTUs, whereas pH and E-Ca were significantly correlated with some OTUs (Figure 4c,d). In the A layer, OTUs 26, 47, 58, and 368 (RB41); OTUs 27 and 49 (subgroup 6); and OTUs 30 and 238 (*Candidatus Solibacter*) of *Acidobacteria* were significantly correlated with TP, T, E-Mg, AK, and EC (Figure 4c). Moreover, OTUs 28 and 124 (*Sphingomonas*), OTU 17 (*Lysobacter*), OTU 54 (*Pedomicrobium*), and OTU 43 (*Steroidobacter*) of *Proteobacteria* were also significantly correlated with TP, T, E-Mg, AK, and EC (Figure 4c). In the A layer, OTUs 1, 2, 9, 31, 52, 410, 823, and 2312 (DA101 soil group) and OTUs 114 and 143 (RB41) of *Verrucomicrobia* and *Acidobacteria* were significantly correlated with SOC and TN

(Figure 4c). In the B layer, OTU 26 (RB41) and OTUs 27 and 69 (subgroup 6) of *Acidobacteria* were significantly correlated with TP, T, E-Mg, AK, and EC (Figure 4d), and OTUs 1, 2, 9, 31, 52, 410, 772, 823, and 2312 (DA101 soil group) of *Verrucomicrobia* were significantly correlated with SOC and TN (Figure 4d), as confirmed by their significant relationships in Tables S2 and S3. Although representing the relationship between soil physicochemical parameters and despite the observation that the most abundant OTUs were different in the three land uses, these tables, on the whole, show a certain regularity (Figure 4c,d and Figure S1). The OTU co-occurrence patterns and the relationships among soil bacterial communities and physicochemical parameters were also investigated. Overall, the ecological networks were markedly different among the bacterial groups at different soil depths. This network was comprised of highly connected genera and soil physicochemical properties, thereby forming a "small world" topology. The nodes in the network were assigned to 11 bacterial phyla (Figure 4e,f). Among these, three phyla (*Proteobacteria*, *Acidobacteria*, and *Verrucomicrobia*) were widely distributed, accounting for over 60% of all nodes. In the surface layer, OTUs 26, 47, and 58 (RB41) and OTUs 1, 2, 9, 31, 410, 823, and 2312 (DA101 soil group) of *Acidobacteria* and *Verrucomicrobia* were keystone taxa (Figure 4e). In the deep layer, OTUs 1, 2, 9, and 2312 of *Acidobacteria* were keystone taxa (Figure 4f). This study indicates that these OTUs may play key roles in maintaining the structure and function of soil bacterial communities. It can be seen that EC, E-Mg, SOC, AK, T, and TN were the most important soil physicochemical factors affecting the bacterial community composition in the A layer, whereas SOC, AK, E-Mg, and TN were the most important factors in the B layer. The networks of competition and cooperation were more complex among bacteria in the surface layer than those in the deep layer. The correlation between bacterial communities and soil physicochemical properties decreased with an increase of soil depth (Figure 4c–f).

4. Discussion

4.1. The Characteristics of the Soil Physicochemical Properties

Land use patterns determine the surface vegetation and soil management method, which in turn result in a difference between soil physicochemical properties [28,29]. In our study, TP, AK, E-Mg, EC, and the moisture in grassland were significantly higher than those in the woodland and shrubland. However, the TN and SOC in woodland were significantly higher than those in shrubland and grassland. It is well known that microorganisms are intimately involved in rock weathering and could use these elements as electron acceptors and nutrients [30]. Consequently, grassland, during the early stages of vegetation succession under the influence of microorganisms on rock weathering, had a high concentration of AK, E-Mg, and TP compared with shrubland and woodland. However, due to the deficient root systems and lower amount of litter in grassland, the SOC and TN were low in the grassland. Moreover, SOC and TN are elements of soil fertility and are closely related to ecosystem stability, environmental protection, and land use [31,32]. Compared with grassland, the litter in woodland was high, and the root system was dense. Moreover, TN and SOC were also positively correlated. Therefore, the contents of TN and SOC in woodland were higher than those in shrubland and grassland. Further, soil nutrient contents decreased gradually with increasing soil depth because the soil's surface layer was the humus layer with rich litter, high nutrient content, a well-developed plant root system, good ventilation, and positive hydrothermal conditions [33–36].

4.2. Distribution of Bacterial Diversity Compositions

Bacterial communities from different land use types and different soil depths were highly diverse. In our study, soil bacterial diversity indices from grassland in the A layer and B layer were significantly higher than those in shrubland and woodland ($p < 0.05$). The diversity indices of soil bacterial communities in the three land use types decreased with increasing soil depth, which was consistent with the changes in soil physicochemical properties. Plant community richness usually increases during late successive stages. Moreover, increased plant community richness can significantly alter soil

bacterial community composition and is negatively correlated with bacterial diversity [37]. An increased plant community can supply a diverse array of resources to the soil, thereby promoting coevolutionary niche differentiation and favoring nonantagonistic microbial communities in which antagonism plays little role in maintaining soil community diversity [38]. The decrease in bacterial diversity with increasing soil depth is due to the reduction in the nutrient substrates for bacteria [39]. This is consistent with the expected depth patterns of soil bacterial diversity found in other studies [40,41].

Beta diversity was used to describe the similarities and differences in community structure. The PCoA distance showed a pronounced influence of land use changes on soil bacterial community structure. In our study, bacterial communities from grassland were significantly different from those in woodland and shrubland. This shows that the rate of species replacement between grassland and shrubland was relatively fast, possibly due to the lack of soil nutrients in grassland and increased competition during successive stages, which intensifies the species replacement between communities [42].

4.3. Relationships of Bacterial Communities with Basic Soil Parameters

Soil physicochemical properties determine the living environment of bacteria, which affect soil bacterial communities [43]. Soil bacteria play an extremely important role in organic matter decomposition, soil nutrient cycling, and ecological environment improvement [44,45]. Changes in bacterial community compositions led us to evaluate the extent of different land uses. Then, in our study, 33 dominant phyla were found in the 18 soil samples. *Proteobacteria*, *Verrucomicrobia,* and *Acrobacteria* were the most abundant dominant soil bacteria from the three land use patterns. These phyla have also been found in different relative proportions in other ecosystems worldwide [46,47], suggesting that they may play a fundamental role in these environments.

Proteobacteria showed no significant difference in the three land use patterns, yet their proportion in surface soil (26.61%) was significantly higher than that in deep soil (20.95%), which could be related to their copiotrophic living attributes. *Proteobacteria* belong to aerobic heterotrophic and facultative trophic bacteria [48,49], which are able to live in soils with high organic matter content. As a result, with an increase in soil depth, the soil nutrients decreased, and the abundance of *Proteobacteria* decreased. *Proteobacteria* were not significantly correlated with other physicochemical factors, except for soil moisture (Figure 5). At the same soil depth, the difference in moisture among the three land use patterns was not significant, and the other physicochemical factors had no significant effect on the distribution of *Proteobacteria* because *Proteobacteria* contain many subgroups with different habits, which are distributed in different niches. The *Proteobacteria's* structure is stable, and its anti-interference ability is strong. In the surface layer, OTUs from *Proteobacteria* were more prevalent in grassland (Figure 2a), and most of the OTUs were significantly correlated with TP, AK, E-Mg, EC, and T (Figure 4c). In the deep layer, *Proteobacteria* were not significantly different in their land use (Figure 2b). Further, the OTUs were not significantly correlated with the soil's physicochemical properties (Figure 4d). These bacterial structural differences reflect the prominent changes in particular groups. The heat map revealed that the distribution of OTUs was strongly affected by different land uses and soil depths, and soil nutrients appear to determine the distribution and frequency of OTUs (Figure 4c,d). Among the most frequent *Proteobacterial* OTUs, six were classified at the genus level (*Variibacter*, *Bradyrhizobium*, *Pedomicrobium*, *Steroidobacter*, *Sphingomonas*, *Lysobacter*). Interestingly, some taxonomically related OTUs from land use, such as *Proteobacteria*-related OTUs (28 and 124, classified as part of the *Sphingomonas* group), exhibited similar occurrence patterns. Some recent advances have demonstrated that *Sphingomonas* have unique abilities in degrading refractory contaminants, serving as bacterial antagonists to phytopathogenic fungi [50]. The genus *Bradyrhizobium* (OTU 4) is one of several genera of nitrogen-fixing bacteria, which play an important role in agricultural productivity and global nitrogen cycling. Previous reports have found that *Bradyrhizobium* are dominant in forest soil [51]. However, in our study, *Bradyrhizobium* were found to be dominant in shrubland and woodland environments.

Verrucomicrobia were the most widely distributed and diverse phylum of bacteria in soil habitats [49]. The proportion of *Verrucomicrobia* in grassland was significantly lower than that in woodland and shrubland at different soil depths. *Verrucomicrobia* were distributed in various soil and aquatic habitats, including environments with poor nutrition, eutrophication, extreme pollution, and man-made habitats [52,53]. *Verrucomicrobia* may be more adaptable to oligotrophic environments in soils [54], which are widely distributed in rhizosphere and aggregate soils. They can use a variety of carbon compounds and may be closely related to the carbon cycle [55]. Our study found that *Verrucomicrobia* were significantly positively correlated with TN and SOC (Figure 5), and significantly negatively correlated with TP, AK, EC, and E-Mg. Because the grassland had more soil nutrients, the proportion of *Verrucomicrobia* in grassland was significantly smaller than that in woodland and shrubland. Moreover, it was found that there was a striking increase in verrucomicrobial abundances at different soil depths (Figure 1). The slow growth rate of *Verrucomicrobia* may allow them to exploit the sparse resources in subsurface soil [56]. In different soil layers, OTUs from *Verrucomicrobia* were enriched in the shrubland (Figure 2a,b). Moreover, most OTUs from *Verrucomicrobia* were significantly correlated with TN and SOC (Figure 4c,d). Among the most frequent *Verrucomicrobia* OTUs, only one (OTU 21) was classified at the genus level (*Candidatus Xiphinematobacter*). Previous studies exposed the difficulty of classifying *Verrucomicrobia* because the portion of culturable bacteria within the *Verrucomicrobia* is quite low [57].

Acidobacteria were widespread in all types of soils with high richness [58]. In the A layer, *Acidobacteria* were significantly positively correlated with EC and E-Mg (Figure 5). The proportion of *Acidobacteria* in grassland was significantly higher than that in woodland and shrubland. In the B layer, *Acidobacteria* had a significantly negative correlation with TP (Figure 5), though the proportion of *Acidobacteria* in the three land use patterns was not significantly different. Moreover, the dominant genera from *Acidobacteria* were the *Blastocatella* (OTU 37) and *Candidatus Solibacter* OTUs (21, 30, and 238). In the surface layer, OTUs from *Acidobacteria* were prevalent in the three land uses, reflecting the high adaptability of this group. In the deep layer, OTUs from *Acidobacteria* were more frequent in grassland and shrubland. In addition, most OTUs were significantly correlated with TP, AK, E-Mg, EC, and moisture. Accordingly, each abundant *Acidobacteria* OTU prevailed in a different niche, reflecting the high adaptability of this group. *Acidobacteria* are acidophilic bacteria, which can decompose animal and plant residues and cellulose to form organic carbon [59]. Consequently, they are more suitable for living in a low organic carbon environment. Our study found that *Acidobacteria* were negatively correlated with TOC. Moreover, there was more litter on the soil's surface, making the surface more suitable for the survival of *Acidobacteria*.

5. Conclusions

Proteobacteria, *Verrucomicrobia*, and *Acidobacteria* were the dominant bacteria, but the abundance of bacterial communities was different. *Verrucomicrobia* were significantly positively correlated with TN and SOC and significantly negatively correlated with TP, AK, EC, and E-Mg. *Acidobacteria* were significantly correlated with EC, E-Mg, and TP. Different land use patterns have significant effects on the soil's physicochemical properties. TP, AK, E-Mg, and EC in the grassland were significantly higher than those in the woodland and shrubland. TN and SOC in the woodland were higher than those in the shrubland and grassland. The soil physicochemical properties decreased with increasing soil depth, and SOC, TN, and AK were the most important physicochemical properties affecting the composition of the bacterial community. The diversity of bacterial communities in the three land use types decreased with an increase of soil depth, which was consistent with the trend of soil physicochemical properties. Different land use patterns and soil depths have significant effects on bacterial communities. Land use shapes strong effects in the soil's bacterial community structure on the soil's surface layer, and the effects of land use attenuation decrease with soil depth. Compared with deep soil, surface soil contains more nutrients that are more suitable for the growth and reproduction of bacteria. Our study provides a basis for understanding the influence of land use patterns and soil

depths on the bacterial community structure in the karst graben basin of Yunnan province, China. Selecting a suitable land use according to the soil bacterial community structure of karst graben basins has great significance. We should also consider the impacts of soil bacterial communities on land use at different soil depths.

Supplementary Materials: The following are available online at http://www.mdpi.com/1999-4907/11/1/51/s1: Table S1: Abundance of dominant phyla in the three land use types. Table S2: Spearman's correlations showing the relationship between soil physicochemical parameters and dominant OTUs in the A layer. Table S3: Spearman's correlations showing the relationship between the soil physicochemical parameters and dominant OTUs in the B layer. Figure S1: Heat map representing the relationship between the soil physicochemical parameters and the most abundant OTUs with abundances >0.5% of the three land uses in different soil layers: woodland in the surface layer (**a**), shrubland in the surface layer (**b**), grassland in the surface layer (**c**), woodland in the deep layer (**d**), shrubland in the deep layer (**e**), and grassland in the deep layer (**f**).

Author Contributions: J.Q. organized the available literature and data, and subsequently developed the original draft of the manuscript. G.L., Y.L., and H.W. collected the soil samples. Q.L. planned and designed the research. Q.L. and J.C. developed the original concept for the project, co-authored the proposal to fund the research, and edited all subsequent drafts of the manuscript. All authors have read and agreed to the published version of the manuscript.

Funding: Project supported by the National Key Research and Development Program of China "Ecological, environmental and geological differentiation of rocky desertification and its driving mechanism in the karst graben basin" (No. 2016YFC0502501).

Conflicts of Interest: The authors declare no conflict of interest.

References

1. Yao, L.S. The formation mechanism and model of faulted karst basins in Yunnan province. *Carsol. Sin.* **1984**, *3*, 48–55. (In Chinese)
2. Wang, Y.; Zhang, H.; Zhang, G.; Wang, B.; Peng, S.H.; He, R.S.; Zhou, C.Q. Zoning of environmental geology and functions in karst fault-depression basins. *Carsol. Sin.* **2017**, *36*, 283–295. [CrossRef]
3. Deng, L.; Zhou, P.; Guan, S.; Li, R. Effects of the grain-for-green program on soil erosion in China. *Int. J. Sediment. Res.* **2012**, *27*, 120–127. [CrossRef]
4. Yang, J. Yunnan Natural Forest Resources Conservation Project Phase II Started in an All-round Way. *Yunnan For.* **2011**, *32*, 24. (In Chinese)
5. Bai, C.L. Deepening Reform and Accelerating Development Creating a New Situation of Natural Forest Protection Project Construction in Yunnan Province. *Yunnan For.* **2007**, *28*, 4–7. (In Chinese)
6. Xu, H.J.; Wang, X.H.; Li, H.; Yao, H.Y.; Su, J.Q.; Zhu, Y.G. Biochar impacts soil microbial community composition and nitrogen cycling in an acidic soil planted with rape. *Environ. Sci. Technol.* **2014**, *48*, 9391–9399. [CrossRef]
7. Zhang, Y.; Du, B.H.; Jin, Z.G.; Li, Z.H.; Song, H.N.; Ding, Y.Q. Analysis of bacterial communities in rhizosphere soil of healthy and diseased cotton (*Gossypium* sp.) at different plant growth stages. *Plant. Soil* **2011**, *339*, 447–455. [CrossRef]
8. McCann, K.S. The diversity-stability debate. *Nature* **2000**, *405*, 228–233. [CrossRef]
9. Suleiman, A.K.A.; Manoeli, L.; Boldo, J.T.; Pereira, M.G.; Roesch, L.F.W. Shifts in soil bacterial community after eight years of land-use change. *Syst. Appl. Microbiol.* **2013**, *36*, 137–144. [CrossRef]
10. Song, M.; Zou, D.S.; Du, H.; Peng, W.X.; Zeng, F.P.; Tan, Q.J.; Fan, F.J. Characteristics of soil microbial populations in depressions between karst hills under different land use patterns. *Chin. J. Appl. Ecol.* **2013**, *24*, 2471–2478. [CrossRef]
11. Edarson, D.C.J.; Terence, L.M.; James, M.T.; Fatima, M.D.S.M. Changes in land use alter the structure of bacterial communities in Western Amazon soils. *ISME J.* **2009**, *3*, 1004–1011. [CrossRef]
12. Bremner, J.M.; Jenkinson, D.S. Determination of organic carbon in soil. I. Oxidation by dichromate of organic matter in soil and plant materials. *Eur. J. Soil Sci.* **2010**, *11*, 394–402. [CrossRef]
13. Parkinson, J.A.; Allen, S.E. A wet oxidation procedure suitable for determination of nitrogen and mineral nutrients in biological material. Commun. *Soil Sci. Plant Anal.* **1975**, *6*, 1–11. [CrossRef]
14. Carson, P.L. Recommended potassium test. In *Recommended Chemical Soil Test Procedures for the North Central Region*; Dahnke, W.C., Ed.; North Dakota Agricultural Experiment Station: Fargo, ND, USA, 1980; Volume 499, pp. 17–18.

15. Wilke, B.M. Determination of chemical and physical soil properties. In *Monitoring and Assessing Soil Bioremediation*; Springer: Heidelberg/Berlin, Germany, 2005. [CrossRef]
16. Li, Q.; Hu, Q.; Zhang, C.; Müller, W.E.G.; Schröder, H.C.; Li, Z. The effect of toxicity of heavy metals contained in tailing sands on the organic carbon metabolic activity of soil microorganisms from different land use types in the karst region. *Environ. Earth Sci.* **2015**, *74*, 6747–6756. [CrossRef]
17. Chan, C.O.; Yang, X.D.; Fu, Y.; Feng, Z.L.; Sha, L.Q.; Peter, C.; Zou, X.M. 16S rRNA gene analyses of bacterial community structures in the soils of evergreen broad-leaved forests in south-west China. *FEMS Microbiol. Ecol.* **2006**, *58*, 247–259. [CrossRef]
18. Magoč, T.; Salzberg, S.L. FLASH: Fast length adjustment of short reads to improve genome assemblies. *Bioinformatics* **2011**, *27*, 2957–2963. [CrossRef]
19. Martin, M. Cutadapt removes adapter sequences from high-throughput sequencing reads. *EMBnet. J.* **2011**, *17*, 10–12. [CrossRef]
20. Quast, C.; Pruesse, E.; Yilmaz, P.; Gerken, J.; Schweer, T.; Yarza, P.; Peplies, J.; Glöckner, F.O. The SILVA ribosomal RNA gene database project: Improved data processing and web-based tools. *Nucl. Acids Res.* **2013**, *41*, D590–D596. [CrossRef]
21. Edgar, R.C.; Haas, B.J.; Clemente, J.C.; Quince, C.; Knight, R. UCHIME improves sensitivity and speed of chimera detection. *Bioinformatics* **2011**, *27*, 2194–2200. [CrossRef]
22. Edgar, R.C. Search and clustering orders of magnitude faster than BLAST. *Bioinformatics* **2010**, *26*, 2460–2461. [CrossRef]
23. Caporaso, J.G.; Kuczynski, J.; Stombaugh, J.; Bittinger, K.; Bushman, F.D.; Costello, E.K.; Fierer, N.; Goodrich, J.K.; Gordon, J.I.; Huttley, G.A.; et al. QIIME allows analysis of highthroughput community sequencing data. *Nat. Methods* **2010**, *7*, 335–336. [CrossRef] [PubMed]
24. Zuur, A.F.; Ieno, E.N.; Smith, G.M. *Analysing Ecological Data*; Springer: New York, NY, USA, 2007.
25. R Core Team. *R: A Language and Environment for Statistical Computing*; R Foundation for Statistical Computing: Vienna, Austria, 2014; Available online: http://www.R-project.org/ (accessed on 15 July 2019).
26. Anderson, M.J.; Willis, T.J. Canonical analysis of principal coordinates: A useful method of constrained ordination for ecology. *Ecology* **2003**, *84*, 511–525. [CrossRef]
27. Bastian, M.; Heymann, S.; Gephi, M.J. An open source software for exploring and manipulating networks. In Proceedings of the Third International Conference on Weblogs and Social Media, ICWSM 2009, San Jose, CA, USA, 17–20 May 2009. [CrossRef]
28. Oberson, A.; Friesen, D.K.; Rao, I.M.; Bühler, S.; Frossard, E. Phosphorus Transformations in an Oxisol under contrasting land-use systems: The role of the soil microbial biomass. *Plant Soil* **2001**, *237*, 197–210. [CrossRef]
29. Batlle-Aguilar, J.; Brovelli, A.; Porporato, A.; Barry, D.A. Modelling soil carbon and nitrogen cycles during land use change-A review. *Agron. Sustain. Dev.* **2011**, *31*, 251–274. [CrossRef]
30. Liu, Y.P.; Lu, M.X.; Zhang, X.W.; Sun, Q.B.; Liu, R.L.; Lian, B. Shift of the microbial communities from exposed sandstone rocks to forest soils during pedogenesis. *Int. Biodeter. Biodegr.* **2019**, *140*, 21–28. [CrossRef]
31. Huang, X.F.; Zhou, Y.C.; Zhang, Z.M. Distribution characteristics of soil organic carbon under different land use in a karst rocky desertification area. *J. Soil Water Conserv.* **2017**, *31*, 215–221. [CrossRef]
32. Tong, J.H.; Hu, Y.C.; Du, Z.L.; Zou, Y.Q.; Li, Y.Y. Effects of land use change on soil organic carbon and total nitrogen storage in karst immigration regions of Guanxi Province, China. *Chin. J. Appl. Ecol.* **2018**, *29*, 2890–2896. [CrossRef]
33. Li, L.; Qin, F.C.; Jiang, L.N.; Yao, X.L. Vertical distribution of soil organic carbon content and its influenceing factors in Aaohan, Chifeng. *Acta Ecol. Sin.* **2019**, *39*, 345–354. [CrossRef]
34. Chaplot, V.; Bouahom, B.; Valentin, C. Soil organic carbon stocks in Laos: Spatial variations and controlling factors. *Glob. Chang. Biol.* **2010**, *16*, 1380–1393. [CrossRef]
35. Kuang, W.N.; Qian, J.Q.; Ma, Q.; Liu, Z.M. Vertical distribution of soil organic carbon content and its relation to root distribution in five desert shrub communities. *Chin. J. Ecol.* **2016**, *35*, 275–281. [CrossRef]
36. Wang, D.; Geng, Z.C.; She, D.; He, W.X.; Hou, L. Soil organic carbon storage and vertical distribution of carbon and nitrogen across different forest types in the Qinling Mountains. *Acta Ecol. Sin.* **2015**, *35*, 5421–5429. [CrossRef]
37. Daniel, C.S.; Matthew, G.B.; James, M.B.; Linda, L.K. Plant community richness and microbial interactions structure bacterial communities in soil. *Ecology* **2015**, *96*, 134–142. [CrossRef]
38. Kinkel, L.L.; Bakker, M.G.; Schlatter, D.C. A coevolutionary framework for managing disease-suppressive soils. *Annu. Rev. Phytopathol.* **2011**, *49*, 47–67. [CrossRef] [PubMed]

39. Zhang, C.; Li, J.; Wang, J.; Liua, G.B.; Wang, G.L.; Guo, L.; Peng, S.Z. Decreased temporary turnover of bacterial communities along soil depth gradient during a 35-year grazing exclusion period in a semiarid grassland. *Geoderma* **2019**, *351*, 49–58. [CrossRef]
40. He, S.B.; Guo, L.X.; Niu, M.Y.; Miao, F.H.; Jiao, S.; Hu, T.M.; Long, M.X. Ecological diversity and cooccurrence patterns of bacterial community through soil profile in response to long-term switchgrass cultivation. *Sci. Rep.* **2017**, *3608*, 7. [CrossRef]
41. Cheng, J.M.; Guanghua Jing, G.H.; Wei, L.; Jing, Z.B. Long-term grazing exclusion effects on vegetation characteristics, soil properties and bacterial communities in the semiarid grasslands of China. *Ecol. Eng.* **2016**, *97*, 170–178. [CrossRef]
42. Wang, S.X.; Wang, X.A.; Guo, H. Change patterns of β-diversity in the succession process of plant communities on Loess Plateau of Northwest China. *Chin. J. Ecol.* **2013**, *32*, 1135–1140. [CrossRef]
43. Tian, Q.; Taniguchi, T.; Shi, W.Y.; Li, G.Q.; Yamanaka, N.; Du, S. Land-use types and soil chemical properties influence soil microbial communities in the semiarid Loess Plateau region in China. *Sci. Rep.* **2017**, *7*, 45289. [CrossRef]
44. Bru, D.; Ramette, A.; Saby, N.P.A.; Dequiedt, S.; Ranjard, L.; Jolivet, C.; Arrouays, D.; Philippot, L. Determinants of the distribution of nitrogen-cycling microbial communities at the landscape scale. *ISME J.* **2011**, *5*, 532–542. [CrossRef]
45. Adria, L.F.; Craig, C.S.; Donald, L.W.; Christopher, S.; Trevor, J.G.; Michael, J.S. Associations between soil bacterial community structure and nutrient cycling functions in long-term organic farm soils following cover crop and organic fertilizer amendment. *Sci. Total Environ.* **2016**, *566*, 949–959. [CrossRef]
46. Manuel, D.B.; Angela, M.O.; Tess, E.B.; Alberto, B.G.; David, J.E.; Richard, D.B.; Fernando, T.M.; Brajesh, K.S.; Noah, F. A global atlas of the dominant bacteria found in soil. *Science* **2018**, *359*, 320–325. [CrossRef]
47. Zhou, J.; Guan, D.W.; Zhou, B.K.; Zhao, B.S.; Ma, M.C.; Qin, J.; Jiang, X.; Chen, S.F.; Cao, F.M.; Shen, D.L.; et al. Influence of 34-years of fertilization on bacterial communities in an intensively cultivated black soil in northeast China. *Soil Biol. Biochem.* **2015**, *90*, 42–51. [CrossRef]
48. Griffiths, B.S.; Philippot, L. Insights into the resistance and resilience of the soil microbial community. *FEMS Microbiol. Rev.* **2013**, *37*, 112–129. [CrossRef] [PubMed]
49. Anna, K.; Jorge, L.M.R.; Eiko, E.K.; Patrick, S.G.C.; Johannes, A.V.V.; George, A.K. Phylogenetic and metagenomic analysis of *Verrucomicrobia* in former agricultural grassland soil. *FEMS Microbiol. Ecol.* **2010**, *71*, 23–33. [CrossRef]
50. David, C.W.; Susan, D.S.; David, B.R. The genus Sphingomonas: Physiology and ecology. *Curr. Opin. Biotechnol.* **1996**, *7*, 301–306. [CrossRef]
51. David, V.; Kendra, R.M.; Erick, C.; Cameron, R.S.; Steven, J.H.; William, W.M. Non-symbiotic *Bradyrhizobium* ecotypes dominateNorth American forest soils. *ISME J.* **2015**, *9*, 2435–2441. [CrossRef]
52. Heinz, S.; Cheryl, J.; Jamest, S. The phylum *Verrucomicrobia*: A phylogenetically heterogeneous bacterial group. *Prokaryotes* **2006**, *7*, 881–896. [CrossRef]
53. Wagner, M.; Horn, M. The *Planctomycetes*, *Verrucomicrobia*, *Chlamydiae* and sister phyla comprise a superphylum with biotechnological and medical relevance. *Curr. Opin. Biotechnol.* **2006**, *17*, 241–249. [CrossRef]
54. Noll, M.; Diethart, M.; Frenzel, P.; Manigee, D.; Liesack, W. Succession of bacterial community structure and diversity in a paddy soil oxygen gradient. *Environ. Microbiol.* **2005**, *7*, 382–395. [CrossRef]
55. Fierer, N.; Ladau, J.; Clementei, J.C.; Leff, J.W.; Owens, S.M.; Katherine, S.P.; Knight, R.; Gilbert, J.A.; McCulley, R.L. Reconstructing the microbial diversity and function of pre-agricultural tallgrass prairie soils in the United States. *Science* **2013**, *342*, 621–624. [CrossRef]
56. Janssen, P.H.; Yates, P.S.; Grinton, B.E.; Taylor, P.M.; Sait, M. Improved culturability of soil bacteria and isolation in pure culture of novel members of the divisions *Acidobacteria*, *Actinobacteria*, *Proteobacteria*, and *Verrucomicrobia*. *Appl. Environ. Microb.* **2002**, *68*, 2391–2396. [CrossRef]
57. Stefan, S.; Boyke, B.; Cathrin, S.; Peter, S.; Manfred, R.; Brian, J.T.; Hans, P.K. Characterization of the first cultured representative of *Verrucomicrobia* subdivision 5 indicates the proposal of a novel phylum. *ISME J.* **2016**, *10*, 2801–2816. [CrossRef]

58. Wang, P.; Chen, B.; Zhang, H. High throughput sequencing analysis of bacterial communities in soils of a typical Poyang Lake wetland. *Acta Ecol. Sin.* **2017**, *37*, 1650–1658. [CrossRef]
59. Zhang, Y.G.; Cong, J.; Lu, H.; Li, G.L.; Qu, Y.Y.; Su, X.J.; Zhou, J.Z.; Li, D.Q. Community structure and elevational diversity patterns of soil *Acidobacteria*. *J. Environ. Sci.* **2014**, *26*, 171–1724. [CrossRef]

forests

MDPI

Article

Effects of Plum Plantation Ages on Soil Organic Carbon Mineralization in the Karst Rocky Desertification Ecosystem of Southwest China

Hui Yang [1,2], Biqin Mo [1,2], Mengxia Zhou [1,2], Tongbin Zhu [1,2,*] and Jianhua Cao [1,2]

[1] Karst Dynamics Laboratory, Institute of Karst Geology (CAGS), Ministry of Natural Resources (MNR) and Guangxi, Guilin 541004, China; yanghui-kdl@karst.ac.cn (H.Y.); mermaid_yh@126.com (B.M.); mengxia.zhou95@gmail.com (M.Z.); jhcaogl@karst.ac.cn (J.C.)

[2] International Research Centre on Karst, Under the Auspices of United Nations Educational, Scientific and Cultural Organization (UNESCO), Guilin 541004, China

* Correspondence: ztb@karst.ac.cn; Tel.: +86-773-583-7840; Fax: +86-773-583-7845

Received: 30 October 2019; Accepted: 2 December 2019; Published: 4 December 2019

Abstract: Soil organic carbon (SOC) mineralization is closely related to carbon source or sink of terrestrial ecosystem. Understanding SOC mineralization under plum plantation is essential for improving our understanding of SOC responses to land-use change in karst rocky desertification ecosystem. In this study, 2-year, 5-year, and 20-year plum plantations and adjacent abandoned land dominated by herbs were sampled, and a 90-day incubation experiment was conducted to investigate the effect of plum plantations with different ages on SOC mineralization in subtropical China. Results showed that: (1) Plum plantation significantly decreased SOC content compared with abandoned land, but there was no significant difference in SOC content among plum plantations with different ages. Oppositely, the accumulative SOC mineralization (C_t) and potential SOC mineralization (C_0) showed different responses to plum plantation ages. (2) The dynamics of the SOC mineralization were a good fit to a first-order kinetic model. Both C_0 and C_t in calcareous soil of this study was several- to 10-folds lower than other soils in non-karst regions, indicating that SOC in karst regions has higher stability. (3) Correlation analysis revealed that both C_t and C_0 was significantly correlated with soil calcium (Ca), suggesting an important role of Ca in SOC mineralization in karst rocky desertification areas. In conclusion, a Ca-rich geological background controls SOC mineralization in karst rocky desertification areas.

Keywords: calcareous soil; plum plantation ages; organic carbon mineralization; fitting parameters; organic carbon accumulation

1. Introduction

Due to the fragile geological and ecological conditions, rocky desertification widely occurs in the southwest karst region of China [1], which is characterized by serious soil erosion, devoid of vegetation and soil [2]. To effectively prevent rocky desertification, a series of ecological restorations have been carried out to increase the forest cover and to mitigate soil erosion by the Chinese government [3]. Consequently, various land uses, including undisturbed (e.g., grassland and shrub) and man-made (e.g., corn, woodland and fruit crop) ecosystems, have been formed in karst rocky desertification regions. These ecological restoration measures have tremendously affected the physical, chemical, and microbiological properties in soils [4]. Plum plantation is one of the local sustainable development models of characteristic agriculture in karst rocky desertification areas, which can not only effectively restore the ecological environment, but also significantly increase farmers' income in local. In recent years, the planting area of plum trees has been increasing continuously in the process of controlling rocky desertification [5].

Dynamic change of soil organic carbon (SOC) is of great significance to global C cycle and current climate change. The quantity and intensity of carbon dioxide (CO_2; an important greenhouse gas) released by SOC mineralization through microbial decomposition can reflect the quality of soil and evaluate soil carbon emissions into the atmosphere [6,7]. In addition, SOC mineralization is closely related to the maintenance of soil nutrients and the formation of CO_2 [8]. The CO_2 emission rate and its dynamic change process are also important indicators reflecting the change of soil quality. Furthermore, SOC concentration at a particular time is controlled by the balance between C input from litter and C output from SOC mineralization [9]. Investigating the SOC mineralization process is the most effective methods to evaluate C loss or stability [10].

Vegetation type influences the rate of accumulation and mineralization of organic matter in forest soil [11]. Some research proved that C loss from soil respiration depends on stand age. It is low in young, high in intermediate, and low again in old stands [12,13]. Plum is one of the principal tree species in the rocky desertification restoration area in the National Sustainable Development Experiment and Demonstration Zone in Gongcheng county. However, there is less study about SOC storage and SOC mineralization in plum forests in rocky desertification restoration areas. In particular, it is not clear whether plum plantation age is the key factor controlling SOC stability and how other factors influence SOC decomposition dynamics. In addition, calcareous soil developed on carbonate rock is characterized by high pH and Ca materials in a karst region [1], which may lead to the obvious differences in SOC mineralization compared to other soil types. The lack of knowledge regarding SOC mineralization under plum plantation during karst rocky desertification restoration limits the ability to predict how this ecosystem will respond to climate change. We hypothesized that both the karst geological background, especially soil pH and Ca concentrations, and plantation ages may play an important role in controlling SOC mineralization.

Therefore, we measured the distribution and mineralization of organic C in soils collected from plum fields with different plantation ages (2 year, 5 year, and 20 year) and adjacent abandoned land in the karst rocky desertification region of subtropical China. The main objectives of this study were to (1) estimate SOC content, mineralization, and soil nutrients under plum plantations with different stand ages; (2) evaluate the relative importance of soil properties affecting SOC content and mineralization; (3) potentially assess mineralization and decomposition rates of SOC.

2. Materials and Methods

2.1. Study Area

The study site was located in the National Sustainable Development Experiment and Demonstration Zone and also a key area of national rocky desertification control in Gongcheng county, Guilin, Guangxi Zhuang Autonomous Region (110°47′4′′ E, 24°54′35′′ N) (Figure 1), which is a subtropical monsoon climate, with an annual average temperature of 19.7 °C and an annual average precipitation of 1438 mm.

The study area is a hilly and middle-low mountain landform. Its parent material is carboniferous limestone. Karst soil is sparse and drought-prone. Because of long-term human activities, natural vegetation is destroyed and large areas of steep slopes are reclaimed, resulting in surface rock bareness, coupled with thin soil layer, shallow bedrock exposure, storm erosion, and a large number of rocks gradually exposed after soil erosion. Severe rocky desertification occurs (Figure S1).

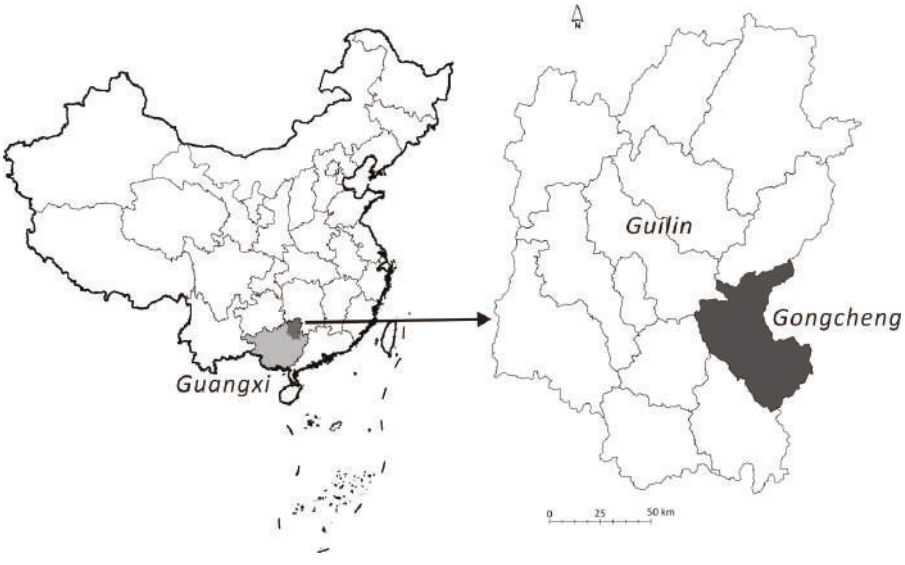

Figure 1. The location of the study area.

2.2. Soil Sampling and Preparation

Soil samples were collected from three plum fields with 2-year, 5-year, and 20-year plantation ages, and abandoned land was used as control. The understory of the plum plantation was dominated by the meda *villosa (Poir.) A. Camus* and *Digitaria sanguinalis (Linn.) Scop.* The dominated plants of the abandoned land were herbs, dominated by *Miscanthus* with a small amount of *Conyza canadensis (Linn.) Cronq*. Fertilizer was applied four times each year, including three times of chemical fertilizer and one time of organic fertilizer. The chemical fertilizer was compound fertilizer (including N 18%, P_2O_5 18%, K_2O 18%). The organic fertilizer was cattle manure (including C 413.8 g kg^{-1}, N 2.7 g kg^{-1}, P_2O_5 1.3 g kg^{-1}, K_2O 6.0 g kg^{-1}). Under each plum tree, an average of 2 kg of chemical fertilizer and 20 kg of organic fertilizer were applied each year. The application rate of N, P_2O_5, and K_2O reached to approximately 250, 100, and 240 kg ha^{-1} $year^{-1}$, respectively.

In November 2015, three representative sites were sampled for plum plantations with different ages and abandoned land as spatial replications, resulting in 12 soil samples. In each site, three 20 m × 20 m plots with similar architecture and growth of plum trees, separated at least 40 m from each other, were randomly selected. Soils of the top 0–10 cm were collected from five quadrats (1 m × 1 m) in each plot; one on each corner and one in the center were mixed to form a composite sample. After removing animal and plant debris and stones, the collected samples were air-dried at room temperature. The composite samples were divided into two parts. One part of the collected sample was passed through a 2-mm sieve to carry out SOC mineralization experiment, and the other part was grinded and passed through a 0.25-mm sieve and homogenized for soil physical and chemical property determination, including pH, SOC, total nitrogen (TN), total phosphorus (TP), total potassium (TK), and calcium (Ca).

2.3. Experiment Design

A laboratory incubation experiment was carried out to determine SOC mineralization. Soil samples were incubated with a constant temperature regime at 20 °C, which was close to the annual mean temperature (19.7 °C) in the sampled area. The incubation temperatures were controlled by digital biochemical incubators (SPX-70B, Hangzhou Julai Instrument Co., Ltd., Hangzhou, China).

Each soil sample (100 g dry), including three repeats, was placed in a 1000 mL incubation jar (Figure S2). The soil moisture content was adjusted to 60% of field capacity prior to incubation. All samples were pre-incubated at 20 °C for 7 days to minimize the burst of respiration due to wetting the dry soils [10]. Then, a 50 mL beaker containing 10 mL of 0.1 mol/L NaOH solution was placed at the bottom of the incubation jar, sealed and capped, and incubated in a 20 °C thermostat in darkness. Three blank controls (no soil addition) were arranged at the same time in order to eliminate the influence of CO_2 in the air when NaOH solution was replaced every time. A total of 39 samples, including 12 soil samples with 3 incubation replicates and 3 blank controls, were used for the incubation experiment. Deionized water was added to the soil twice a week to keep the loss of soil water within 2% [14]. The 50 mL beaker containing 10 mL of 0.1 mol/L NaOH solution was replaced at days 2, 5, 8, 14, 20, 26, 32, 38, 44, 62, 74, and 90. The amount of CO_2 released during incubation can be calculated by titrating residual NaOH with 0.1 mol/L HCl solution.

2.4. Methods

Soil pH was determined at a 1:2.5 (w/v) soil/water ratio by a digital millivolt pH Meter-2 (DMP-2 mV/pH) detector (Quark Ltd., Nanjing, China); SOC was determined using the $K_2Cr_2O_7$–H_2SO_4 volumetric dilution heating method; total nitrogen was determined using the Kjeldahl procedure [15]; total potassium (TK) concentration was determined with the HF–$HClO_4$ flame photometric method; and total phosphorus (TP) was measured using $HClO_4$–H_2SO_4 digestion followed by an Mo–Sb colorimetric assay [1]; soil calcium (Ca) was extracted by HNO_3–HF–$HClO_4$ and analyzed by inductively coupled plasma–atomic emission spectrometry (ICP–AES). Three replicates were performed for each soil sample.

The mineralization of SOC was calculated by the following Equation (1).

$$C_m = C_{HCl} \times (V_0 - V_1) \times 22/0.1 \quad (1)$$

where C_m was the amount of CO_2 release (mg CO_2/kg soil); C_{HCl} was the concentration of hydrochloric acid (mol/l); V_0 was the volume of hydrochloric acid consumed in blank titration (ml); V_1 was the volume of hydrochloric acid consumed in titration of samples (ml); 22 was half of the Molar mass of CO_2 (mol/kg); 0.1 was soil weight (kg).

2.5. Data Analysis

The data was fitted in an exponential model using the data analysis and graphing software (Origin ver. 7.5; Origin Lab Corp., Northampton, MA, USA) to obtain kinetics of SOC mineralization (Equation (2)) [16].

$$C_t = C_0 (1 - e^{-kt}) \quad (2)$$

where C_t was the cumulative mineralization of SOC after t days; C_0 was amount of potential mineralizable SOC (mg/kg); k for constant of mineralization rate of SOC (/day).

The half-turnover period was calculated by Equation (3).

$$T_{1/2} = 1n2/k \quad (3)$$

where $T_{1/2}$ was half the turnover period (day).

The obtained data were statistically analyzed using the analysis Statistical Package Social Science (SPSS ver. 20.0; IBM Corp., Armonk, NY, USA) to compare the analysis of variance. Tukey's honestly significant difference (HSD) was then calculated for indicating the significant differences in soil properties and SOC mineralization ($p < 0.05$). Graphs were plotted using the Origin 7.5 program. The correlations between the SOC mineralization and the soil chemical properties were analyzed by the Pearson correlation test.

3. Results

3.1. Soil Chemical Properties as Affectted by Plantation Age

Compared to abandoned land, plum plantation significantly decreased pH and the contents of SOC and TN ($p < 0.05$) (Table 1), but there was no significant difference among plum plantations with different ages ($p > 0.05$). Although C/N ratios in soils under plum plantation were lower than that under abandoned land, the significant difference was not found between abandoned land and plum plantations. There was no significant difference in TP contents among abandoned land and three plum plantations ($p > 0.05$). The highest TK contents were found in soils under 5-year plum plantation and abandoned land, which were significantly higher than 2-year and 20-year plum plantations. Plum plantation significantly decreased Ca contents compared with abandoned land ($p < 0.05$), with the lowest in soil under 5-year plum plantation.

Table 1. Soil properties under plum plantations with different ages.

	pH	SOC (g/kg)	TN (g/kg)	C/N	TP (g/kg)	TK (g/kg)	Ca (%)
CK	6.60 ± 0.10 ^{a}	22.38 ± 0.53 ^{a}	1.01 ± 0.04 ^{a}	25.97 ± 1.62 ^{a}	0.49 ± 0.08 ^{a}	18.07 ± 0.05 ^{a}	0.97 ± 0.13 ^{a}
2 year	5.31 ± 0.32 ^{b}	11.87 ± 3.18 ^{b}	0.61 ± 0.18 ^{b}	22.83 ± 2.82 ^{a}	0.55 ± 0.25 ^{a}	14.56 ± 0.55 ^{b}	0.54 ± 0.23 ^{b}
5 year	5.91 ± 0.51 ^{c}	10.17 ± 3.28 ^{b}	0.74 ± 0.20 ^{ab}	17.96 ± 8.61 ^{a}	0.44 ± 0.21 ^{a}	19.47 ± 1.68 ^{a}	0.27 ± 0.10 ^{c}
20 year	5.17 ± 0.28 ^{b}	11.70 ± 5.27 ^{b}	0.66 ± 0.27 ^{b}	21.34 ± 6.50 ^{a}	0.63 ± 0.31 ^{a}	15.06 ± 1.25 ^{b}	0.40 ± 0.16 ^{bc}

Note: CK represents abandoned land; 2 year represents plum forest plantation for 2 years; 5 year represents plum forest plantation for 5 years; 20 year represents plum forest plantation for 20 years. SOC represents soil organic carbon; TN represents total nitrogen; C/N represents the molar ratio of soil organic carbon (SOC)/TN; TP represents total phosphorus; TK represents total potassium; Ca represents calcium. Identical letters indicate no significant differences in the average values among soils under different plantation ages at the 0.05 level.

3.2. Mineralization Rate of Soil Organic C under Plum Plantations with Different Ages

Soil organic carbon mineralization rate decreased with incubation time (Figure 2), and accorded with logarithmic function $y = a + b\ln(x)$ (Table 2), indicating that SOC mineralization rate would change b% absolute value when incubation time changed by 1% unit.

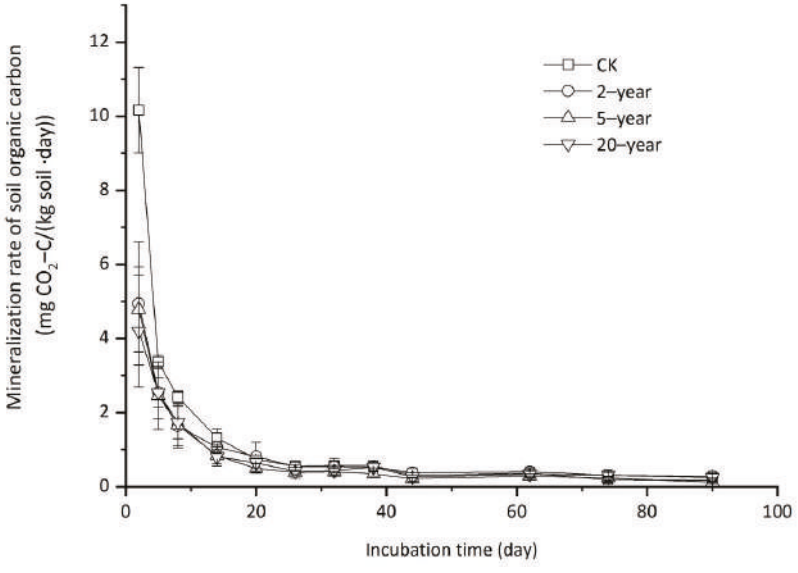

Figure 2. Daily mineralization rate of soil organic carbon.

Table 2. Regression equation of SOC mineralization rate relative to plum plantation age.

Treatment	Regression Equation	R^2
CK	$y = 8.221 - 2.101\ln(x)$	0.734 **
2 year	$y = 4.499 - 1.078\ln(x)$	0.835 **
5 year	$y = 4.736 - 1.085\ln(x)$	0.831 **
20 year	$y = 4.040 - 0.971\ln(x)$	0.853 **

Note: y represents CO_2 production rate; x represents incubation day; ** means significant correlation at 0.01 level.

Based on the decline rate of SOC mineralization (Figure 2), it can be divided into three stages. The first stage (2–14 days) was the early stage of the incubation. The rate of CO_2 production decreased rapidly from the peak (2 days) and changed greatly. There was no significant difference in the mineralization rate of SOC among three planting ages, but it was significantly lower than CK. The second stage (14–62 days) was the medium stage of the incubation, and the rate of CO_2 production declined from a slow stage to a stable stage. The SOC mineralization rate of CK was higher than that in the three planting ages. At the last stage (62–90 days), the SOC mineralization rate of CK began to be lower than that of soils under plum plantations with different ages, and the difference was significant.

3.3. Cumulative Mineralization of Soil Organic Carbon Under Plum Plantations with Different Ages

Carbon mineralization showed a curvilinear relationship with time over the incubation period (starting from 0 to day 90) (Figure 3). Across different plantation ages, cumulative CO_2–C emission varied from 2.29 mg CO_2–C/kg soil (day 2) to 61.17 mg CO_2–C/kg soil (day 90).

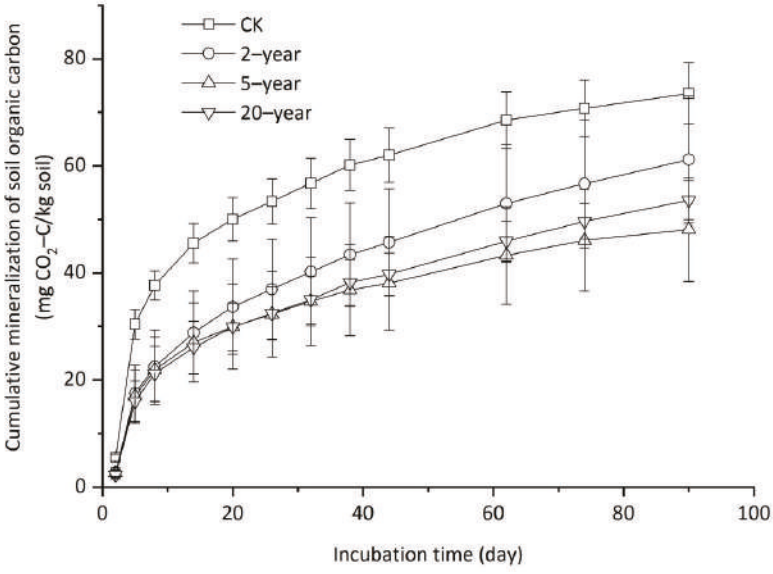

Figure 3. Cumulative mineralization of SOC relative to plum plantation age.

The cumulative release of CO_2 increased with incubation time, but the cumulative release intensity gradually slowed down. During the whole incubation, the cumulative release of CO_2 was higher in CK than that in plum plantations with different ages. The cumulative release of CO_2 was ranked as 2-year, 20-year, and 5-year plantations.

3.4. Parameters of Soil Organic Carbon Mineralization Kinetic Equations Under Plum Plantations with Different Ages

The first-order kinetic equation was used to fit the cumulative mineralization of SOC under plum plantations with different ages, and the fitting results were good ($R^2 > 0.90$). The potential mineralization of SOC (C_0) and constant for SOC mineralization rate (k) estimated from the first-order kinetic equation are shown in Table 3. The values of C_0 ranged from 44.13 (5-year) to 67.10 mg/kg (CK), and it was significant higher in CK than that in plum plantations ($p < 0.05$). The CO_2–C release from mineralization of soil potential organic C, i.e., the turnover rate (k) of bioactive organic carbon pool, ranged from 0.043 (2-year) to 0.079 day^{-1} (CK), and the half-turnover period was 8.80 (CK)–16.1 day (2-year) (Table 3). The values of k for different plum plantation ages showed the same trend with C_0. With increasing plum plantation age, soil potential mineralized C pool decreased, but soil potential mineralized C pool increased slightly after 20-year plum plantation, although the difference was not significant between 5-year and 20-year plum plantations ($p > 0.05$).

Table 3. Cumulative mineralization of SOC after the 90 days of incubation and parameters of its kinetic equations.

Treatment	C_t (mg/kg)	C_0 (mg/kg)	k (/d)	$T_{1/2}$ (d)	C_0/SOC (%)	R^2
CK	73.52 ± 8.43 ^{a}	67.10 ± 7.56 ^{a}	0.079 ± 0.003 ^{a}	8.80	0.30	0.93
2-year	61.17 ± 5.56 ^{b}	57.92 ± 1.33 ^{b}	0.043 ± 0.001 ^{b}	16.1	0.49	0.96
5-year	48.09 ± 3.27 ^{c}	44.13 ± 5.71 ^{c}	0.060 ± 0.001 ^{c}	11.6	0.43	0.93
20-year	53.60 ± 4.11 ^{c}	49.85 ± 2.55 ^{c}	0.046 ± 0.002 ^{b}	15.1	0.43	0.94

Note: C_t represents cumulative mineralization of SOC; C_0 represents amount of potential mineralizable SOC; k represents constant of mineralization rate of SOC; $T_{1/2}$ represents half-turnover period; C_0/SOC represents ratio of potential mineralizable organic carbon to total organic carbon in soil. Values followed by different letters in the same column mean significance at 0.05 level.

3.5. SOC Mineralization as Affected by Chemical Properties

Many environmental factors might influence the mineralization of SOC [17]. Soil organic carbon content was positively correlated with C_t and C_0. Therefore, the difference of SOC mineralization in plum plantations with different ages was mainly due to the difference in SOC content. The proportion of active organic C varies with the content of SOC. Among the many factors, the Ca content and C/N ratio significantly affect SOC mineralization (Table 4). The mineralization rate of SOC was the highest in the abandoned land with the highest Ca content and C/N ratio.

Table 4. Correlations between the C parameters and soil property factors.

	pH	SOC	TN	C/N	TP	TK	Ca
C_t	0.593	0.923 **	0.690	0.974 **	−0.035	−0.079	0.959 **
C_0	0.524	0.883 *	0.621	0.981 **	0.014	−0.159	0.931 **
k	0.986 **	0.823 *	0.983 **	0.423	−0.627	0.741	0.733

* Significant correlation ($p < 0.05$); ** Extremely significant correlation ($p < 0.01$).

4. Discussion

4.1. Effects of Plantation Ages on Soil Chemical Properties

Plum plantation significantly reduced SOC content by about 50% compared with abandoned land, which may be attributed to the changes in agricultural managements (e.g., the clear-cut of forest, tillage and mineral N fertilizer). Except for the direct reduction in litter input to soil, weed control, tillage, and mineral N fertilizer can also stimulate the decomposition of SOC, thereby lowing SOC content. Despite applying large organic fertilizer during plum plantation, it may not counterbalance the negative effect on SOC consumption through litter reduction and agricultural managements. However,

SOC contents did not exhibit the obvious differences among plum plantations with different ages, suggesting that SOC pool is maintained at the relatively stable level once grassland is converted to plum, irrespective of plum plantation years.

The C/N value in the studied soils was relatively stable, and no significant difference was found among plum plantations with different ages. This was in agreement with the previous result that the C/N ratio was relatively stable and was insignificantly affected by climate, although C and N concentrations had great spatial variability [1]. Compared with abandoned land, TP content in soil under plum plantation did not significantly change, which was consistent with a previous study that TP was mainly derived from the weathering release of soil minerals, rather than from the short-term biological cycle in karst rocky desertification areas [1]. Oppositely, potassium sources in soil are mainly derived from potassium minerals and fertilization. With the increase of plum plantation ages, Ca content in soil decreased obviously, which may be because plum trees absorb a lot of Ca as one of the nutrient elements in the process of growth.

4.2. SOC Mineralization and Affecting Factors

In this study, CO_2 production rate is faster in the initial stage of incubation, possibly owing to the priming effect [18]. After pre-incubation, a large number of active organic substances such as sugars and proteins can be effectively decomposed by microorganisms in the initial stage of mineralization [8]. Greater SOC mineralization in abandoned land than plum plantations was often attributed to greater total SOC [19] or greater labile SOC, e.g., dissolved organic carbon (DOC) and microbial biomass C (MBC), which could stimulate the abundance and activity of microorganisms, and subsequently accelerate SOC mineralization [20,21]. With the prolongation of incubation time, the mineralization rate of SOC gradually decreased with decreasing decomposable organic matter. At the later stage of incubation, the organic matter in soil was mainly composed by cellulose and lignin [18], which were difficult to decompose and could not be utilized by microorganisms, resulting in the decline of the mineralization rate of organic carbon. The CO_2 efflux rate in this study showed a similar trend with many research results [8,18,22]. In addition, the relationship between SOC mineralization rate and incubation time was logarithmic function, which was consistent with previous research results [8,23,24].

The cumulative mineralization and mineralization rate of SOC under plum plantations with different ages decreased compared to abandoned land. High CO_2 emissions probably indicate high biological activities in soil [25] and this might take place through microbial exhalation [26], as well as the emissions of CO_2 during organic matter decomposition [27]. Thus, it is no wonder to find out that the efflux rate of CO_2 from the plantation soils was lower than that in abandoned land. The long-term application of chemical fertilizer during plum plantation is not conducive to the formation of soil aggregates. This may exacerbate the microbial growth environment, resulting in the decrease of soil microbial biomass [28]. It may also be that N in fertilizer combines with lignin in soil to form more stable organic compounds [29], which then inhibits the mineralization of SOC. The mechanism of soil characteristics affecting microbial species and activities in plum forests of different ages in karst mountainous areas remains to be further studied.

4.3. Carbon Pool Stability and Factors that Potentially Affect SOC Decomposition

Both cumulative CO_2–C emission and potential mineralizable SOC in calcareous soil of this study was several- to 10-folds lower than that in other soils [8,13,17], similar to the results in soils of karst regions [30], indicating that SOC in karst regions has higher stability. Both Ca and C/N were important factors affecting SOC mineralization in this study. Soil C/N affects the abundance, activity, and community composition of microorganisms [31]. Calcium is the necessary metabolic component of microbial growth, and fungal and bacterial heterotrophs may access and accumulate root Ca to form oxalates, which can be used to maintain microbial metabolism under unfavorable soil conditions. Therefore, it has an important influence on the decomposition of SOC.

5. Conclusions

The amount of SOC mineralization is governed by the net C content in soil. Results of this research showed that mineralization of SOC occurred, but was somewhat several- to 10-folds lower in karst soils, indicating that SOC in karst regions has higher stability. The higher SOC and the consequent higher release of CO_2 in this study may indicate a reversible equilibrated process between decomposition of soil organic matter and buildup of more stable organic components at the same time. The mineralization of SOC under plum plantation is significantly correlated with soil Ca, suggesting an important role of Ca in SOC mineralization in rocky desertification areas. Furthermore, it was also found that agricultural management, e.g., fertilization and weed control under plum forests, may play an important role in SOC mineralization.

Supplementary Materials: The following are available online at http://www.mdpi.com/1999-4907/10/12/1107/s1: Figure S1. Rocky desertification in the study area; Figure S2. The sketch of the incubation device.

Author Contributions: Conceptualization, J.C.; writing—original draft preparation, H.Y.; investigation, B.M. and M.Z.; writing—review and editing, T.Z.

Funding: This study was supported by the National Key Research and Development Program of China (No.2016YFC0502501; No.2017YFC0406104), the Guangxi National Science Foundation (2017GXNSFAA198153) and the Guangxi Scientific Research and Technology Development Project Guikeneng 1598023-1, the CAGS research Fund (YWF201715, 201724), and the program of Hainan Association for Science and Technology Plans to Youth R & D Innovation (QCXM201713).

Acknowledgments: Special thanks to the anonymous referees for their valuable comments and suggestions. The authors also thank Chunlai Zhang and Bing Bai for their help with field work.

Conflicts of Interest: The authors declare no conflicts of interest.

References

1. Yang, H.; Zhang, P.; Zhu, T.; Li, Q.; Cao, J. The characteristics of soil C, N, and P stoichiometric ratios as affected by geological background in a karst graben area, Southwest China. *Forests* **2019**, *10*, 601. [CrossRef]
2. Yuan, D.X. Rock desertification in the subtropical Karst of South China. *Z. Geomorphol.* **1997**, *108*, 81–90.
3. Li, W.H. Degradation and restoration of forest ecosystems in China. *For. Ecol. Manag.* **2004**, *201*, 33–41.
4. Singh, K.; Singh, B.; Singh, R.R. Changes in physico-chemical, microbial and enzymatic activities during restoration of degraded sodic land: Ecological suitability of mixed forest over monoculture plantation. *Catena* **2012**, *96*, 57–67. [CrossRef]
5. Guangxi Daily. Available online: http://www.forestry.gov.cn/main/138/20190613/075621420562132.html (accessed on 13 June 2019).
6. Li, S.J.; Qiu, L.P.; Zhang, X.C. Mineralization of soil organic carbon and its relations with soil physical and chemical properties on the Loess Plateau. *Acta Ecol. Sin.* **2010**, *30*, 1217–1226. (In Chinese)
7. Smith, P. Carbon sequestration in croplands: The potential in Europe and the global context. *Eur. J. Agron.* **2004**, *20*, 229–236. [CrossRef]
8. Guo, Z.; Wang, X.L.; Duan, J.J.; Jiao, K.Q.; Sun, S.S.; Duan, Y.H.; Zhang, Y.R.; Li, Y.; Jiang, T.M. Long-term fertilization and mineralization of soil organic carbon in paddy soil from yellow earth. *Acta Pedol. Sin.* **2018**, *55*, 225–235. (In Chinese)
9. Vesterdal, L.; Elberling, B.; Christiansen, J.R.; Callesen, I.; Schmidt, I.K. Soil respiration and rates of soil carbon turnover differ among six common European tree species. *For. Ecol. Manag.* **2012**, *264*, 185–196. [CrossRef]
10. Huang, J.; Lin, T.C.; Xiong, D.; Yang, Z.; Liu, X.; Chen, G.; Xie, J.; Li, Y.; Yang, Y. Organic carbon mineralization in soils of a natural forest and a forest plantation of southeastern China. *Geoderma* **2019**, *344*, 119–126. [CrossRef]
11. Malý, S.; Fiala, P.; Reininger, D.; Obdržálková, E. The relationships among microbial parameters and the rate of organic matter mineralization in forest soils, as influenced by forest type. *Pedobiologia* **2014**, *57*, 235–244. [CrossRef]
12. Pregitzer, K.S.; Euskirchen, E.S. Carbon cycling and storage in world forests: Biome patterns related to forest age. *Glob. Chang. Biol.* **2004**, *10*, 2052–2077. [CrossRef]

13. Liu, L.; Wang, H.; Dai, W. Characteristics of soil organic carbon mineralization and influence factor analysis of natural Larix olgensis forest at different ages. *J. For. Res.* **2019**, *30*, 1495–1506. [CrossRef]
14. Chen, X.; Tang, J.; Jiang, L.; Li, B.; Chen, J.; Fang, C. Evaluating the impacts of incubation procedures on estimated Q10 values of soil respiration. *Soil Biol. Biochem.* **2010**, *42*, 2282–2288. [CrossRef]
15. Gao, Y.; He, N.; Yu, G.; Chen, W.; Wang, Q. Long-term effects of different land use types on C, N, and P stoichiometry and storage in subtropical ecosystems: A case study in China. *Ecol. Eng.* **2014**, *67*, 171–181. [CrossRef]
16. Stanford, G.; Smith, S.J. Nitrogen mineralization potentials of soils 1. *Soil Sci. Soc. Am. J.* **1972**, *36*, 465–472. [CrossRef]
17. Ahmed, A.A.; Mohamed, H.H.A.; Tamer, M.S.A.; Walid, E.B.; Samira, E.M. Mineralization of organic carbon and nitrogen in semi-arid soils under organic and inorganic fertilization. *Environ. Technol. Innov.* **2018**, *9*, 243–253.
18. Munda, S.; Bhaduri, D.; Mohanty, S.; Chatterjee, D.; Tripathi, R.; Shahid, M.; Kumar, U.; Bhattacharyya, P.; Kumar, A.; Adak, T.; et al. Dynamics of soil organic carbon mineralization and C fractions in paddy soil on application of rice husk biochar. *Biomass Bioenergy* **2018**, *115*, 1–9. [CrossRef]
19. Yang, K.; He, R.; Yang, W.; Li, Z.; Zhuang, L.; Wu, F.; Tan, B.; Liu, Y.; Zhang, L.; Tu, L.; et al. Temperature response of soil carbon decomposition depends strongly on forest management practice and soil layer on the eastern Tibetan Plateau. *Sci. Rep.-UK* **2017**, *7*, 4777. [CrossRef]
20. Wang, J.; Song, C.; Zhang, J.; Wang, L.; Zhu, X.; Shi, F. Temperature sensitivity of soil carbon mineralization and nitrous oxide emission in different ecosystems along a mountain wetland-forest ecotone in the continuous permafrost of Northeast China. *Catena* **2014**, *121*, 110–118. [CrossRef]
21. Chen, Y.; Chen, G.; Robinson, D.; Yang, Z.; Guo, J.; Xie, J.; Fu, S.; Zhou, L.; Yang, Y. Large amounts of easily decomposable carbon stored in subtropical forest subsoil are associated with r-strategy-dominated soil microbes. *Soil Biol. Biochem.* **2016**, *95*, 233–242. [CrossRef]
22. Xiao, D.; Huang, Y.; Feng, S.; Ge, Y.; Zhang, W.; He, X.; Wang, K. Soil organic carbon mineralization with fresh organic substrate and inorganic carbon additions in a red soil is controlled by fungal diversity along a pH gradient. *Geoderma* **2018**, *321*, 79–89. [CrossRef]
23. Li, Z.; Zhang, T.; Chen, B. Dynamics of soluble organic carbon and its relation to mineralization of soil organic carbon. *Acta Pedol. Sin.* **2004**, *41*, 544–552. (In Chinese)
24. Chen, T.; Hao, X.; Du, L.; Lin, B.; Feng, M.; Hu, R.; Gao, J. Effects of long-term fertilization on paddy soil organic carbon mineralization. *Chin. J. Appl. Ecol.* **2008**, *19*, 1494–1500. (In Chinese)
25. Worrell, E.; Price, L.; Martin, N.; Hendriks, C.; Meida, L.O. Carbon dioxide emissions from the global cement industry. *Annu. Rev. Energy Environ.* **2001**, *26*, 303–329. [CrossRef]
26. Davidson, E.A.; Verchot, L.V.; Cattânio, J.H.; Ackerman, I.L.; Carvalho, J.E.M. Effects of soil water content on soil respiration in forests and cattle pastures of eastern Amazonia. *Biogeochemistry* **2000**, *48*, 53–69. [CrossRef]
27. Paustian, K.; Six, J.; Elliott, E.T.; Hunt, H.W. Management options for reducing CO2 emissions from agricultural soils. *Biogeochemistry* **2000**, *48*, 147–163. [CrossRef]
28. Yu, S.; Wang, J.; Gao, Y. Effect of plastic mulching and different fertilization treatments on soil microbial biomass carbon and nitrogen. *J. Shenyang Agric. Univ.* **2006**, *37*, 602–606. (In Chinese)
29. Ågren, G.I.; Bosatta, E.; Magill, A.H. Combining theory and experiment to understand effects of inorganic nitrogen on litter decomposition. *Oecologia* **2001**, *128*, 94–98. [CrossRef]
30. Ci, E.; Mahdi, A.-K.; Wang, L.; Ding, C.; Xie, D. Soil organic carbon mineralization as affected by cyclical temperature fluctuations in a karst region of southwestern China. *Pedosphere* **2015**, *25*, 512–523. [CrossRef]
31. Wang, H.; Fan, Z.; Deng, D. Effects of environmental factors on soil organic carbon mineralization in a pinus sylvestris var. mongolica plantation. *Chin. J. Ecol.* **2008**, *27*, 1469–1475. (In Chinese)